Engineered tools for studying the malaria parasite *Plasmodium falciparum*

by

Bridget Wall

B.A., Illinois Wesleyan University (2008)

Submitted to the Department of Biological Engineering in Partial Fulfillment of the Requirements for the Degree of

Doctor of Philosophy

at the

Massachusetts Institute of Technology

June 2015

Author.....

Bridget Wall

Department of Biological Engineering, MIT

Certified by.....

Jacquin C. Niles

Associate Professor of Biological Engineering, MIT

Thesis Supervisor

Approved by.....

Forest M. White

Professor of Biological Engineering, MIT

Chair, Course 20 Graduate Program Committee

This doctoral thesis has been examined by a committee of the Department of Biological Engineering as follows:

Certified by.....

Leona Samson

Associate Department Head/Director of Biological Engineering, MIT

Thesis Committee Chair

Certified by.....

Jacquin C. Niles

Associate Professor of Biological Engineering, MIT

Thesis Supervisor

Certified by.....

Forest M. White

Professor of Biological Engineering, MIT

Thesis Committee Member

Engineered tools for studying the malaria parasite *Plasmodium falciparum*

by

Bridget Wall

Submitted to the Department of Biological Engineering on May 22nd, 2015 in Partial Fulfillment of the Requirements for the Degree of Doctor of Philosophy in Biological Engineering at the Massachusetts Institute of Technology

ABSTRACT

New techniques to both prevent and treat the disease malaria are necessary. To develop these novel strategies, innovative tools must be designed to study the basic biology within *Plasmodium falciparum* and characteristics of the pathological relationship between host and parasite. These tools will be diverse in nature, yet all seek to address the same fundamental question: what are the characteristics of the parasite that can be exploited to decrease the burden this parasite places on the human species? First, the relationship between nitric oxide and the parasite-infected red blood cell will be measured using a microfluidic device. Second, a toolkit to determine the essentiality of genes of unknown function will be engineered and tested with three separate genes to improve and demonstrate usability. Third, a mutator strain will be engineered and defined for eventual use in the study of drug resistance and the characterization of the resistance potential of anti-malarial drugs.

Thesis Supervisor: Jacquin C. Niles

Title: Associate Professor of Biological Engineering

Contents

0.1 Acknowledgements and Attributions

First, thank you to the entire Niles Lab, past and present, for their support and contributions. Much of the work described herein was performed as a team or collaboration. The work described in Chapter 2 contains work by Niles Lab postdoc Erika Bechtold and Han Lab member Sha Huang. The data they generated is attributed specifically to them in the figure legends. Many thanks to Jay Han for his assistance and support on this collaboration. The work described in Chapter 3 is built on other Niles Lab technology development. The original set of TetR-binding RNA aptamers was discovered by Jacquin Niles. The first characterizations of TetR-aptamer interactions were performed by Brian Belmont [1, 2]. Characterizations of the TetR aptamer in the parasite was performed by Steve Goldfless and Jeff Wagner [3] and the system was extended by Suresh Ganesan (unpublished). Sebastian Nasamu designed and cloned constructs for the 5' Aptamer portion of the toolkit, and Aleja Falla and Sumanta Dey are also contributing to the completion of the toolkit in its entirety. The work described in Chapter 4 is entirely my own work.

Thank you to my family and friends for their support.

Thank you my funding sources: MIT startup funds, the Biological Engineering Department, the first year Cargill Fellowship, and the NIEHS Training Grant.

1 Introduction

1.1 The Malaria Parasite

Five different species of the malaria parasite have been found to infect humans: *Plasmodium falciparum*, *Plasmodium vivax*, *Plasmodium knowlesi*, *Plasmodium ovale*, and *Plasmodium malariae*. *Plasmodium falciparum* is the most virulent, causing the majority of malaria-related mortality and morbidity, especially in children under the age of five [4]. Approximately 200 million people are infected by the parasite each year, and just under one million die from malarial infections. The life cycle of the *Plasmodium falciparum* parasite occurs in two different hosts: female *Anopheles spp.* mosquitoes and humans. There are over 200 other malaria species that infect birds, reptiles, and other mammals, and these species are differentiated by their host, vector, geography, and pathological characteristics.

In humans, the contact with a parasite begins when a mosquito takes a blood meal from a human and sporozoites are injected into the skin (Figure 1 on page 11). The sporozoites travel to the liver and infect hepatocytes, undergoing initial replication termed exo-erythrocytic schizogony. After an approximately two week incubation period, asexual stage merozoites are released into the blood stream. Merozoites reinvade a new cell in 30-90 seconds [5], and begin a 48 hour cycle that includes three main stages: ring, trophozoite, and schizont. At this point in the cycle, the red blood cells rupture and release from 2-20 new merozoites, and the cycle begins again. Sometimes, the parasite differentiates into the sexual stages, termed gametocytes, which are taken up during a mosquito blood meal. Within the gut, gametocytes differentiate into gametes, and undergo fertilization. The zygote develops into an ookinete and invades the wall of the gut, forms an oocyst, and undergoes meiosis. The oocyst grows for 1-3 weeks, and divides to form haploid sporozoites. These migrate to the mosquito salivary gland, mature, and the cycle begins again when the mosquito takes a blood meal and deposits sporozoites into another human.

Symptoms of malaria arise during the asexual cycle in the red blood cells, usually a week to a month following infection. The clinical symptoms can range from the somewhat mild to severe. Mild symptoms include fever, chills, headache, vomiting, and diarrhea, and are similar to the symptoms of the flu. More severe cases of malaria can result in an enlarged spleen, anemia, lung and kidney dysfunction, and neurological maladies. While the pathophysiology of the parasite is complicated and not well understood, sequestration of infected red blood cells in the microvasculature seems to be the culprit in severe and fatal cases of the disease. Sequestration prevents full oxygenation of tissues, which can result in brain damage, loss of a fetus during pregnancy, and death.

1.2 The Need for Tool Development

The malERA Consultative Group on Basic Science and Enabling Technologies wrote a review in 2011 stating the basic science goals surrounding the biology of the malaria parasite and the tools required to make changes at the global scale:

> Research priorities include the development of in vitro culture systems for the complete life cycle of *P. falciparum* and *P. vivax* and the development of an appropriate liver culture system to study

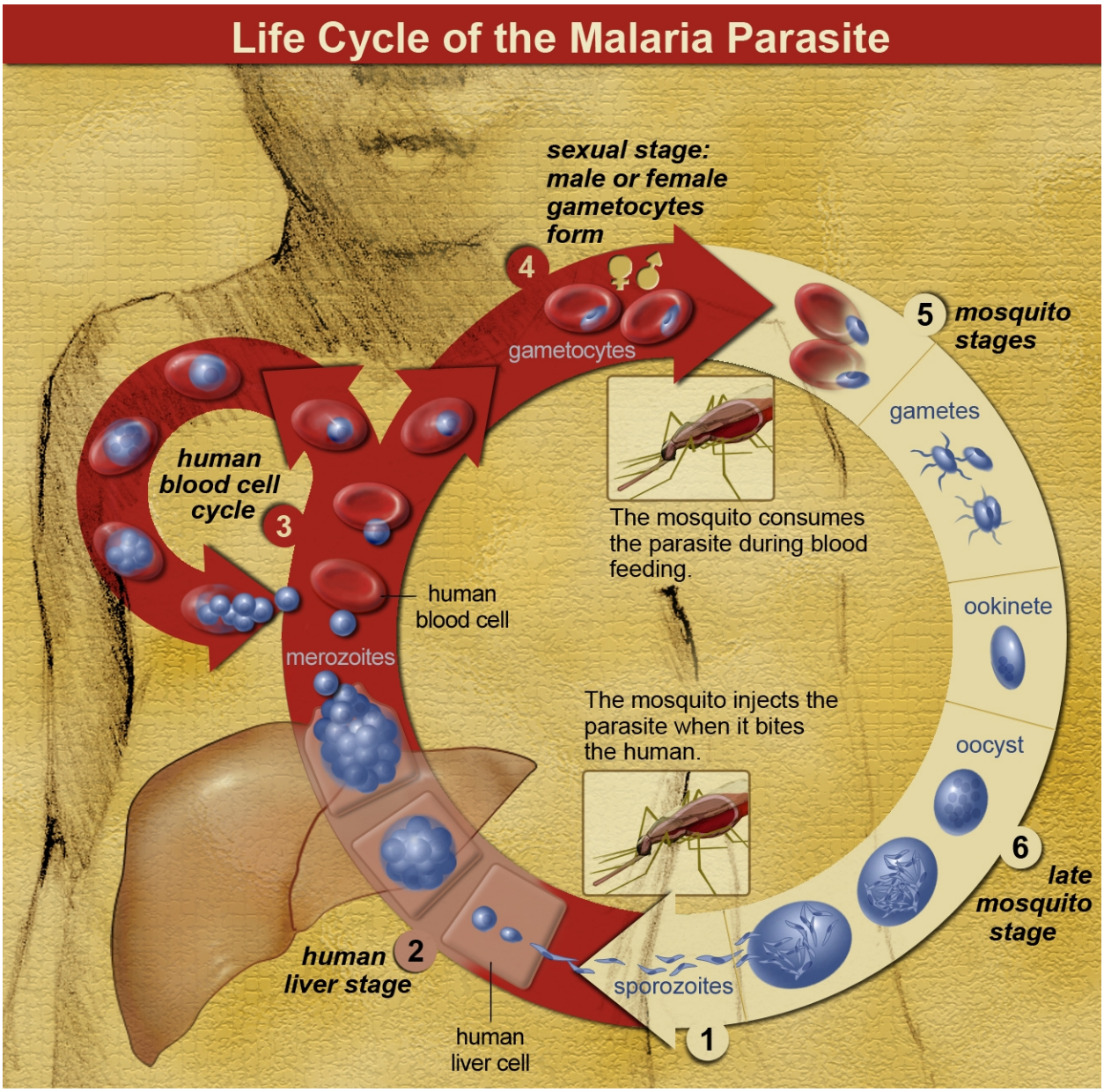

Figure 1: The life cycle of *Plasmodium falciparum* (National Institutes of Health).

hepatic stages. In addition, genetic technologies for the manipulation of Plasmodium need to be improved, the entire parasite metabolome needs to be characterized to identify new druggable targets, and improved information systems for monitoring the changes in epidemiology, pathology, and host-parasite-vector interactions as a result of intensified control need to be established to bridge the gap between bench, preclinical, clinical, and population-based sciences. [6]

These research priorities directly interface with the goals of this thesis, and each chapter addresses a component of these priorities.

1.2.1 malERA Priority: Developing appropriate culture systems to study the malaria parasite

One notable challenge in the study of malaria is the lack of a true animal model that mimics known human-parasite characteristics of infection. There are several rodent and simian systems utilized to study the molecular mechanisms of infection. However, given that these *in vivo* systems utilize primarily rodent and simian parasites, they are unable to recapticulate some of the biology unique to the human-parasite system. Though the parasites are indeed related, evolution has rendered them unpredictably different from their human parasite relatives. For example, rodent and human malaria parasites possess orthologs of parasitophorous vacuole membrane proteins in common (ETRAMPs). An ETRAMP called UIS4 was found to be essential in liver stage rodent parasites. However, when the putative ortholog from the human malaria parasite was expressed in rodent parasites lacking the native UIS4 gene, the rodent parasites were unable to progress through the liver stage [7].

Essentially, while there does seem to be overlap between different parasite species, they are still imperfect model systems that should not be used as direct evidence for human-parasite interactions. Advances in humanized mouse models have facilitated unique *in vivo* studies yet also remain unreliable [8]. However, the alternative of using *in vitro* models using the human parasite and human blood come with their own negative characteristics as well. Without the complex environments present within the *in vivo* setting, many of the chemical and mechanical nuances experienced are left unmeasured and unrealized. Thus, there is a clear need for a system that recapitulates the biology of both the host organism and host parasite. In the meantime, isolating particular biological molecules and looking for cause and effect will help begin to fill in the substantial gaps in what is known about the relationship between parasite and host.

For my first aim, I address a portion of this problem by using a microfluidic deformability device to examine the relationship between the chemical nitrite and the mechanical deformability of parasite-infected red blood cells, in order to learn more about the effects of immune system-produced chemicals on the physical state of the parasite in the microvasculature.

1.2.2 malERA Priority: Improve technologies for genetic manipulation of the malaria parasite

There are many challenges in the parasite that make manipulation of the genome challenging:

- The genome is AT-rich. On average, coding regions are 80% AT, and non-coding regions are 90% AT [9]

- 60% of *Plasmodium falciparum* genes were classified as having no known homology to any other known gene [9]
- Transfections are extremely time-consuming [10, 11, 12]
- There are only four viable resistance genes for use in the parasite
- Proper localization is non-trivial [13]
- Knocking out essential genes is fraught with complications: while transfecting in a donor plasmid and hoping that it undergoes homologous recombination has yielded successful knockouts in the past, it takes from months to years, and is only feasible for those genes that are non-essential in the blood stage parasite.

Yet, the Niles lab has worked hard to overcome these challenges and design modular and efficient systems for investigating basic biology in the parasite. These tools include utilizing the CRISPR/Cas9 system for editing the genome, adapting the TetR aptamer system for conditional protein expression in the parasite, and improving cloning techniques.

For my second aim, I will contribute to a toolkit that brings together these tools in order to address the essentiality of genes in order to find potential drug targets in the vast numbers of undefined parasite genes.

1.2.3 malERA Priority: Monitor changes in epidemiology

Epidemiology encompasses the incidence, distribution, and control of a given disease. Currently, a pressing issue of disease control in malaria is the rapid emergence of resistance to anti-malarials. Anti-malarial resistance directly affects patient care and mortality rates, and it is clear that a new approach is needed to address drug-resistant parasite populations.

As resistant malaria has arisen against every antimalarial employed against the disease [14], it is important to learn more about the mechanisms of drug resistance and the resistance potential of single drugs and drug combinations. However, studying drug resistance in the laboratory is hampered by many factors [15].

First, while there have been drug resistant strains selected *in vitro* for almost 40 years, the process remains time-consuming and unpredictable. Artemisinin is currently the first choice for treatment, and is now used in the form of artemisinin-combination therapy, since parasites resistant to artemisinin are now commonplace. Yet, until 2014, artemisinin-resistant parasites had not been created *in vitro*, and that process took five years. Creating a lab strain that is able to more efficiently and predictably create drug resistance parasites that can be characterized and studied is desirable.

For my third aim, I will make a mutator strain that has the potential to help address these concerns and provide a much-needed straightforward *in vitro* test for determining characteristics of resistance to specific drugs and drug combinations.

2 Defining the nitrite/nitrate-dependent infected red blood cell phenotype and investigation of potential mechanisms mediating this phenotype

An important note on the collaborative nature of this project:

- Niles Lab postdoc Erika Bechtold and Han Lab member Sha Huang contributed to this project, and the data that they generated is attributed to them in the figure legends.

2.1 Introduction

One of the hallmarks of malaria pathology is the sequestration of infected red blood cells in the microvasculature. This process allows parasites to evade clearance and destruction by the spleen. The process is not well understood, but both chemical and mechanical properties of the infected red blood cell increase their ability to sequester successfully. In addition, the exact nature of the relationship between the immune system and process of parasite sequestration is still in the very early stages of research. Of particular interest is the relationship between the humoral immune system mediator nitric oxide and the mechanical properties of the infected red blood cell during sequestration.

2.1.1 Chemical Properties of the Infected Red Blood Cell

When the parasite invades the red blood cell, significant changes occur. First, as the red blood cell is filled with hemoglobin, the parasite begins to break down this protein in order to harvest amino acids for growth, but also to allow for space for the parasite to increase in size [16, 17]. Cellular heme is detoxified and processed into a heme crystal known as hemozoin. Permeability also increases upon infection [18]. The infected red blood cell loses the characteristic bi-concave shape, becoming spherical. As the parasite grows, over 400 proteins are exported to the surface, and approximately 10,000 elevated knobs form, changing the structure of the red blood cell [19, 20, 21] and altering the adhesive properties of the red blood cell membrane [22]. The biophysical relationship between the lipid bilayer in the red blood cell and the cytoskeleton remains under investigation [23, 24]. Identified cell surface proteins, namely KAHRP, various PfEMPs, RESA, MESA, and MAHRP, function primarily in cytoadhesion, interacting both with the red blood cell cytoskeleton and receptors on epithelial cells [25, 26, 27, 28]. This characteristic of adherence contributes to the infected red blood cell's ability to sequester in the microvasculature and avoid destruction in the spleen [29, 30, 31]. Notably, different species of the parasite have preferential sequestration patterns in different organs at different points in their life cycle [32].

2.1.2 Mechanical Properties of the Infected Red Blood Cell

One of the key defining mechanical properties of red blood cells is their ability to deform through small spaces in the microvasculature and the slits in the spleen. Those red blood cells that are unable to deform through these sieve-like slits are phagocytized and broken down[33]. In healthy humans, these red blood cells are usually at the end of their 120 day life span. In malaria patients, infected red blood cells become stiffer and the spleen is able to remove infected cells [34]. *Ex vivo* spleen studies have demonstrated this ability by showing the retention of infected red blood cells and heat-stiffened uninfected cells using a perfusion experiment [35]. In fact, one of the symptoms of malaria is an enlarged spleen, and the size of the spleen is a clinical tool used to estimate characteristics of malaria transmission [36]. Those patients without spleens display an increased parasitemia when infected with malaria despite use of a wide range of antimalarials[37].

Thus, it is hypothesized that parasites evolved mechanical and chemical means of avoiding the spleen by sequestering in the microvasculature [38]. Essentially, increasing their stiffness and expressing membrane-associated proteins that bind to epithelial cells both upregulate their ability to sequester and avoid splenic

clearance. Deformability in red blood cells is thought to be caused by cross-linking of membrane-bound proteins and the cytoskeleton [39, 40]. Thus, in infected red blood cells, the expression of parasite proteins that interact with the red blood cell cytoskeleton are hypothesized to significantly change the deformability of the red blood cell membrane [38, 41].

However, many of these studies were done in isolation without the greater microenvironment in mind. These properties have not been evaluated in the dynamic and complex environment possessing components of the host immune system. These unknowns include the milieu concentrations of cytokines and chemicals like nitric oxide, the types and numbers of immune cells present, but also the microenvironment's pH and ion concentrations. For instance, it is logical to think that if cells are sequestered in the microvasculature alive and respiring, the pH of the local environment would go down following release of carbon dioxide as carbonic acid in the surrounding plasma. These components are likely contributing to the progression of disease in patients, and further study of the effects of these microenvironments will help define the pathophysiology of sequestration in the disease and possibly provide potential drug targets. Therefore, the mechanical properties of infected red blood cells should be measured while perturbing certain components of the complicated microvasculature milieu.

2.1.3 Measuring Mechanical Properties of the Infected Red Blood Cell

Given the importance of the mechanical changes of the infected red blood cells in the pathology of malaria, a variety of methods have been used to measure deformability of infected red blood cells:

- Optical Tweezers - measures the membrane shear modulus in individual cells
  - An optically trapped Con A-coated polystyrene bead is attached to one side of an RBC, while the opposite side is attached to a cover slip. Force is applied to the coverslip and force displacement responses are measured by detecting the changes in position of the bead. During these stretching experiments, a shear modulus is determined, and the deformability can be calculated using computational modeling [42, 43].
- Micropipette Aspiration - measures the membrane shear modulus in individual cells
  - Cells are aspirated by a 1 µM diameter pipette, and the leading edge of the aspired cell is tracked in order to calculate the elastic shear modulus using the spherical cap model [44].
- RBC membrane fluctuations - measures the refractive index of individual cells
  - Tomographic phase microscopy (TPM) utilizes laser interferometery with a rotating incident beam to provide a 3D distribution of refractive index [45].
- Ektacytometry - measures the elongation index in bulk
  - A laser-assisted optical rotational cell analyzer is used to analyze the elongation index of a group of cells over a range of shear stresses [46].

- Microfluidic Flow Cytometry - measures transit velocity of individual cells through a microfluidic challenge
  - The velocity of individual cells is measured as they move through a microfluidic device that is has pores small enough that force constant deformation [34, 44].

All studies have concluded that parasitized red blood cells are stiffer than uninfected red blood cells. Note that one group has confirmed a bystander effect in their optical tweezer experiment, where uninfected red blood cells in a culture of infected cells had different deformability readings than uninfected red blood cells cultured alone [43].

However, the multifactorial nature of cell deformability means that different measurement tools can lead to slightly different results, as occurs in the above studies [44, 47]. Important variables of deformability include cell geometry, the viscosity of the cytoplasm, and membrane viscoelasticity. Different tools measure different components of these variables. Single cell approaches like micropipette aspiration and membrane fluctuations are time-consuming and low throughput. Measurements using bulk approaches like ektacytometry may be influenced by cell to cell interactions. Thus, microfluidic flow cytometry is the tool of choice in this study because it is able to measure the entire deformability of a specific cell at a given time, yet in a timely manner.

2.1.4 The Infected Red Blood Cell and the Human Immune System

The human immune system has a combined cellular and humoral response to malarial infection. Adaptive immunity to malaria can be acquired, but it is a slow process and incomplete, hence why children under the age of five with incomplete resistance profiles are the main victims of malaria [48]. This is thought to be due in part to the complicated process malaria parasites employ for antigenic variation [49, 50, 51].

However, it appears as if protective immunity can also be mediated by a combination of T cells, IFN-γ, and nitric oxide rather than antibodies [52]:

- First, when sporozoites enter the liver, parasite antigens induce formation of CD8+ and CD4+ T cells, which target infection by producing interferon-gamma (IFN-γ), which activates the nitric oxide pathway either in the endothelial cells or in macrophages [53, 54, 55, 56].
- CD4+ T cells have two subpopulations, TH1 and TH2. TH1 cells protect against a murine malarial infection by a nitric oxide-dependent mechanism, while TH2 cells act by inducing increased production of a G1 antibody [57].
- Monocytes also take up more uninfected red blood cells during infection, something that could contribute to the anemia often seen in malaria patients [58].
- Natural killer cells interact with dendritic cells and secrete cytokines. In malarial infection, they are a source of (IFN-γ) following an interaction with infected red blood cells [59, 60]
- IFN-γ activates monocyte-derived macrophages, which proceed to kill infected parasites [61].

- Hemozoin also has been shown to increase IFN-γ induced nitric oxide generation from macrophages [62] and in general affect the innate inflammatory response [63]. Unprocessed hemoglobin released following hemolysis during infection contributes to infection-based inflammation and damage [64].

As articulated above, the main cellular components of the immune system exert their effects using cytokines, and these chemicals have a dynamic role in malaria infection, one that is capable of both protecting and exacerbating the disease [62]. The particular nature of their role is difficult to determine given the challenges in measuring accurate cytokine concentrations and outcomes *in vivo*. However, it is argued that their contribution should be acknowledged in the pathology of disease along with mechanical sequestration [65, 66, 67, 68, 69]. For example, a high parasite burden can lead to an increased production of pro-inflammatory mediators, which has been shown to suppress erythropoiesis in the bone marrow, contributing to the pathology of malaria [70].

To add even greater complexity to the mix, individuals have highly variable cytokine response dynamics [71]. A recent study profiled the responses of mice to murine malaria, finding that they fall into three categories of differential immune response [72]. Another study shows that IL-12 induces protection against blood stage murine malaria using IFN-γ and TNF-α through a nitric oxide-dependent mechanism, and the concentration of applied IL-12 drastically changed the concentrations of measured cytokines [73].

It is clear from these studies that nitric oxide in particular contributes to the pathophysiology of malaria, though the full extent of the relationship between infected red blood cells and nitric oxide remains to be elucidated.

2.1.5 Nitric Oxide Biology

Reactive nitrogen species (RNS) and reactive oxygen species (ROS) are important players in the immune system as downstream effectors following cytokine activation (Figure 2 on page 19) [75]. These species cause a myriad of downstream effects to a diverse set of molecules: proteins, carbohydrates, nucleic acids, and lipids.

Nitric oxide is produced by three isoforms of nitric oxide synthase: iNOS (inducible), eNOS (endothelial) and nNos (neuronal). NOS enzymes catalyze the change of the substrates arginine, a hydrogen ion. two oxygen gas molecules and NDAPH to produce citrulline, nitric oxide, and NADP+. eNOS and nNOS are both constitutively expressed, and use nitric oxide as a signaling molecule, especially in vasodilation. iNOS was originally found in macrophages, and produces nitric oxide in response to stimulation by other upstream components of the immune system. In regions of inflammation as a result of infection, the local concentration of nitric oxide and other RNS/ROS can be quite high, causing damage to the local host cells as well as the infectious agent. The particular consequences of nitric oxide are determined by several factors: [75]

- diffusion rate
- distance between generation of nitric oxide and potential targets
- concentration of targets (whether they are other components of the RNS/ROS family or cellular targets)

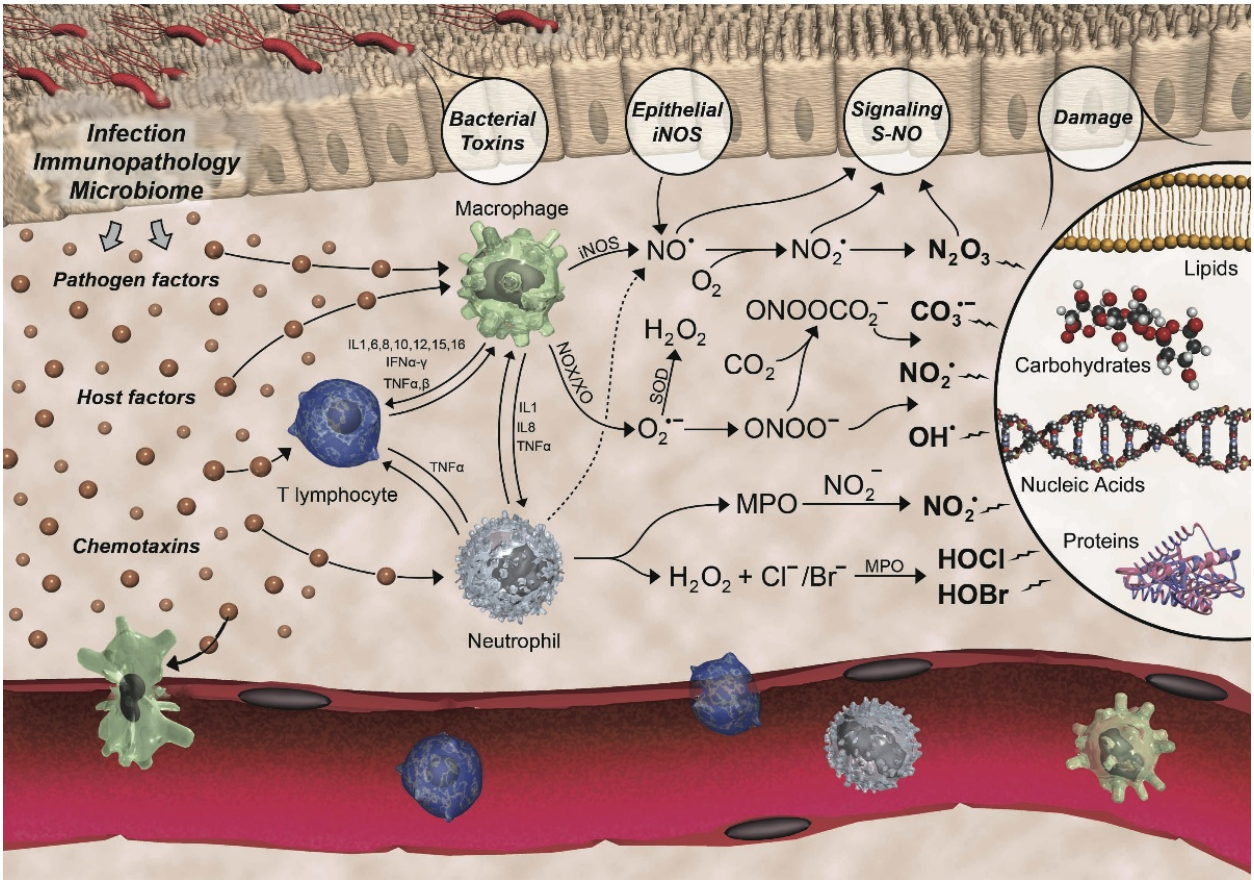

Figure 2: The complex relationships between reactive nitrogen and oxygen species continue to be elucidated. Figure courtesy of Peter Dedon (this is an updated version of the figure published in Lonkar 2011 [74]).

- concentration of enzymes like catalase and superoxide dismutase
- concentration of antioxidants like glutathione
- concentration of substrate (arginine)

As red blood cells are carriers of a high concentration of iron-containing hemoglobin, and assist in oxygen transport, they are exposed to significant oxidative stress in the form of RNS/ROS [76]. Importantly, within the red blood cell, nitric oxide binds readily to hemoglobin to form S-nitrosohemoglobin and nitrosylhemoglobin, acting in a regulatory capacity, cycling between a sink and a donor of NO depending on the local microenvironment [77, 78]. Hemoglobin is also able to react with a variety of other ligands, including carbon monoxide, sulfide, cyanide, and hydrogen peroxide. The population of hemoglobin also cycles between oxidation states of Fe^{2+} and oxidized met-hemoglobin (Fe^{3+}), the latter of which is unable to bind oxygen and is a marker for oxidative stress [79]. Additionally, red blood cells express an arginase enzyme, as well as an active and functional endothelial nitric oxide synthase (eNOS), localized to both their cell membrane and cytoplasm [78].

It is important to mention that measuring nitrite in biological systems is difficult; not only does the oxidation of nitrite occur very quickly, but the levels are low, approaching the limit of detection, even using technologies like an nitric oxide analyzer (NOA). Such technologies also require very stringent preparation of standard curves and controls, making it difficult to increase experimental throughput [80]. Additionally, levels tested in plasma do not accurately reflect the concentration of nitrite or other relevant species at the level of the microvasculature.

However, to provide context for concentrations of nitrite relevant to this study, provided below are experimentally measured levels of nitrite:

- Red blood cells
  - 200 and 300 nM [81]
  - 50 to 436 nM (mean of 288 ± 47 nM) [80]
- Human plasma
  - 75 to 167 nM (mean of 114 ± 11 nM) [80]
- Whole blood
  - 65 to 290 nM (mean of 181 ± 29 nM) [80]
- Malaria-infected red blood cells in culture
  - 11 mM (+/- 3 mM) [82]

2.1.6 Nitric Oxide and Malaria Infection

With regards to malaria-infected red blood cells, production of reactive nitrogen and oxygen species in the parasite has been confirmed [83]. Antioxidants were found to have anti-malarial activity when given to mice with murine malaria [84], and a range of outcomes are known from different antioxidants on malarial parasites [85]. The redox buffering systems of the malaria parasite are not fully defined, though much is known about the main players like glutathione and thioredoxin [86, 87, 88, 89, 90].

While many RNS and ROS are under investigation for their interactions with malaria infected red blood cells, many studies have focused on nitric oxide in particular:

- Increased nitric oxide levels have been measured in mice [57] and in patients, where they are associated with severe disease and clinical cure, suggesting their presence as beneficial [91, 92]
- Inducible nitric oxide synthase (iNOS) knockouts in mice show similar levels of parasitemia following infection with *P. berghei*, a murine malaria strain. Yet, these infected knockouts present early mortality, increased leukocyte rolling, and liver damage [93]
- Low nitric oxide bioavailability and an increase in endothelial dysfunction and sequestration is seen in a cerebral malaria model in mice [64, 94]
- The presence of nitric oxide has been shown to protect against experimental cerebral malaria in mice by inhibiting CD4+ and CD8+ T cells [95]
- A study released in 2014 shows that *P. falciparum* proteins undergo s-nitrosylation and could be components of the nitric oxide pathway in the parasite, both in terms of signaling and toxicity [96]

However, the parameters of the relationship between nitric oxide and infected red blood cells are not fully understood, especially in non-mouse models. It is acknowledged however, similar to cytokines, the presence of nitric oxide can be beneficial or detrimental, depending on concentration, timing, location, and surrounding environment [62, 90, 97, 98, 95, 99]. This could even be true in the same patient at different times during infection or different environments within the body. As with cytokines, the contribution of oxidative stress and chemicals like nitric oxide to the pathology of sequestration events in malaria is being investigated. Thus, investigating the effects of nitric oxide on the mechanical deformability of infected red blood cells is of particular interest.

2.1.7 Nitric Oxide and Uninfected Red Blood Cell Deformability

Nitric oxide has been found to be an important mediator of cell stiffness as measured by a variety of deformability measurement techniques: electron paramagnetic resonance, shear stress laser defractometry, ektacytometry, and filter membranes. The NO-donor *S*-nitroso-*N*-acetylpenicillamine (SNAP) was found to increase membrane fluidity and deformability, a phenotype that was rescued by nitric oxide synthase inhibitor L-NAME [100]. Two different nitric oxide-producing drugs were found to increase the deformability of rat erythrocytes, a phenotype also rescued by nitric oxide synthase inhibitor L-NAME [101]. Rats treated with

LPS have significantly stiffer and more fragile red blood cell membranes, and NO-donors were found to rescue that phenotype [102]. This suggests that preventing additional nitric oxide release maintained the normal plasticity and robustness of the cell membrane. Low RBC deformability due to L-NAME treatment was rescued by NO donors SNP and DETA-NONOate [46]. When *ex vivo* RBCs are treated with L-arginine (the substrate processed with oxygen to become L-citrulline and nitric oxide), deformability of cells increases. However, when a NOS inhibitor is added (L-NNA), red blood cell deformability is reduced [78].

However, it is important to remember that these results, whether measured *in vitro* or *ex vivo*, may not accurately portray the dynamics occurring *in vivo*. Yet, all studies assert that nitric oxide plays a role in the manipulation of red blood cell membrane deformability, in addition to the role it plays in vasodilation and in the immune system. This evidence suggests the hypothesis that nitric oxide affects infected red blood cell deformability.

2.1.8 Red Blood Cell Membrane Deformability, Malarial Infection, and Nitric Oxide

Dynamic concentrations of nitric oxide are present in the microvasculature during malarial infection. Sources of nitric oxide are the immune system, the red blood cell itself and the vascular endothelium. Many processes and cell types contribute to these shifts: the concentration of nitric oxide synthase (NOS) enzymes, the presence of specific immune effectors, both cell-mediated and humoral, and even the concentration of arginine, the substrate used by NOS enzymes to make nitric oxide.

Only one paper to date, published in January of 2014, has looked specifically at the relationship between malaria infected red blood cells and nitric oxide [103]. Their results compared the blood of malaria patients to that of healthy individuals using ektacytometry, a technique that uses bulk measurements rather than measuring single cells. Low levels of arginine in the blood were correlated to low deformability of red blood cells taken from malaria patients. Additionally, adding nitric oxide donors L-NAME or L-arginine to red blood cells in vitro resulted in a slightly but reproducibly increased deformability. Thus, the authors suggest that hypoarginemia that occurs during malarial infection contributes to the reduced deformability of infected RBCs.

Indeed, these results suggest that higher nitric oxide increases the deformability of infected red blood cells, but the mechanism is unclear. The bulk measurement technique and a simple correlation of plasma levels to deformability do not show a direct relationship between nitric oxide and deformability. To do that, experiments should be done on a single cell level, and by varying the concentration of nitric oxide (or a nitric oxide donor) and directly measuring deformability in order to define the relationship between nitric oxide and infected red blood cells.

These measurements of deformability will provide experimental evidence to elucidate a portion of the complicated pathophysiology of the malaria parasite, especially with regards to the process of sequestration. This could lead directly to an improved understanding of preventative measures or treatments for the disease. Additionally, developing and refining a process to make these measurements could be used to characterize how particular candidate treatments for malaria affect the phenotype of sequestration.

Thus, this study looks to measure individual cell deformability and the mechanism by which nitric oxide could be affecting the deformability of malaria-infected red blood cells.

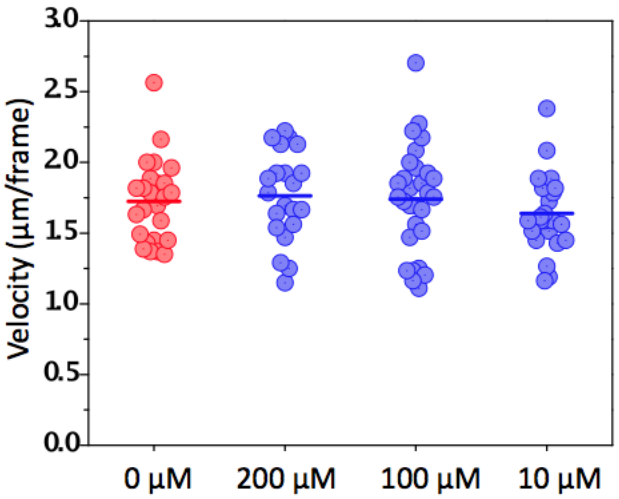

Figure 3: Uninfected red blood cells treated with a panel of nitrite concentrations have similar deformability measurements. Data generated by Sha Huang and Erika Bechtold.

2.2 Preliminary Experiments

Jay Han's graduate student Sha Huang adapted a device to measure the mechanical deformability of red blood cells as well as red blood cells infected with the malaria parasite [104]. In order to parse how specific immune effectors affect the infected red blood cell, both uninfected red blood cells and infected red blood cells were treated with nitrite, a likely chemical effector present in the microvasculature. Preliminary results from Sha and former postdoc Erika Bechtold's work demonstrate that parasites become stiffer upon treatment with nitrite.

2.2.1 Deformability of Uninfected Red Blood Cells Treated with Nitrite

An important control was the treatment of uninfected red blood cells with nitrite. Uninfected red blood cells were treated with the specified concentrations of nitrite and their velocity was determined by using the microfluidic device as described in the methods section. Deformability was tested three separate times. First, a panel of nitrite concentrations was tested (Figure 3 on page 23), and all treated cells had similar deformability measurements. A second test was done testing a greater range of concentrations (Figure 4 on page 24), also measuring similar deformability results. The final test re-measured the nitrite concentration of 1000 µM, and found that the cells that were not treated with nitrite were approximately the same stiffness as those cells treated with nitrite (Figure 5 on page 24).

It was concluded that nitrite had no significant affect on red blood cell deformability for a range of concentrations.

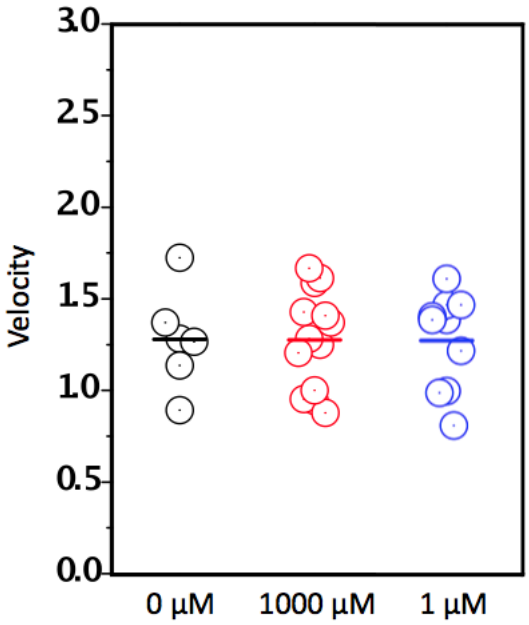

Figure 4: Uninfected red blood cells treated with 1000 µM or 1 µM nitrite had similar deformability measurements. Data generated by Sha Huang and Erika Bechtold.

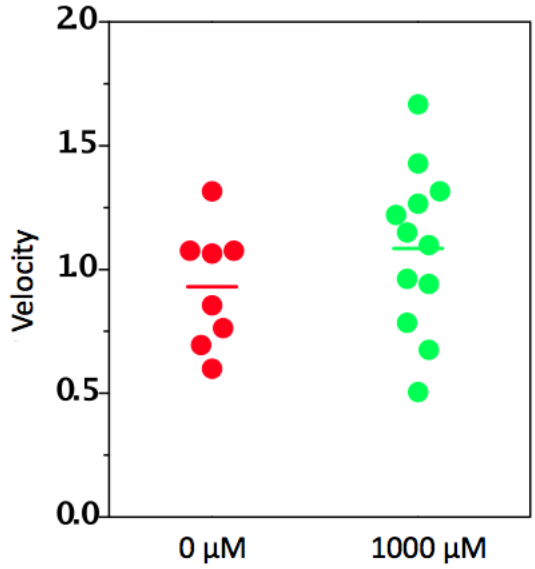

Figure 5: Uninfected red blood cells treated with 1000 µM nitrite are more deformable than untreated cells. Data generated by Sha Huang and Erika Bechtold.

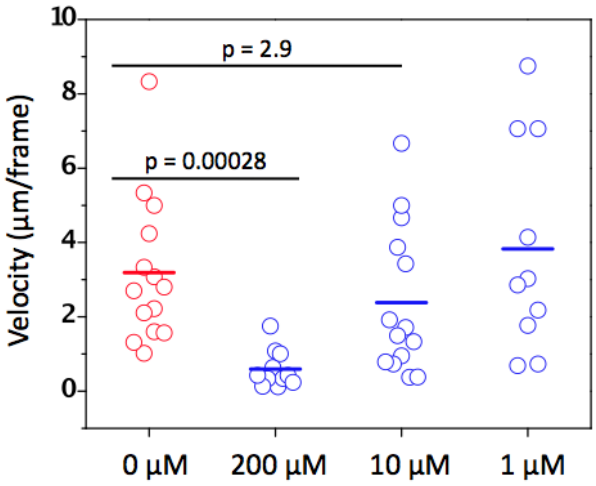

Figure 6: Infected red blood cells treated nitrite concentrations of 200 µM, 10 µM and 1 µM demonstrate a dose dependent shift in deformability. Data generated by Sha Huang and Erika Bechtold.

2.2.2 Deformability of Infected Red Blood Cells Treated with Nitrite

Next, infected red blood cells were tested with three nitrite concentrations: 200 µM, 100 µM, and 10 µM (Figure 6 on page 25). In this first test, the cells treated with 200 µM nitrite were significantly stiffer than untreated cells. The experiment was repeated with the nitrite concentrations of 10 µM and 1000 µM. The deformability phenotype was maintained (Figure 7 on page 26). A final test was done to confirm the phenotype by again treating cells with 1000 µM nitrite (Figure 8 on page 26). Cells treated with this concentration of nitrite were stiffer than control cells that were untreated. Of note with all these graphs is the sample size; for a deformability study where cells are significantly stiffer, this sometimes leads to a reduction in sample size due to device clogging.

With the deformability phenotype confirmed, the next step was to determine if the applied nitrite was having an effect in the media extracellularly, or internally.

2.2.3 Nitrite and Nitrate Uptake

A nitric oxide analyzer (NOA) was utilized to measure the change in extracellular nitrite concentration in the media following introduction of sodium nitrite to infected or uninfected red blood cells. In a closed system, reduced extracellular nitrite concentration corresponds to increased nitrite uptake. While this technique cannot directly address the question of whether nitrite is having an effect specifically intracellularly or extracellularly, any difference between the nitrite uptake of the uninfected cells compared to the infected cells would allow a correlation of uptake to deformability. After incubating cells with nitrite for 60 minutes, the nitrite concentration in a cell free media was unchanged (not shown). However, at 10% hematocrit, significant nitrite uptake was seen both in uninfected and infected RBCs, as evidenced by the drop in extracellular nitrite concentrations. However, *P. falciparum*-infected RBCs take up nitrite to an extent comparable with or greater than uninfected RBCs. (Figure 9 on page 27).

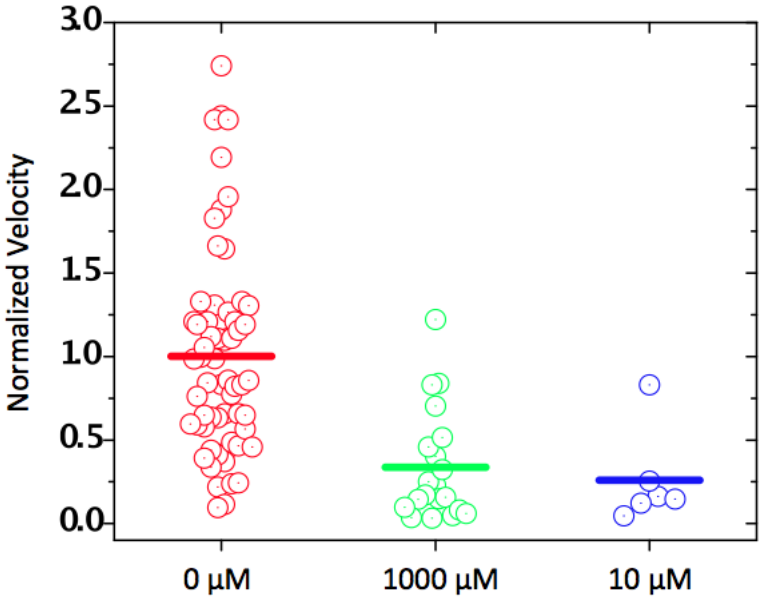

Figure 7: Infected red blood cells treated with 1000 µM nitrite are stiffer than untreated cells, as are cells treated with the concentration of 10 µM nitrite. Data generated by Sha Huang and Erika Bechtold.

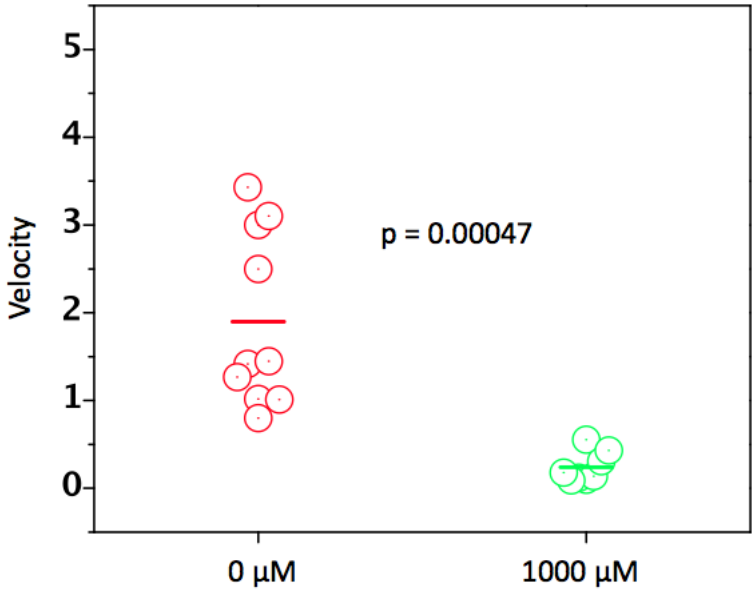

Figure 8: Infected red blood cells treated with 1000 µM nitrite are more deformable than untreated cells. Data generated by Sha Huang and Erika Bechtold.

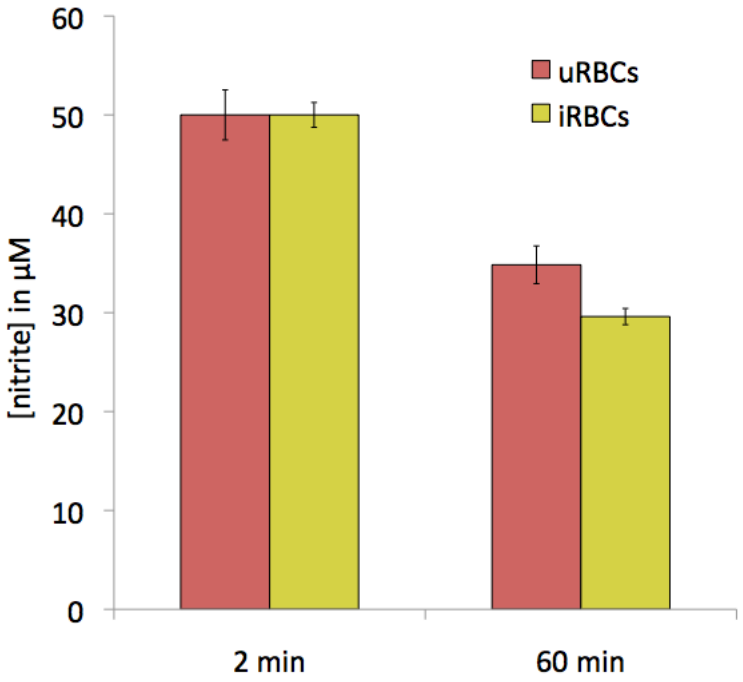

Figure 9: After a 60 minute exposure to nitrite, significant nitrite uptake is seen in both uninfected and infected RBCs. Data generated by Erika Bechtold.

2.2.4 Cell Size and Deformability

Because infection with malaria parasite changes the red blood cell significantly, it is important to determine whether the size of an infected red blood cell could affect deformability. First, samples of uninfected and infected red blood cells were analyzed by Coulter Counter to determine the range of their diameters and their average size (Figure 10 on page 28). As expected, infected red blood cells have a significantly larger diameter than uninfected red blood cells.

Next, infected red blood cells were treated with nitrite and their diameter was measured compared to a media-only control (Figure 11 on page 28). The diameter of infected red blood cells treated with nitrite is not significantly different from infected red blood cells incubated with media only. Thus, nitrite does not affect infected red blood cell diameter.

In order to establish that differences in the sizes of infected red blood cells treated with nitrite do not affect the deformability measured by the microfluidic device, infected red blood cells were artificially swelled by adding sorbitol to induce osmotic changes in size.

Infected red blood cells were treated with nitrite for one hour, washed, and resuspended in nitrite free media containing 2.5%, 0.64%, or 0.32% sorbitol. A portion of the population was measured using a Coulter Counter. As expected, those treated with the highest concentration of sorbitol had the largest diameter (Figure 12 on page 29). A portion of the treated population of cells from the same treatment groups was sent through the device to assess if the deformability changed upon nitrite and sorbitol treatment and it was found that there was not a significant change in deformability between cell sizes (Figure 13 on page 30). A no-sorbitol control was not included, so the experiment was repeated.

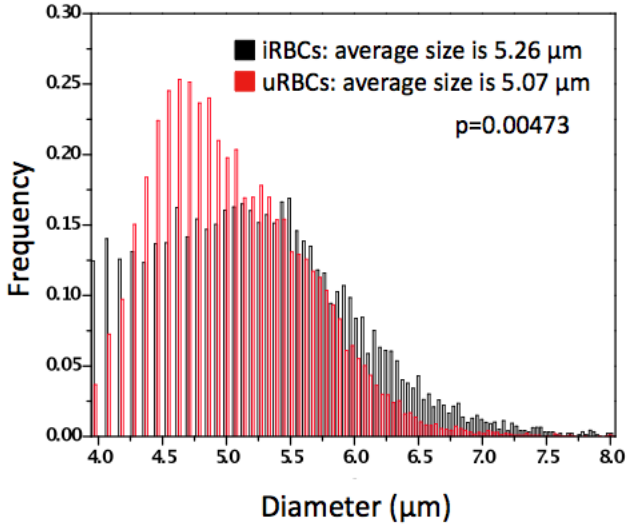

Figure 10: Infected red blood cells are larger than uninfected red blood cells as measured by Coulter Counter. Data generated by Sha Huang and Erika Bechtold.

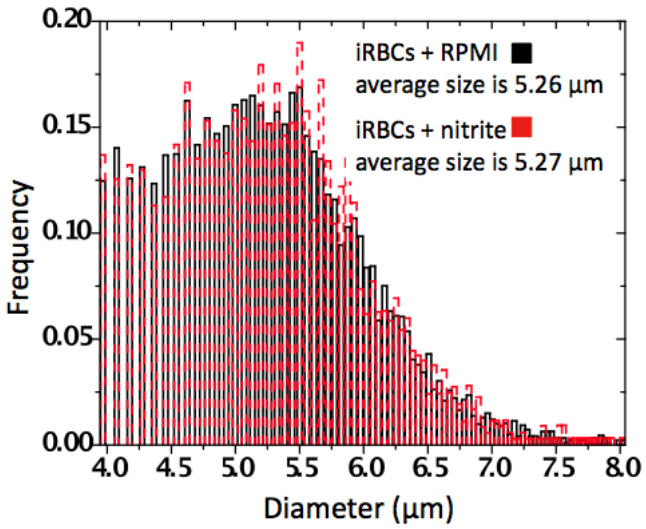

Figure 11: Infected red blood cells treated with nitrite or left untreated have the same diameter as measured by Coulter Counter. Data generated by Sha Huang and Erika Bechtold.

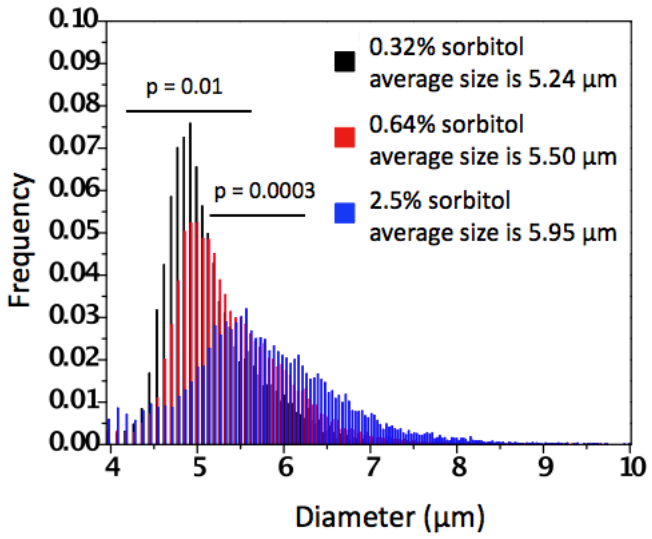

Figure 12: Size of sorbitol-treated infected red blood cells as measured by Coulter Counter. Data generated by Sha Huang and Erika Bechtold.

These experimental repeats were done on two consecutive days using blood from the same donor. All experimental data was gained within two hours of the post-incubation wash and resuspension. As expected, cells swelled with sorbitol treatment (Figure 14 on page 30). On the two separate experiment days, there were slightly different deformability results (Figure 15 on page 31). While there were statistically significant results in both experimental days that support the hypothesis that cell size does change deformability, the cell size that causes deformability to change was inconsistent. From these results, it can be concluded that osmotic and hydrostatic changes do not account for the nitrite-induced iRBC stiffening phenotype.

2.3 Investigating the pH-Dependent Deformability Phenotype

A dose dependent increase in stiffness was measured when infected red blood cells were treated with different concentrations of nitrite. However, these measurements do not take into account the potential pH shift seen in the microvasculature surrounding sequestered infected red blood cells. It is reasonable to assume that sequestered cells that are alive and respiring release carbon dioxide as carbonic acid, acidifying the local microenvironment and potentially changing how molecules like nitrite interact with their targets. Therefore, the pH and nitrite-dependent deformability phenotype will be measured.

2.3.1 Re-testing the Deformability Phenotype at pH 6.8

In order to test the pH and nitrite deformability phenotype, different nitrite concentrations were applied to cells at pH values of 6.8. These represent physiological pH and the potential local pH surrounding sequestered infected red blood cells.

Two samples of infected red blood cells were incubated with 1000 µM nitrite or no nitrite at pH 6.8. Surprisingly, there was no difference in deformability between the samples (Figure 16 on page 32).

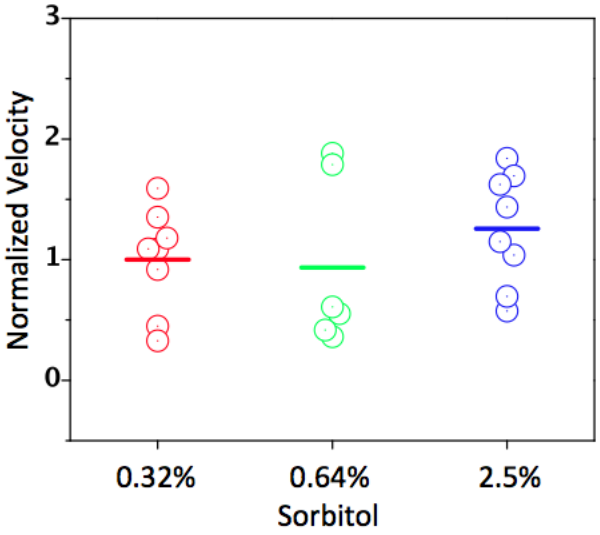

Figure 13: Deformability of sorbitol-treated infected red blood cells. Data generated by Sha Huang and Erika Bechtold.

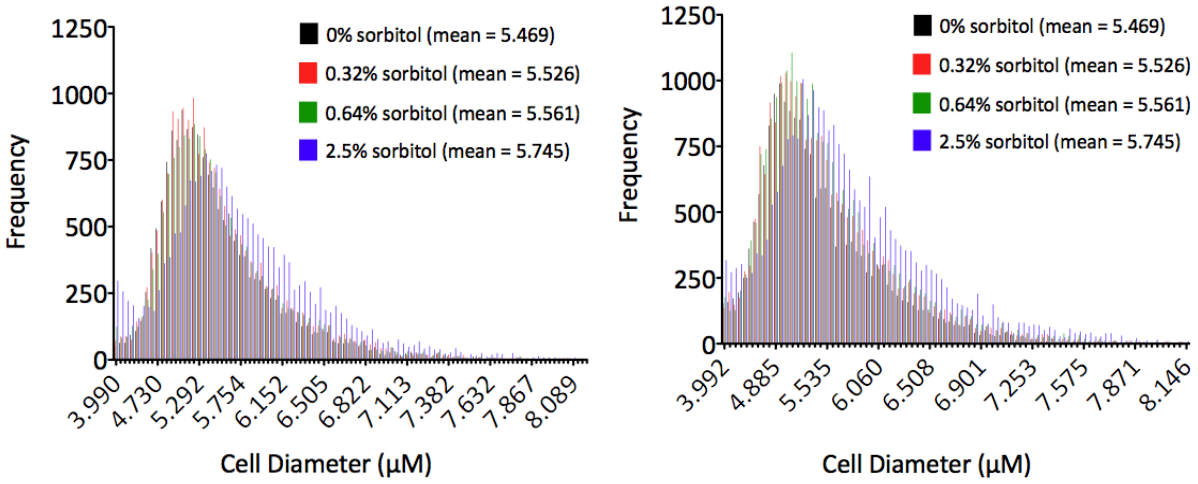

Figure 14: Cell diameter results from two sequential experimental days (6.10.14 and 6.11.14), analyzed using coulter counter. Data generated by Bridget Wall

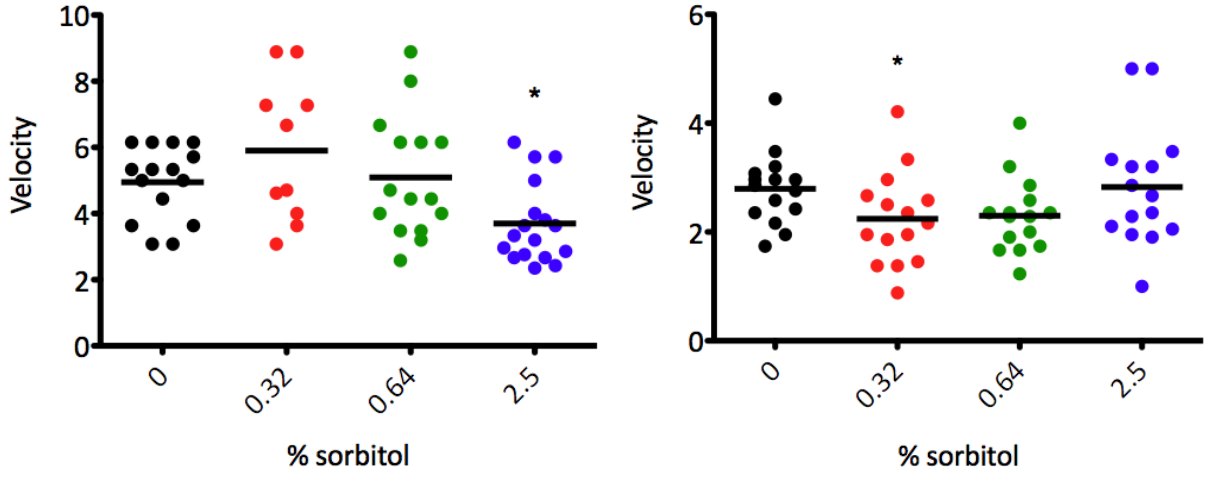

Figure 15: Deformability results from two sequential experimental days (6.10.14 and 6.11.14), analyzed using the microfluidic device. The asterisk (*) denotes statistical significance compared to the no sorbitol control in black; p value between 0.01 and 0.05. Data generated by Bridget Wall.

In order to address concentrations closer to the expected physiological concentration, three samples of infected red blood cells were incubated with 200 µM nitrite, 25 µM nitrite, or no nitrite at pH 6.8. In this experiment, only the 200 µM nitrite treatment was significantly stiffer than the control, compared to the preliminary experiments where 10 µM nitrite was statistically significantly stiffer than control (Figure 7 on page 26). However, in repeating this experiment exactly, the cells treated with 200 µM or 25 µM were both statistically stiffer than untreated cells (Figure 18 on page 33).

Now that the phenotype of increased deformability upon exposure to nitrite was confirmed at pH 6.8, the experiment was extended to include pH 7.4 conditions. This experiment would allow for a direct comparison of the effects of nitrite on infected red blood cells at varying pH conditions. After all, while the pH in the microvasculature may eventually lower to a value of 6.8, this would be a dynamic process, and confirming the deformability phenotype at different pH values could help assist in building a more complete model.

Five samples of infected red blood cells were used in this experiment: a zero nitrite control, and two samples containing the nitrite concentrations of 200 µM and 25 µM at each pH. Surprisingly, however, with this experiment, there was no difference in deformability between any of the samples (Figure 19 on page 33).

This experiment was repeated with only nitrite concentrations of 200 µM in order to increase the sample number measured. The deformability phenotype returned, yet only for cells in buffer at pH 7.4 (Figure 20 on page 34).

Notably, all experiments in this chapter were set up to have replicates on two sequential days using the same donor's blood in order to make biological replicates as similar to one another as possible. However, several variables made it difficult for these experiments to proceed fully without problems (parasitemia was not high enough, enrichment was poor, the parasites did not invade the blood very well, devices did not bond well, devices did not wash well, cells clogged devices too quickly, cells appeared dead after the enrichment and

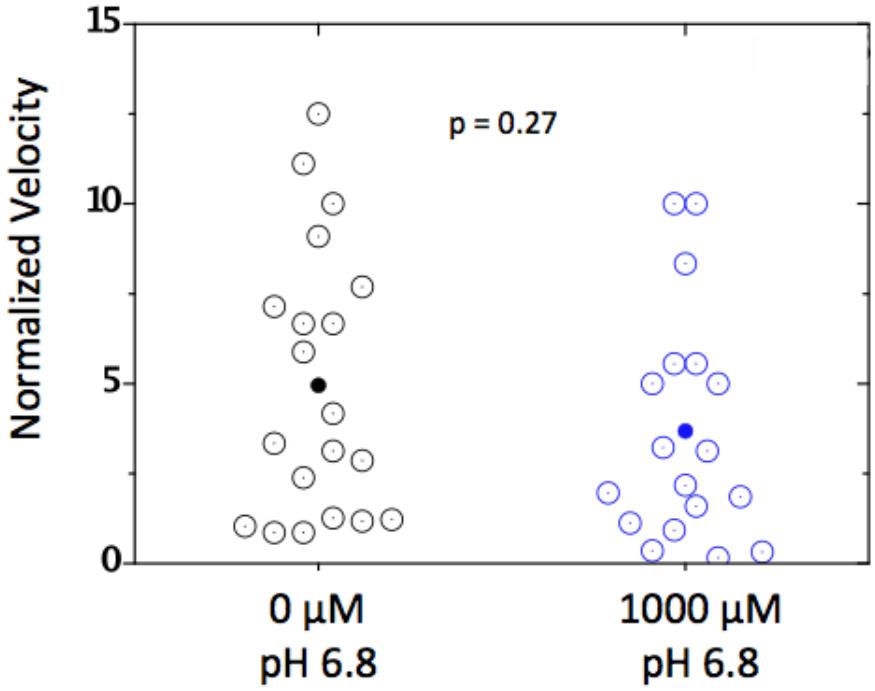

Figure 16: Infected red blood cells treated with nitrite had similar deformability scores to those cells without nitrite. Data generated by Sha Huang and Bridget Wall.

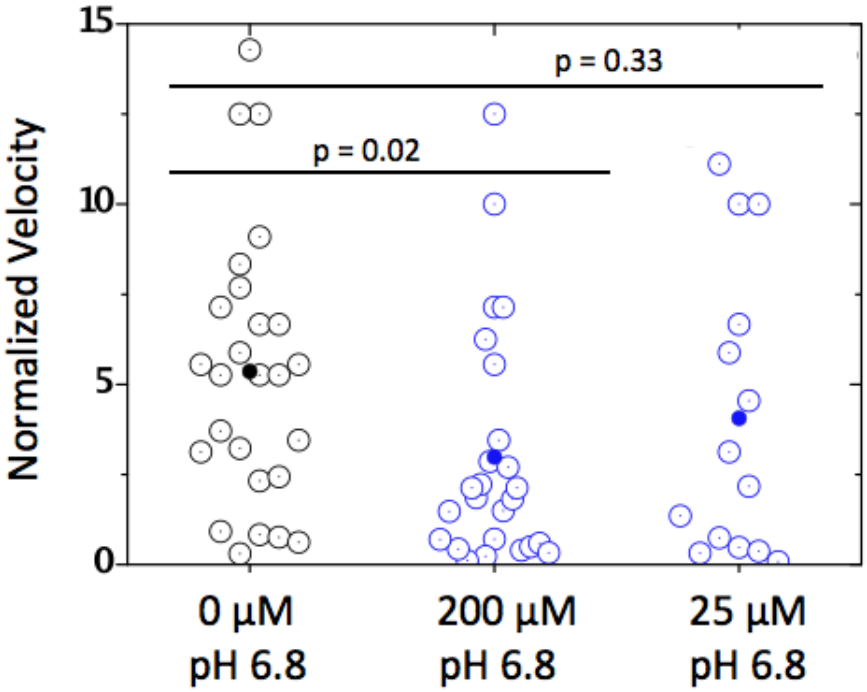

Figure 17: Infected red blood cells treated with 200 µM nitrite were statistically stiffer than the no nitrite control. Data generated by Sha Huang and Bridget Wall.

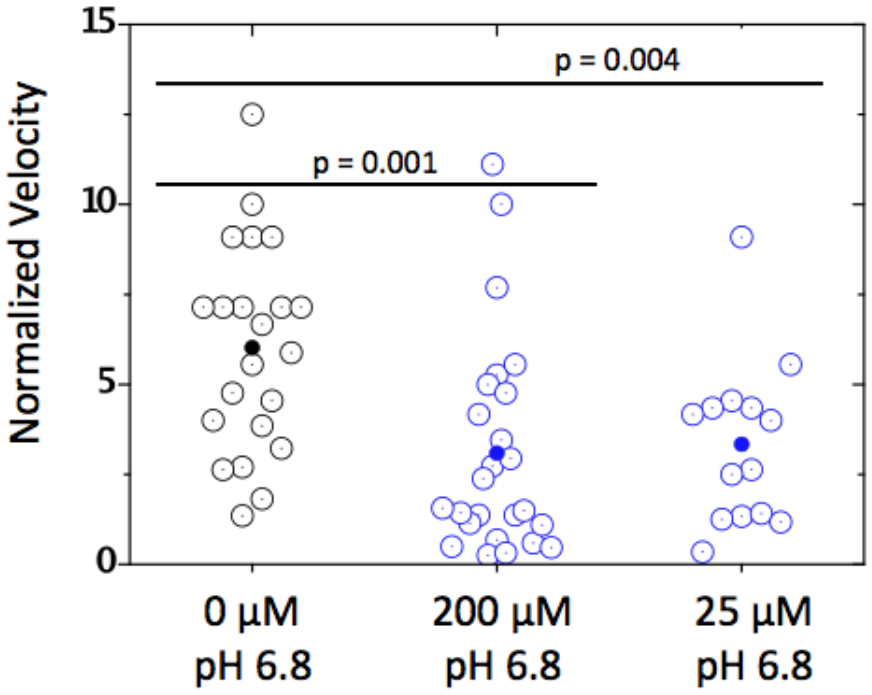

Figure 18: Infected red blood cells treated with 200 µM or 25 µM nitrite are significantly stiffer than the no nitrite control. Data generated by Sha Huang and Bridget Wall.

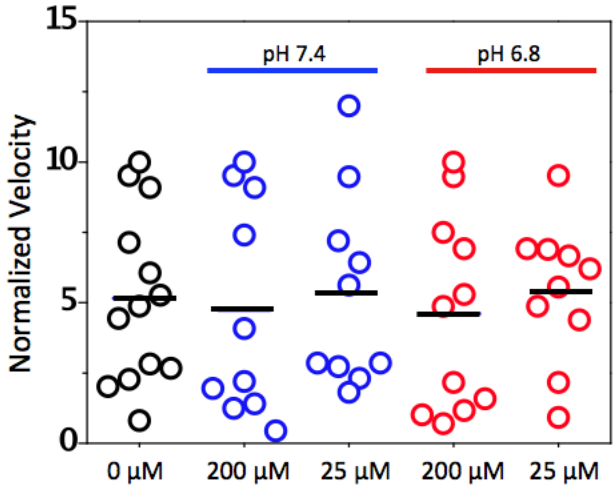

Figure 19: Infected red blood cells treated with 200 µM or 25 µM nitrite in pH conditions of 6.8 or 7.4 have the same deformability as the no nitrite control. Data generated by Sha Huang and Bridget Wall.

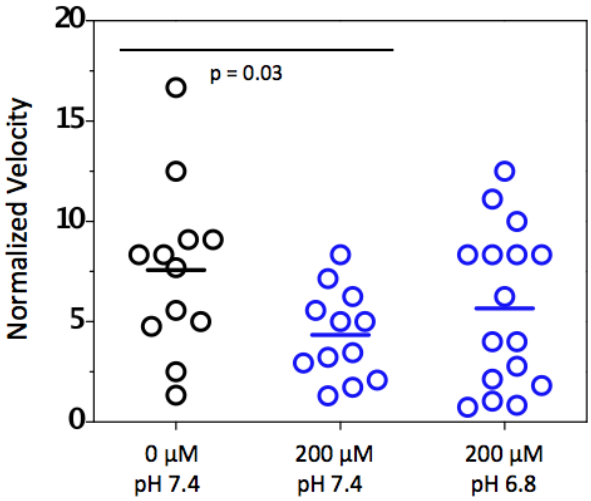

Figure 20: Infected red blood cells treated with 200 µM nitrite in pH conditions of 6.8 or 7.4 are stiffer than the no nitrite control, but the difference is stiffness is only significant for the cells in media at pH 7.4. Data generated by Sha Huang and Bridget Wall.

nitrite incubation process). However, in the following two experiments, these were both successful biological replicates on successive days.

Four sets of infected red blood cells were prepared containing zero and 200 µM nitrite at both pH 6.8 and pH 7.4. On both experimental days, both samples treated with nitrite were stiffer than their untreated controls (Figure 21 on page 35). However, there is a clear difference between experiment days as to the magnitude and range of cell deformability measurements. Sample size was also a problem; as seen in the graphs, there would sometimes be as few as three cells in a given treatment condition.

This exact experiment was repeated one week later. Nitrite treated cells in pH 6.8 buffer were stiffer than the untreated control, but between days, the treated cells in pH 7.4 buffer were either the same as the untreated control cells or stiffer (Figure 22 on page 35). Due to problems with devices, there were no cells in pH 6.8 buffer on the second day.

The clear conclusion of these experiments: the results were inconsistent. Overwhelmingly, in light of these results, defining the deformability phenotype became the top priority. Many technical challenges needed to be addressed in order to confirm the original data, thus, answering questions about mechanism of action and the biochemistry involved in the nitrite-dependent deformability phenotype would be a secondary priority.

2.4 Repeating Initial Experiments

Note: at this point, my collaborator Sha was graduating and leaving the country, leaving me as the sole scientist repeating these experiments. I worked with Sha and did several test runs, learning how to operate the microfluidic device and analyze the videos from the experiments to extract deformability measurements. I re-analyzed videos from a prior date and our results to be comparable (data not shown).

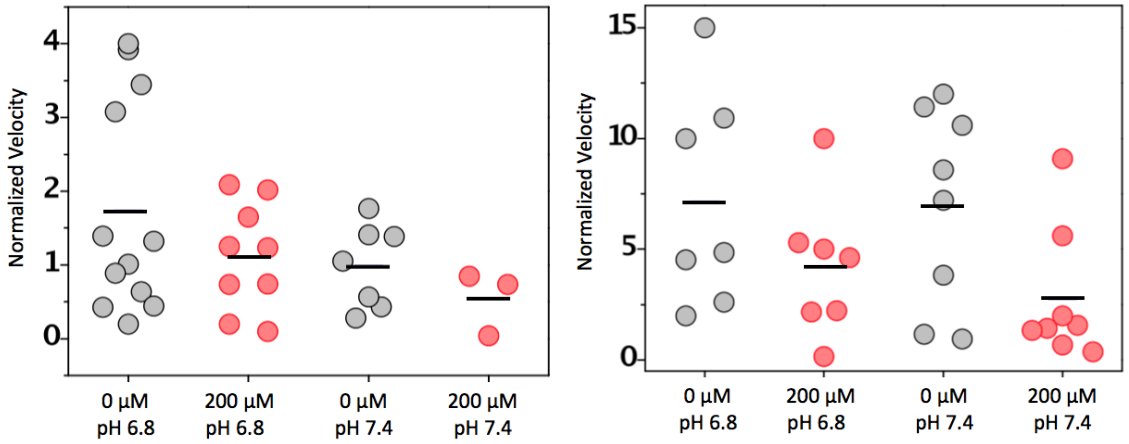

Figure 21: Deformability results from two sequential experiment days (9.27.13 and 9.28.13) using the same blood donor. Data generated by Sha Huang and Bridget Wall.

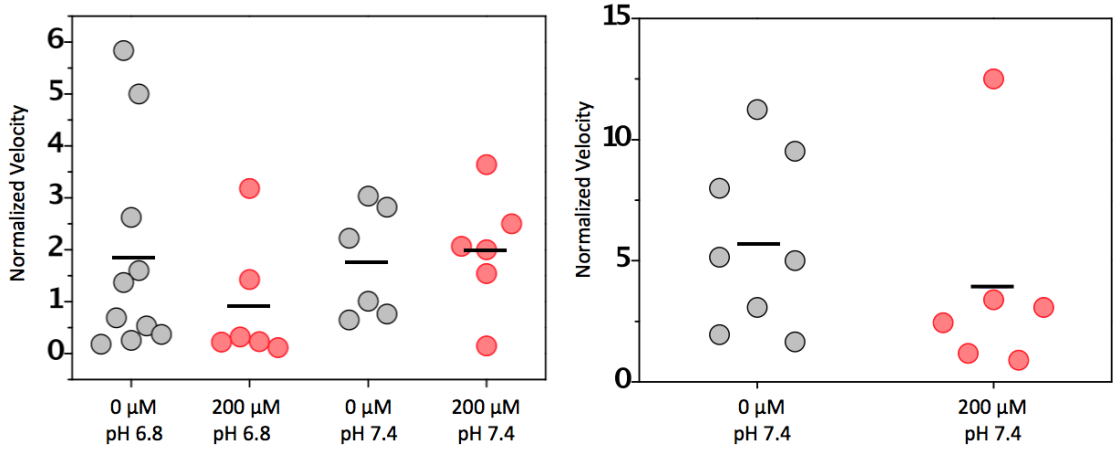

Figure 22: Deformability results from two sequential experiment days (10.1.13 and 10.2.13) using the same blood donor. Data generated by Sha Huang and Bridget Wall.

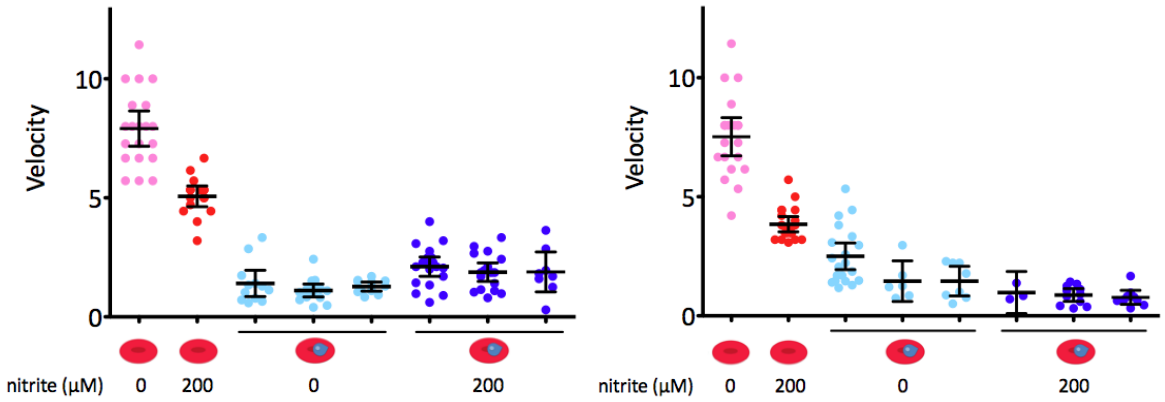

Figure 23: Deformability results from two sequential experimental days (6.25.14 and 6.26.14) using the blood from the same donor. The results on the left graph are from cells treated with 200 µM nitrite at pH 7.4. The results on the right graph are from cells treated with 200 µM nitrite at pH 6.8. Each separate grouping (column) of cells was measured in a separate microfluidic device. Data generated by Bridget Wall.

Prior to making conclusions about the deformability phenotype following nitrite treatment, it must be defined both reliably and reproducibly. This includes investigating every angle of the technical space, from buffer composition to inclusion of more controls, to device variation.

2.4.1 Addressing device variation and uninfected red blood cell treatments with samples at both pH 7.4 and pH 6.8

The first experiment included an uninfected red blood cell control that was treated with nitrite, and addressed device variation by running the same treated cells through multiple devices. These experiments were also done on sequential days using the blood from the same donor. This experiment contained four separate samples: uninfected red blood cells treated with 200 µM nitrite or a no nitrite control, and infected red blood cells treated with 200 µM nitrite or a no nitrite control. On day one, these four samples were incubated in buffer at pH 7.4, and on day two, these four samples were incubated in buffer at pH 6.8 (Figure 23 on page 36). In these graphs, each column represents the cells that go through a particular device. On the first day in buffer at pH 7.4, the untreated infected cells were stiffer than all of the uninfected cells, but also the treated infected cells, which was unexpected. On the second day in buffer at pH 6.8, the treated infected cells appear stiffest. On both days, the uninfected red blood cells are much stiffer following treatment with nitrite. This was especially concerning, given the original data that on uninfected red blood cells that showed no change between treated and untreated cells (Figure 3 on page 23, Figure 4 on page 24, Figure 5 on page 24).

2.4.2 Repeating pH 7.4 Experiments with a Modified Incubation Buffer

The next priority was to repeat this experiments at pH 7.4, including a 1000 µM nitrite treatment to reference back to the prior experiments. In addition, the nitrite incubation buffer was modified to have four times

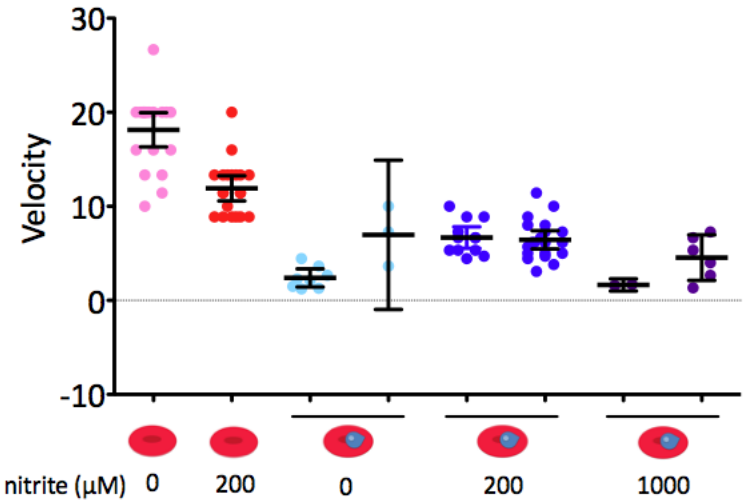

Figure 24: Deformability results from one experimental day (7.3.14). The prior day's experiment was voided due to problems with the microscope's computer. Each separate grouping (column) of cells was measured in a separate microfluidic device. Cells were run in pH 7.4 media that was nitrite free and had four times the buffering capacity (4X NF RPMI). Data generated by Bridget Wall.

the buffering capacity with the hypothesis that this would stabilize reaction conditions. This buffer will be referred to as 4X NF RPMI.

For this experiment, five different conditions were measured in 4X NF RPMI at pH 7.4: uninfected red blood cells treated with 200 µM nitrite or no nitrite controls, and infected red blood cells treated with 1000 µM nitrite, 200 µM nitrite, or no nitrite controls (Figure 24 on page 37). First, uninfected red blood cells treated with nitrite were stiffer than uninfected cells that were no nitrite controls. Second, there was a definite lack of consistency between cells measured in different devices but with the same nitrite treatment. Another issue of note is the challenge of low numbers of usable cells in a given device, a known technical challenge. However it does appear as if all infected red blood cells are stiffer than uninfected red blood cells.

2.4.3 Changing the incubation concentration to 2% hematocrit, and continuing use of the 4X NF RPMI buffer at pH 7.4

Next, in order to repeat the earliest deformability experiments, cells were incubated at 2% hematocrit instead of 0.01% in order to better mimic the high density conditions in the microvasculature.

Thus, nitrite incubations for the next set of experiments were done at 2% hematocrit in 4X NF RPMI buffer at pH 7.4, and washed and resuspended to the appropriate concentration for running on the microfluidic device prior to use. For this experiment, there were five separate conditions as before: two uninfected red blood cell conditions, one treated with 200 µM nitrite and one no nitrite control, and three infected red blood cell conditions, 1000 µM, 200 µM, and a no nitrite control.

First, unlike the most results from 6.25.14, 6.26.14 (Figure 23 on page 36), and 7.3.14 (Figure 24 on page 37), uninfected red blood cells that were not treated with nitrite were stiffer than those treated with nitrite

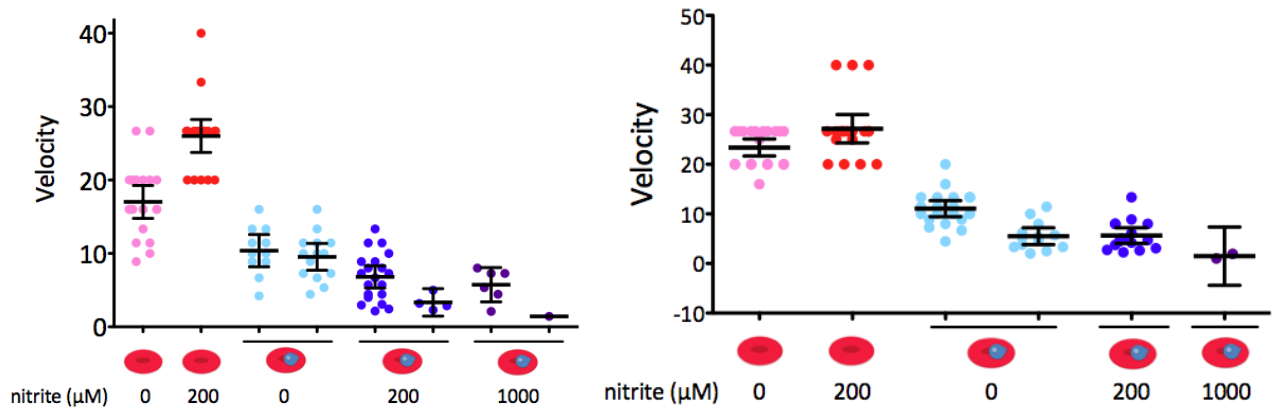

Figure 25: Deformability results from two sequential experimental days (7.9.14 and 7.10.14) using the blood from the same donor. Each separate grouping (column) of cells was measured in a separate microfluidic device. On 7.10.14, there was a problem with the flow rate in three of the infected red blood cell samples (the second untreated sample, and both the 200 µM and 1000 µM sample). Data generated by Bridget Wall.

(Figure 25 on page 38). Given the very clear previous results concluding the deformability of uninfected red blood cells was not affected by nitrite treatment, this began to call into question our basic assumptions about this system, and how to proceed with experiments and statistical analysis of said experiments. On 7.9.14, the uninfected cells that are not treated with nitrite are stiffer than those untreated, and on 7.10.14, they are also stiffer, but to a lesser degree. With this donor's blood, the phenotype seemed to be consistent between the two days; uninfected untreated cells were stiffer than uninfected treated cells; all infected red blood cells are stiffer than uninfected red blood cells, and the greater the nitrite concentration, the stiffer the cells are. However, there continued to be a disparity between the deformability of cells with the same nitrite treatment being measured in different devices. For example, the infected red blood cells treated with 200 µM nitrite on 7.9.14 had two very different mean velocities, but given the fact that there were only four cell measurements in the second device, it's difficult to make any conclusions about whether this is significant. However, in the case of the untreated infected red blood cells on 7.10.14, they each have over 10 cells and a tight distribution of velocities, but different mean velocities. Additionally, on 7.10.14, there was an issue with flow rate in the device. While there is no way to measure flow rate using this gravity-based method, a cursory check between every device when moving the inlet tubing showed a large difference to the expected rate of liquid moving from the syringe through the tubing.

These experiments were repeated with the same conditions the next week, and again there was a difference in the deformability of uninfected red blood cells (Figure 26 on page 39). On 7.16.14, treated uninfected cells were stiffer than untreated red blood cells, but on 7.17.14, the red blood cells had approximately the same stiffness. All infected red blood cells were stiffer than uninfected blood cells, but cells from the same treatment in different devices continued to have different deformability measurements. There was a weak trend among infected red blood cells; the more nitrite, the stiffer they were.

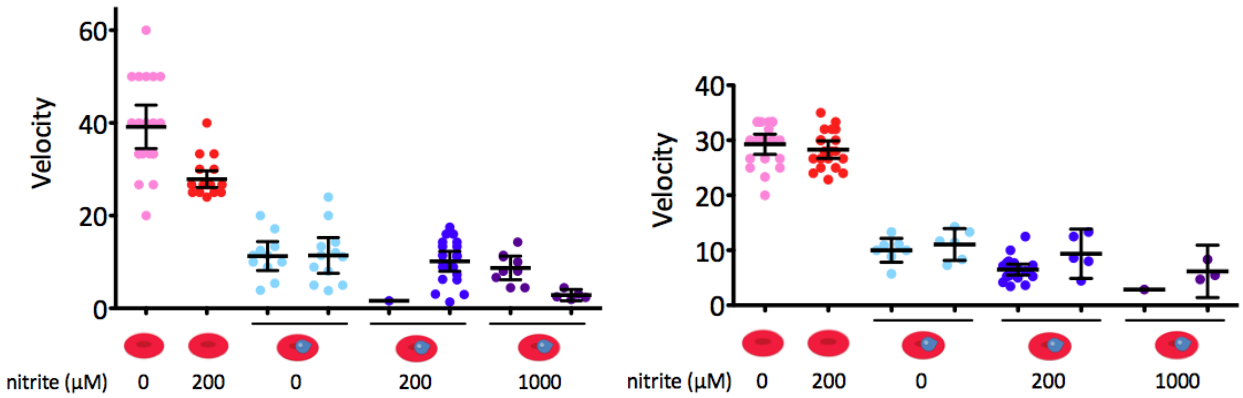

Figure 26: Deformability results from two sequential experimental days (7.16.14 and 7.17.14) using the blood from the same donor. Each separate grouping (column) of cells was measured in a separate microfluidic device. Data generated by Bridget Wall.

2.4.4 Using an orbital shaker for equal distribution of nitrite, and examining time as a variable while maintaining 2% hematocrit, 4X NF RPMI, and pH 7.4 conditions

In designing the next experiment, the entire flow of the experiment was re-examined. One prior variable left unaddressed until now was the issue of cell settling. As cells settle if kept static for one hour, it was decided to incubate cells on an orbital shaker during the incubation in order to keep them suspended and exposed to similar amounts of nitrite. Another variable was the time at which samples were actually measured going through the device. The time limit of two hours post washing after the nitrite incubation had been followed, but examining whether the time affected deformability had not been attempted.

For this particular experiment, each uninfected red blood cell condition was tested once and each infected red blood cell condition was tested twice. This was done twice, denoted "early" and "late" in the below graphs. These experiments retained the five conditions similar to the recent experiments.

First, the samples were graphed on separate graphs, early and late (Figure 27 on page 40). Uninfected red blood cells treated with nitrite were stiffer than uninfected red blood cell controls in both early and late cases, but for the later time points, this stiffness appeared to be on par with the stiffness of the infected red blood cells. Both time points had a lack of consistency between the same sample run through different devices.

Second, to show the range of deformabilities in each separate device, all of the early and late devices were graphed on a single graph (Figure 28 on page 41). On this graph, the differences in deformability for cells treated the same way is particularly evident, yet it doesn't seem to be time-dependent.

Third, the results were batched in two different ways in an attempt to further clarify time dependence as a cause of deformability changes (Figure 29 on page 41). For the left graph, all of the samples from each replicate are batched together (eg, both the early and late uninfected and untreated cells are together, as are the early and late results from the first replicate of the untreated infected red blood cells). For the right

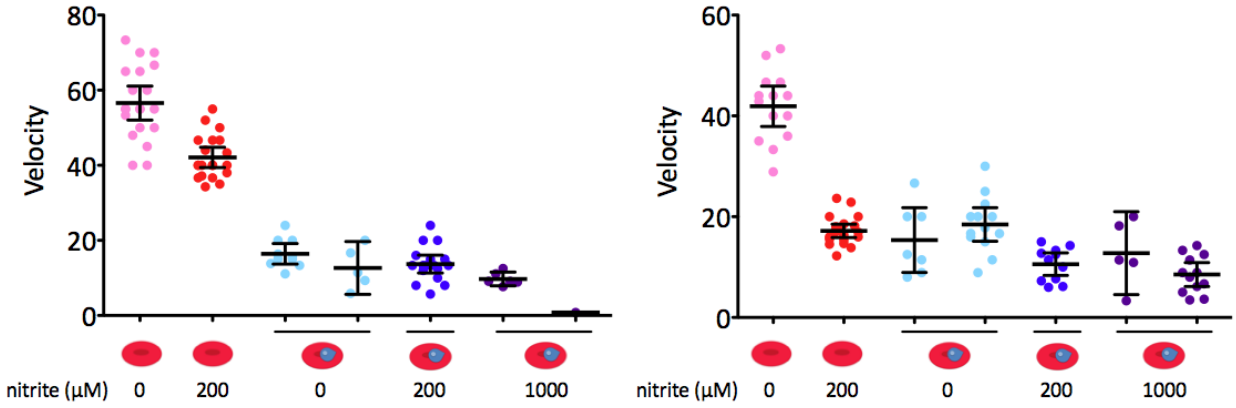

Figure 27: Deformability results from a single day (7.23.14). Each separate grouping (column) of cells was measured in a separate microfluidic device. The graph on the left shows the samples from the early set of devices, and the graph on the right shows the samples from the late set of devices. Data generated by Bridget Wall.

graph, the early and late results are batched together (eg, since there was only replicate of uninfected red blood cells, they were plotted, alone, but both early replicates for the untreated infected cells were batched together). Notice in particular the bi-modal distribution of treated uninfected red blood cells in the left graph.

This experiment was repeated on the next day, and all analysis methods were repeated (Figure 30 on page 42). Similar to the experiments on 7.23.14, there is a great deal of variance between the early and late time point as well as between samples. This is especially evident in the graph displaying all microfluidic devices run on that day (Figure 31 on page 42). When comparing the batched results, there is no discernible trend between early and late time points (Figure 32 on page 43).

What is completely clear from these results is that the inter-device variation is by far the most significant contributor to the inconsistencies and lack of reproducibility in the data, far more than the time elapsed following nitrite treatment.

2.4.5 Using "contaminating" uninfected red blood cells as an in-device control while using an orbital shaker for equal distribution of nitrite, and examining time as a variable while maintaining 2% hematocrit, 4X NF RPMI, and pH 7.4 conditions

For the next experiment, addressing the inter-device variation by adding in a control for each individual device was deemed appropriate. Even though parasite cultures are enriched to a high parasitemia, some number of uninfected red blood cells remain in the mixture as "contaminants." They are easily distinguishable when analyzing the infected red blood cells as they look quite different from infected red blood cells both in terms of contents and speed. Even if there is a change between the deformability of the uninfected red blood

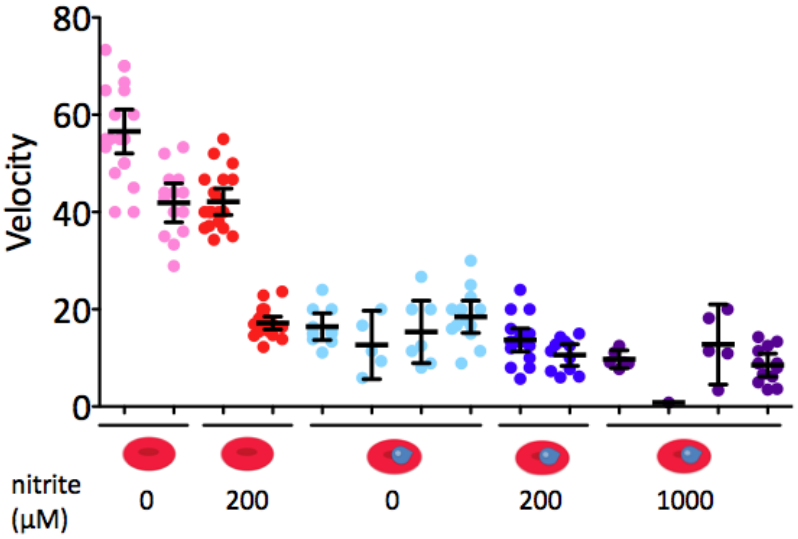

Figure 28: Deformability results from a single day, all plotted on one graph (7.23.14). Each separate grouping (column) of cells was measured in a separate microfluidic device. The early result is shown first, followed by the later result. For the 200 µM nitrite condition, the replicate did not contain usable cells in either time point, so what is shown is the only data available, one early column, and one late column. Data generated by Bridget Wall.

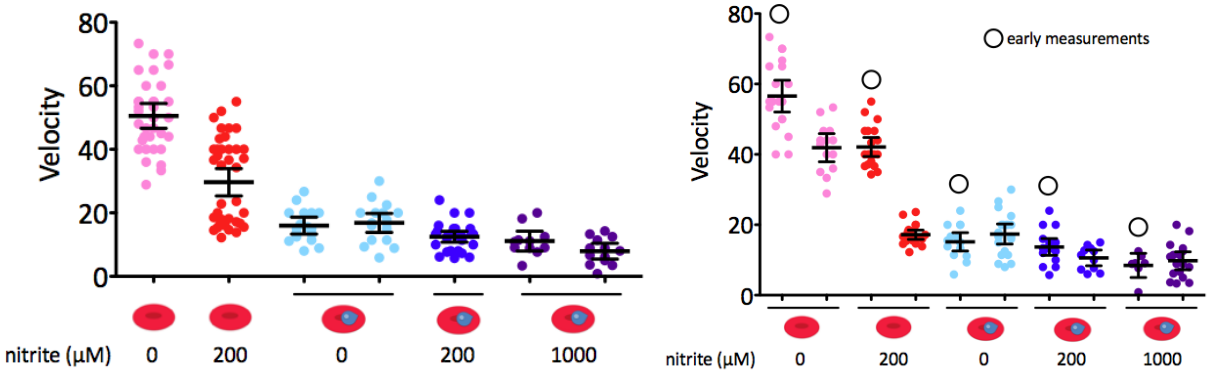

Figure 29: Deformability results from a single day, batched in two different ways. For the left graph, all of the samples from each replicate are batched together (eg, both the early and late uninfected and untreated cells are together, as are the early and late results from the first replicate of the untreated infected red blood cells). For the right graph, the early and late results are batched together (eg, since there was only one replicate of uninfected red blood cells, they were plotted alone, but both early replicates for the untreated infected cells were batched together). Data generated by Bridget Wall.

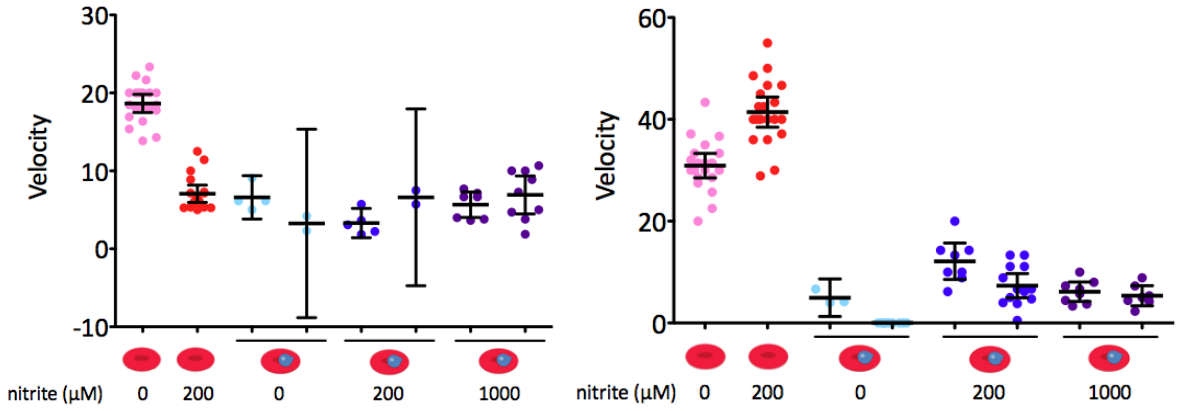

Figure 30: Deformability results from a single day (7.23.14). Each separate grouping (column) of cells was measured in a separate microfluidic device. The graph on the left shows the samples from the early set of devices, and the graph on the right shows the samples from the late set of devices. Data generated by Bridget Wall.

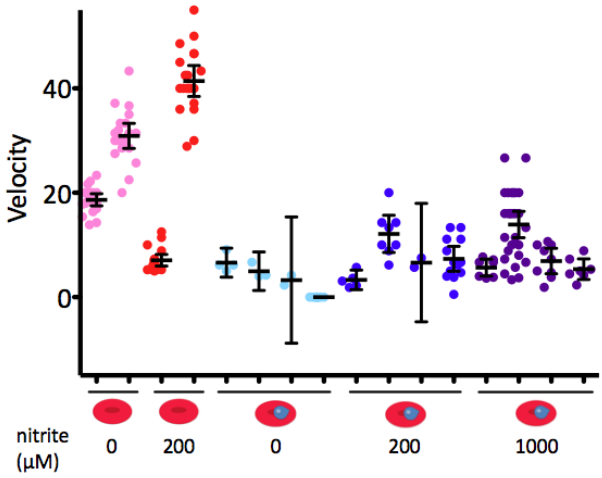

Figure 31: Deformability results from a single day, all plotted on one graph (7.24.14). Each separate grouping (column) of cells was measured in a separate microfluidic device. The early result is shown first, followed by the later result. Data generated by Bridget Wall.

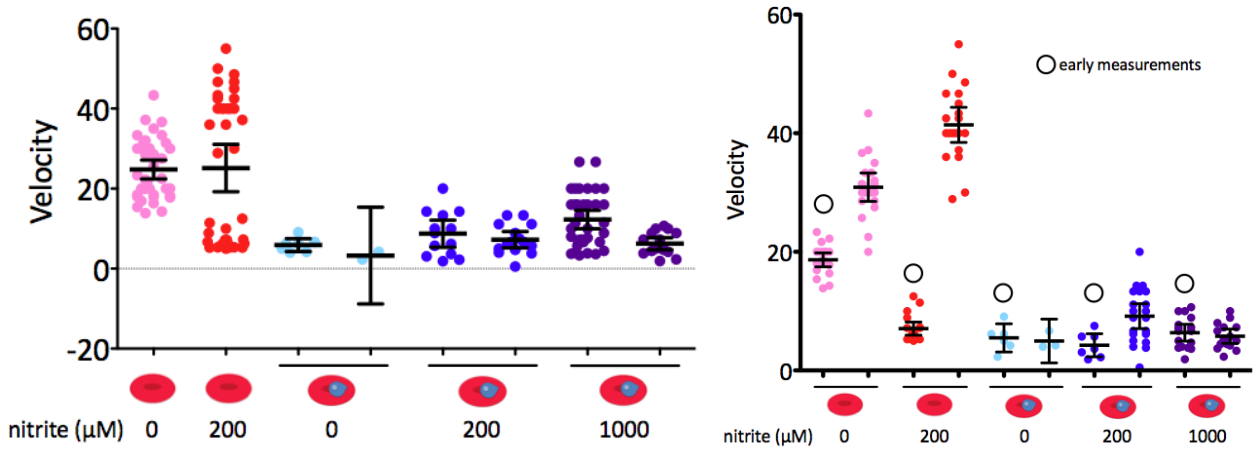

Figure 32: Deformability results from a single day, batched in two different ways. For the left graph, all of the samples from each biological replicate are batched together (eg, both the early and late uninfected and untreated cells are together, as are the early and late results from the first replicate of the untreated infected red blood cells). For the right graph, the early and late results are batched together (eg, since there was only one replicate of uninfected red blood cells, they were plotted alone, but both early replicates for the untreated infected cells were batched together). Data generated by Bridget Wall.

cells when treated with nitrite, if they are present in the mixture during treatment, they would experience the same exposure to nitrite as the infected red blood cells. Therefore, in order to have enough of these uninfected red blood cell contaminants, the wash step will be cut back to one column volume (6 mL instead of 12 mL) in hopes of increasing the uninfected red blood cell concentration to a level at which they could be used as a normalization factor to compare between different devices. This lack of ability to compare between devices is the main force behind the lack of statistical analysis of this work as a whole; plainly put, the results are not comparable at this juncture.

The experiments above with five separate conditions were repeated, this time with a less stringent wash step to allow for a greater contamination of uninfected red blood cells (Figure 33 on page 44). However, despite such efforts, the number of usable uninfected red blood cells in each device was too small for the mean deformability to be used as a normalization value ($n < 5$). Yet, even without such data, the graphs again speak to the variance of deformabilities seen across different devices. Uninfected cells behave differently on either day, and the infected red blood cell deformabilities were also quite variable.

Sha Huang was consulted to see if there were any particularly intra-device variations we could account for, and the unfortunate answer was no. Device manufacture and flow rate seem to be variables for which there is not much control. However, she did suggest using a smaller sized device for our uninfected red blood cell samples. This device would force the uninfected red blood cells to deform, rather than slide through the larger device on their sides. in addition, reducing the wash volume from 6 mL to 4 mL could assist in the normalization scheme.

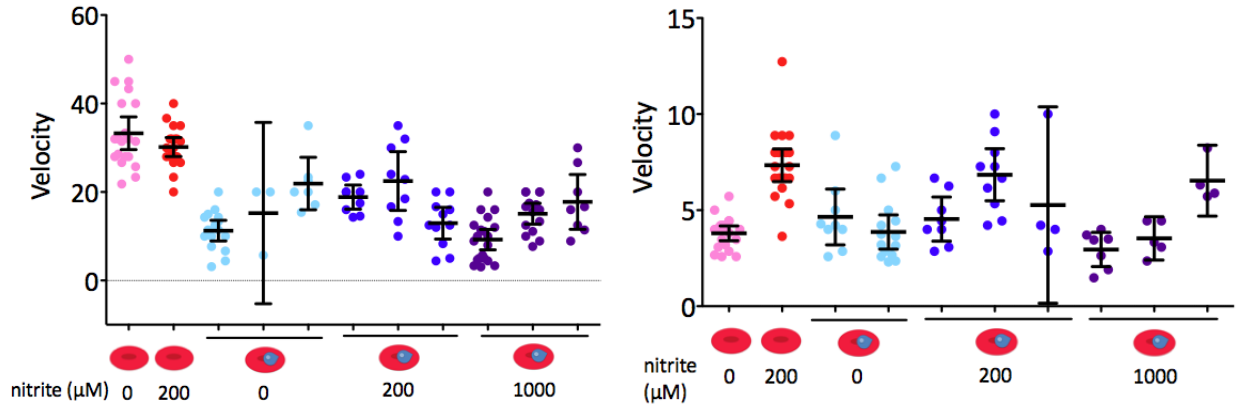

Figure 33: Deformability results from a two sequential experiments (8.21.14 and 8.22.14), using the same blood donor. Each separate grouping (column) of cells was measured in a separate microfluidic device. Data generated by Bridget Wall.

2.4.6 Using a smaller device for uninfected red blood cells, while maintaining the use of "contaminating" uninfected red blood cells as an in-device control while using an orbital shaker for equal distribution of nitrite, and examining time as a variable with incubation conditions of 2% hematocrit, 4X NF RPMI, and pH 7.4 conditions

The experiment was repeated as previously described with five conditions, but the wash volume to 4 mL and utilizing a smaller device for uninfected red blood cells (Figure 34 on page 45). The trend of inconsistency continued on these two experimental days. The contaminating red blood cell "n" was also too small for the mean velocity to be used as a normalization value.

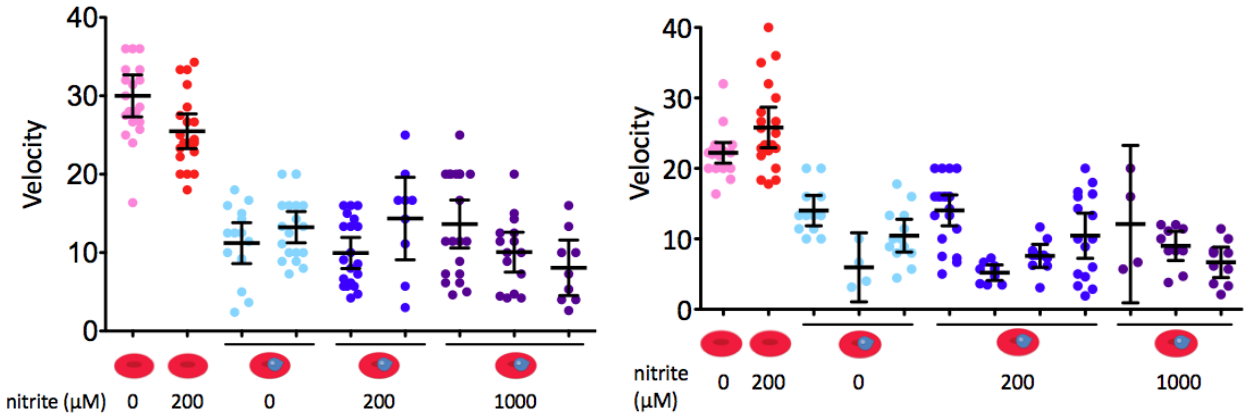

Figure 34: Deformability results from a two sequential experiments (8.28.14 and 8.29.14), using the same blood donor. Each separate grouping (column) of cells was measured in a separate microfluidic device. Uninfected red blood cells were measured using a smaller, 4.2 µM device. Infected red blood cells were measured using a larger, 5.3 µM device. Data generated by Bridget Wall.

2.5 Discussion

After thoroughly investigating the deformability phenotype following nitrite treatment, it became clear that this particular multivariate problem too challenging to address directly. Both technical challenges and the complicated nature of biology contribute to these challenges.

2.5.1 Technical Challenges

Microfluidic flow cytometry was the tool of choice for this experiment because it reflects the capability of individual cells to deform as a whole rather than more isolated tools that don't account for the entirety of the system [44]. However, this does not mean that this experimental setup is without challenges. The results of these experiments were inconsistent and lacked reproducibility, resulting in a great deal of troubleshooting both in technical hardware space and analysis techniques. Much progress was made in isolating potential sources of variability, with device variation and flow rate as likely culprits.

2.5.2 Biological Challenges

It is also possible that the results are an artifact of true biology, in addition to the technical challenges in this space. Sha's thesis work confirms the variability of red blood cell deformability based on blood donor. And indeed, many studies of red blood cell storage demonstrate the variability inherent to these human samples [105, 106, 107, 108, 109, 110, 111, 112, 113, 114]. As such, it is important to realize that this variability could be compromising the ability of our system to measure a "real" effect. Perhaps the effect being measured is indeed "real" but differs for different blood donors and is therefore a significant component of malaria pathophysiology, and one that is dependent on characteristics and biology of the host.

2.5.3 Next Steps

To move forward in such a challenging space requires resolving the uncertainty surrounding our main deformability assay using the microfluidic device. This would require measuring flow rate into the device as well as developing a methodology to account for device variations. The use of uninfected red blood cells as a control is potentially a possibility, but there are still differences in uninfected cell deformability that could obscure our results. Even better would be a non-deforming and inert entity that could act as a control in either setting.

Following resolution of the technical challenges, learning more about the basics of nitric oxide treatment on uninfected red blood cells as well as their variability in deformability in this type of experiment would be prudent. Such experiments could examine the results of applications of different chemicals or cytokines, and broaden our understanding of the dynamics of membrane fluctuation in the red blood cell Additionally, these experiments could be designed to address questions about the potential dynamic response to these molecules. Finally, defined donors with specific diseases or conditions could be sought out to determine additional characteristics of red blood cell membrane deformability.

Once these are elucidated, returning to investigating the infected red blood cell phenotype would be possible. Once the phenotype of nitric oxide-induced deformability was defined, the mechanisms behind this phenotype could be explored.

2.6 Methods

2.6.1 Materials

- Miltenyi Biotech
  - MACS LD columns
- US Biological
  - RPMI 1640 Medium w/o L-Glutamine (Calcium Free)
- Gibco Life Technologies
  - Albumax II
  - 1X PBS, pH 7.4
- Goldbio
  - Gentamicin
- Nordsen
  - Precision Tips for Engineered Fluid Dispensing (23 GA, 0.13x0.25; orange)
- Sigma
  - All remaining chemicals

2.6.2 Culturing *Plasmodium falciparum*

The 3D7 strain of *P. falciparum* was cultured in leukocyte-free human RBCs (stored in acid-citrate-dextrose anticoagulant; from Research Blood Components, Brighton, MA) under an atmosphere of 5% O_2, 5% CO_2, and 95% N_2 at 2% hematocrit as previous described [115]. Parasites were synchronized weekly at a consistent time with 5% sorbitol (w/v) as previously reported [116] to ensure schizont-stage parasites prior to all experiments.

Nitrate Free RPMI Media

- RPMI 1640 Medium w/o L-Glutamine and Calcium Free (10.04 g/L)
- Hypoxanthine (30 mg/L)
- 25 mM HEPES-KOH (7.0825 g HEPES/L)
- Gentamicin (50 mg/L)

- Albumax II (5 g/L)
- Glutamine (150 mg/L)
- $CaCl_2$ (47 mg/L)
- Sodium bicarbonate (2 g/L)

Nitrate Free RPMI Media (4X buffering capacity)

- RPMI 1640 Medium w/o L-Glutamine and Calcium Free (10.04 g/L)
- Hypoxanthine (30 mg/L)
- 100 mM HEPES-KOH buffer (23.88 g HEPES/L)
- Gentamicin (50 mg/L)
- Albumax II (5 g/L)
- Glutamine (150 mg/L)
- $CaCl_2$ (47 mg/L)
- Sodium bicarbonate (2 g/L)

2.6.3 Enrichment of iRBCs Using MACS Separation

Enrichment of late trophozoite and schizont iRBCs was accomplished using MACS LD magnetic columns with minor changes to the published protocol [117]. During the process of heme detoxification, the iron in heme becomes paramagnetic, a characteristic that means infected red blood cells stick to magnets. An LD column was washed with 6 mL of pre-warmed nitrate free RPMI media. Following this wash step, 6 mL of parasitized culture was loaded on to the column and allowed to flow through using gravity. This 6 mL of culture was concentrated from a 30-40 mL culture at 2% HCT and 8-12% parasitemia. The flow through from the column was discarded, and the column was washed with additional pre-warmed nitrate free RPMI. This step increased stringency and enrichment parasitemia. Volumes for this washing step varied; the default volume was 6 mL. However, in some experiments, 4 mL was used to create a population of cells with a lower parasitemia and higher concentration of uninfected RBCs. In other experiments, 12 mL (two column volumes) was added to increase the enrichment parasitemia to an even higher yield. Following this wash step, the column was removed from the magnet, and infected cells retained on the column were eluted in 1 mL nitrate free RPMI to yield an enriched culture of 85-99% parasitemia. Pre- and post-enrichment parasitemias were determined using Giemsa-stained blood smears visualized using 100X oil immersion microscopy. Cells were resuspended to the desired hematocrit and used immediately. If there were any delays, cells were kept in a suspended mixture in a 37^{o}C incubator.

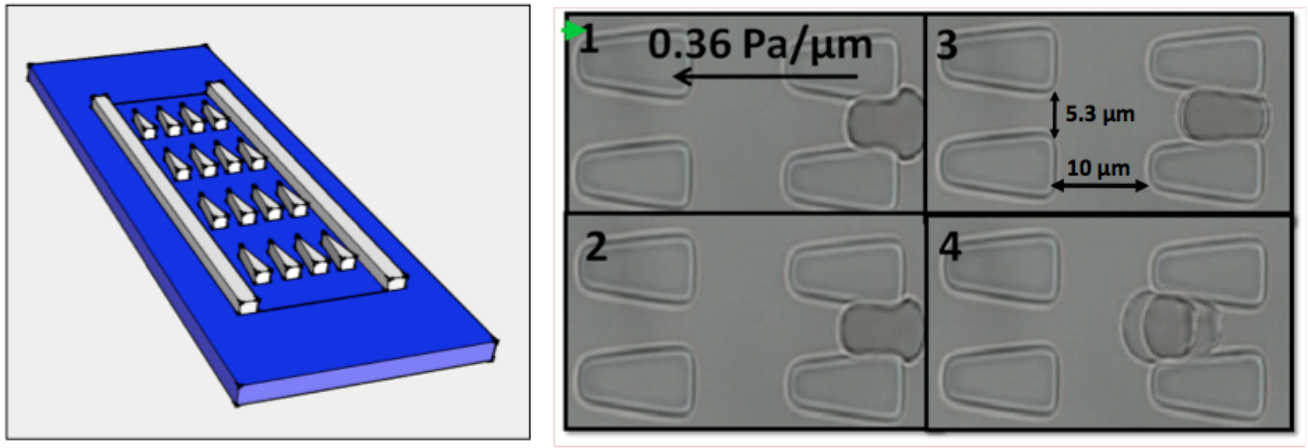

Figure 35: A schematic of the microfluidic device in 3D, as well as from above. Note that for these experiments, the hexagonal pillars were used for analysis, as seen in Figure 36 on page 50.

2.6.4 Nitrite and Other Chemical Exposures

In order to provide a proper matched control that minimizes differences due to culturing conditions or the age of human blood, uninfected red blood cells were sham cultured in nitrate free RPMI media identically to the infected red blood cells. Uninfected red blood cells were also kept at room temperature during the enrichment process, though they were not sent over a MACS column. Identical volumes of infected RBCs and uninfected RBCs were brought up to 0.1%, 2% or 10% hematocrit as required by individual experiments. Experiments were run in nitrate free RPMI media with 100 mM HEPES (4X NF RPMI) or with the regular 25 mM HEPES in the culture media (NF RPMI). The 4X NF RPMI was used to prevent acidification of the RPMI by the enriched cell suspensions at high hematocrit. NOA uptake experiments were run at 10% hematocrit with all other conditions being identical. For nitrite exposures, nitrite was brought up in degassed NF RPMI or 4X NF RPMI and then applied to parasite pellets in the appropriate volume to result in a 2% or 10% hematocrit solution. All cells were washed and resuspended in a nitrate free media prior to analysis.

2.6.5 Microfluidic Flow Cytometry Deformability Assay

Microfluidic-based deformability experiments were performed using a pillar array structure as previously reported [104]. Hexagon-shaped pillars were used to achieve optimal experimental results (Figure 35 on page 49).

For experiments comparing uRBC deformability only, an inter-pillar gap size of 3.0 µm and a channel depth of 4.2 µm were used to ensure that uRBCs experience sufficient deformation when traveling through the microchannels. For experiments measuring the deformability of schizont-stage iRBCs, a different gap size of 4.0 µm with a channel depth of 5.3 µM to minimize channel clogging. For some experiments, uRBCs were run with 5.3 µM devices. All experiments were performed at room temperature.

To prepare devices, they were first washed from right to left with 1% BSA in PBS (pH 7.4). A needle attached to a 2 cm length of tygon tubing was screwed into a 10 mL syringe and filled with buffer; the tygon tubing

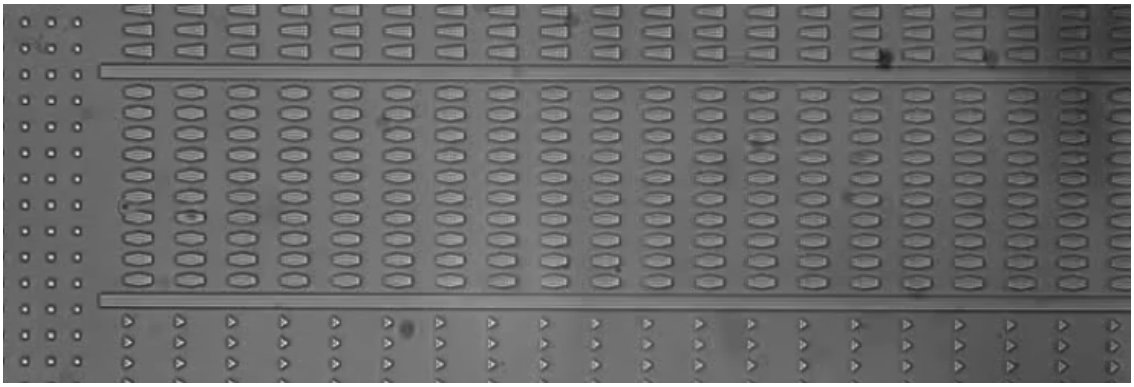

Figure 36: Screenshot of video taken of channels. Note the infected red blood cell entering the channel.

was inserted into the micro-well on the right side of the device and the syringe was depressed slowly. The washing of the device was carefully monitored to ensure all rows of the device were being filled with buffer, and that there was a clear path from the rows of the device to the left micro-well. If they weren't adequately filled, the fluid dynamics inside the device would change, skewing the deformability values. Thus, any devices that didn't meet this criteria were discarded at this point. Washed devices were used immediately or within one hour of washing.

Synchronized and enriched iRBCs and uRBCs were pelleted and resuspended to 0.1% hematocrit and injected using a gel loading pipette tip into the micro-well on the left side of the device. Another needle was attached to a length of tygon tubing, though this time it was approximately 20 cm long. This needle was screwed into a 60 mL syringe, which was mounted in a clamp on a ring stand so that the base of the syringe barrel was 20 cm above the microscope stage during the experiment. The clamp was then lowered to the level of the stage. Approximately 5 mL of 1X BSA in PBS (pH 7.4) was added to the syringe, and allowed to drip through the tygon tubing (the plunger of the syringe was not re-inserted). The tubing was attached to the left micro-well, and the microscope was focused and prepared for video analysis. Once everything was ready, the clamp was re-placed at 20 cm above the microscope stage, beginning the constant gravity-induced pressure gradient across the device. Under the inverted microscope (Olympus IX 71 with phase contrast attachment), infected RBCs were distinguished from contaminating uninfected red blood cells by the presence of black dots inside RBCs (hemozoin crystals within the food vacuole of the parasite). The movement of cells was captured by a CCD camera (Hamamatsu Photonics, C4742-80-12AG, Japan) and images were acquired using IPLab (Scanalytics, Rockville, MD).

The free software imageJ (NIH) was used to process all the images (Figure 36 on page 50). Transit velocity of individual cells was defined as the distance travelled per unit time, and utilized as the proxy for deformability. Cells were all analyzed by eye, and each cell had to be carefully tracked to insure proper identity of an analyzable cell. Cells are classified into four different groups, and individually tracked over the length of the device as seen through the video to ensure correct phenotype classification (Figure 37 on page 51). Both absolute value and proportions of the cells in these groups vary between devices, conditions, and experimental days.

1. Confirmed infected RBC (black dots of the infected red blood cells are surrounded by a red blood cell membrane, no strange morphology)

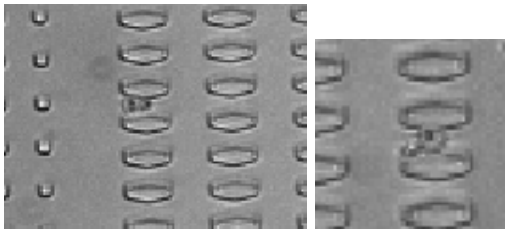

Figure 37: A cell that usable data could be taken from is on the left, and an iRBC with a "tail" that cannot be used for taking usable data is on the right.

2. Confirmed uninfected RBC (moves quickly through the device; possesses a uniform concave appearance)
3. Unusable iRBC (presence of a "tail," strange morphological shape, lack of RBC membrane)
4. Unidentified cell (could be a red blood cell ghost, random membrane, or a cell where identity cannot be confirmed)

Additionally, cells must be within the pillar array, and not between the pillar array and the sides of the device. If more than five lanes are clogged, this also interferes with the fluid dynamics and invalidates the velocities of any cells past that point. Any given confirmed cell must move at least three pillars prior to being clogged for the velocity to be included in analysis. Clogging rates were also calculated for each device based on when they entered, and are classified into three groups.

1. Not Clogged (cell does not clog in the 100 frames after entering the device)
2. Mixed (cell stays clogged for some amount of time in the 100 frames following entrance into the device)
3. Clogged (cell stays clogged in the entrance of the device for 100 frames)

Cells are viable for two hours following nitrite treatment.

2.6.6 NOA Chemiluminescence Assays

Nitrite and nitrate quantification was done using a Nitric Oxide Analyzer model 280i (NOA, Sievers-GE Analytical Instruments) according to the manufacturer's protocol. Argon was bubbled through a purge vessel containing potassium iodide (KI, 50 mg) in glacial acetic acid (6 - 8 mL) and the nitrite-derived NO was quantified by chemiluminescence. A population of uninfected red blood cells and infected red blood cells at 10% hematocrit were exposed to 200 µM $NaNO_2$, and measurements were taken using the NOA at 2 minutes and 60 minutes.

2.6.7 Coulter Counter quantification of cell size distribution

A 60 µL aliquot of infected red blood cells at 1% hematocrit in nitrate free media was mixed with 240 µL sorbitol solution to a final sorbitol concentration of 2.5%, 0.64%, 0.32%, and 0%. These samples have a final

concentration of 0.2% hematocrit, an appropriate concentration for analysis on both the coulter counter and using the microfluidic device. Cells were incubated at 37^{o}C for 30 minutes. The diameter of infected red blood cells was quantified using a Coulter Counter (Beckman Coulter, Fullterton, CA). Infected RBCs were diluted with ISOTON II diluent to a final cell count close to 1 million. An aperture of 100 µm was used and the upper and lower target diameters were set to be 12.4 µm and 2.8 µm, respectively. Cell size was presented in the form of "effective diameter," assuming the cells are spherical in shape.

2.6.8 Statistics

P values were calculated using Prism Software (Graphpad Softward, California). All p values are the result of paired two-tailed T-tests.

3 Complete toolkit for functional genetics in the parasite *Plasmodium falciparum*

This particular project builds on a great deal of work done by other lab members:

- Stephen Goldfless and Brian Belmont developed and refined the TetR aptamer system.
- Jeffrey Wagner developed a functional CRISPR system for use in the parasite.
- Sebastian Nasamu designed and cloned the vectors utilized in the toolkit.

3.1 Introduction

There is a great need for additional tools to study the basic biology of the malaria parasite to learn more about preventing and treating the disease. In 2011, the Malaria Eradication Research Agenda (malERA) convened in Boston to discuss the major gaps in the basic science that should be addressed in order to have an impact on malaria eradication. Five main recommendations were proposed, and one was improving genetic technologies to manipulate the parasite genome [118].

First, it is important to understand some of the parasite's inherent biology that has complicated this challenge for many years.

- There are three genomes in the parasite: the 14-chromosome genome found in the nucleus, the 6 kb genome found in the mitochondria, and the 35 kb genome found in the apicoplast [9].
- The genome is 80% AT, and 90% AT in non-coding regions [9].
- In 2002, when the genome sequence of the 3D7 strain was first published, 60% of the genes were classified as having no known homology to any other known gene [9]. Today, the number remains at approximately 50% [119].
- Transfection of the parasite requires the crossing of many membranes and spaces (red blood cell membrane, red blood cell cytosol, red blood cell membrane (parasitophorous vacuole) vacuolar space, parasite membrane, parasite cytosol, nuclear membrane). As such, even with DNA concentrations of 50-100 µg, the number of successful transfection events is so low that it takes 4-6 weeks to bring up a population of parasites containing the desired genetic material. While new methods such as chemical induction [10] and lipid nanoparticle conjugation [12] have been shown to be effective, electroporation remains the standard method of choice. However, advances continue to be made in refining traditional electroporation, such as electroporation of uninfected cells to preload them with DNA and using them as the uninfected red blood cell donors for invading merozoites [11].
- Transfection of malaria parasites remains time and resource intensive, from the cost of reagents to the time it takes to manage flasks. Parasites are cultured in liquid, and must be attended to every single day. Blood must be added every other day.
- There are only four viable resistance genes and drug combinations, and they have variable effectiveness in certain pairings which makes it difficult to design multiple plasmids for concurrent use.
- Episomal expression of a protein in the parasite was first completed successfully in 1995, in a method that most clearly echoes guess and check (different untranslated regions were placed before and after a gene, transfected, and see what happens) [120].
- Given the number of potential localization sites in the parasite, ensuring an episomally-expressed protein ends up where expected is non-trivial [13].
- When genome modification is desired, a population of parasites must be cloned out in order to separate episomal populations from genome-modified populations, another time-intensive process. Additionally, until the cost and ease of genome sequencing of parasite DNA is low enough, very time-intensive Southern blots must be utilized to show genome loci modification.

- Homologous recombination of a donor plasmid into the genome has been accomplished using various drug cycling methods, but is incredibly time-consuming (one month to years). However, this only applies to genes that are non-essential in the intra-erythrocytic development cycle.
- Targeting essential genes for a knockout results in a difficult problem: if you are unable to knock out a gene, that does not mean that the gene is essential.

Members of the Niles Lab have worked on many different components in order to build a unified toolkit to study many different aspects of parasite biology, especially that of essential genes. As half of the genes in the genome still have no known homology to any other genes, those genes that are essential among that pool are excellent potential drug targets.

A recent review [119] details the progress the Niles lab and the field have made in the last five years, stating:

> To increase the chance of observing a mutational phenotype in the short window between gene ablation and death, the more elegant inducible mutational systems are required to target these genes in order to view their mutational phenotype.

This precise methodology has been successfully utilized in the Niles lab, and the toolkit to make this technology available and useful for other science is the one I am helping develop and test.

3.1.1 Conditional gene expression using the TetR aptamer system

The TetR aptamer system allows for conditional protein expression by turning translation on and off at the level of the mRNA. This system has been tested in bacteria, yeast, and *Plasmodium falciparum* in the Niles lab [121, 1, 3, 2, 122]. Briefly, a sequence that, when transcribed, folds in such a way to have high binding affinity to the TetR protein, is placed in the untranslated region before a gene. This is a TetR-binding aptamer. When TetR binds to the aptamer structure, translation is turned off. When a small molecule that has higher affinity to the TetR protein is added, the TetR protein ceases binding to the TetR-binding aptamer, which allows the ribosome to read through the gene and translate protein (Figure 38 on page 56). The sequence of the aptamer and characteristics are shown in Figure 39 on page 57.

This system was adapted for use in the *Plasmodium falciparum* parasite by Stephen Goldfless [122, 3]. The system works much the same as described above, but is modified for expression using validated parasite promoters and measured using well-characterized parasite outcome assays (Figure 40 on page 58). Of particular interest is the work he did showing that aptamer "tagged" transcripts were still successfully exported to the correct cellular compartments (Figure 41 on page 59).

3.1.2 Improved cloning techniques using linear vectors

Tradition cloning reactions in *Plasmodium falciparum* are challenging: there is a lack of a robust system that allows for easy manipulation of the AT-rich genes of many different size ranges. When such AT-rich

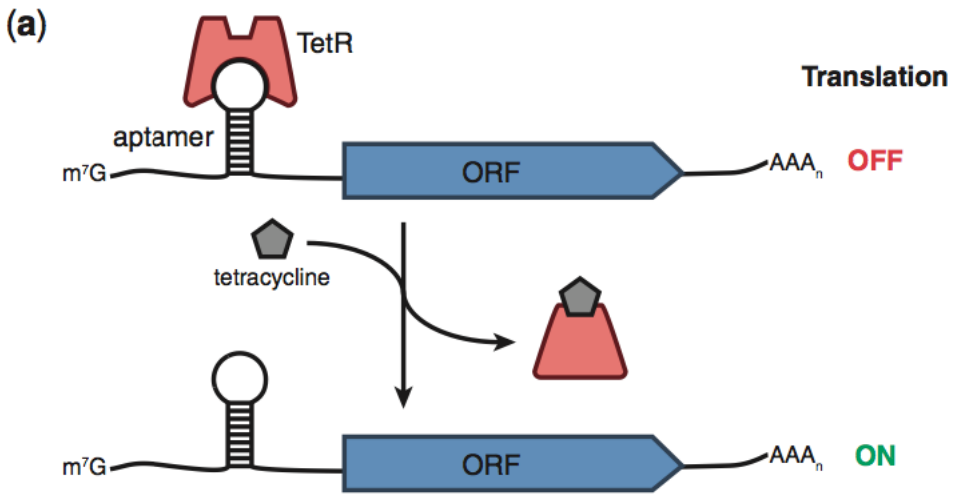

Figure 38: Figure 1A from [1]. Illustration of the regulation scheme used to demonstrate functionality of the TetR–aptamer module. TetR binding to the aptamer element within the 50-UTR of the regulated ORF inhibits its translation. Tetracycline analogs (e.g. aTc and Doxycycline) induce translation by disrupting the TetR–aptamer interaction.

regions are present on typical circular plasmids, there is a high chance of rearrangement and deletion, and sequencing remains challenging. While our lab has found yeast homologous recombination and Gibson to be helpful in addressing these problems [123], the use of linear vectors has further reduced the cloning bottleneck in our lab. The pJazz system from Lucigen and a system to rescue said linear vector into a large bacterial artificial chromosome (BAC) [124] from the were adapted by Sebastian Nasamu and Alejandra Falla in the lab to best suit the challenges presented by the parasite. Unfortunately, transfection of linear DNA does not work on larger timescales (it can be used for transient transfections) [125]. The pJazz system has been used successfully with the AT-rich DNA of another *Plasmodium* genus parasite, *Plasmodium berghei* [126].

3.1.3 Utilizing CRISPR for knockouts of non-essential genes

Jeff Wagner in the lab pioneered a system to cause double strand breaks and successful incorporation of donor DNA by engineering the CRISPR/Cas9 design to function in the parasite. First, he was able to produce non-coding RNA in the parasite using T7 RNA polymerase (Figure 42 on page 60). Next, he used this system to produce gRNA that targets a spot in the genome for a double strand break using the Cas9 nuclease Figure 43 on page 61. He successfully knocked out two known non-essential genes, knob-associated histidine rich protein (KAHRP) and erythrocyte binding antigen 175 (EBA-175), the former of which has data shown here [127]. He verified both of the knockouts using:

- Renilla luciferase expression (Figure 44 on page 61)
- PCR of the edited genomic region (Figure 45 on page 62)
- Southern blot (Figure 46 on page 62)

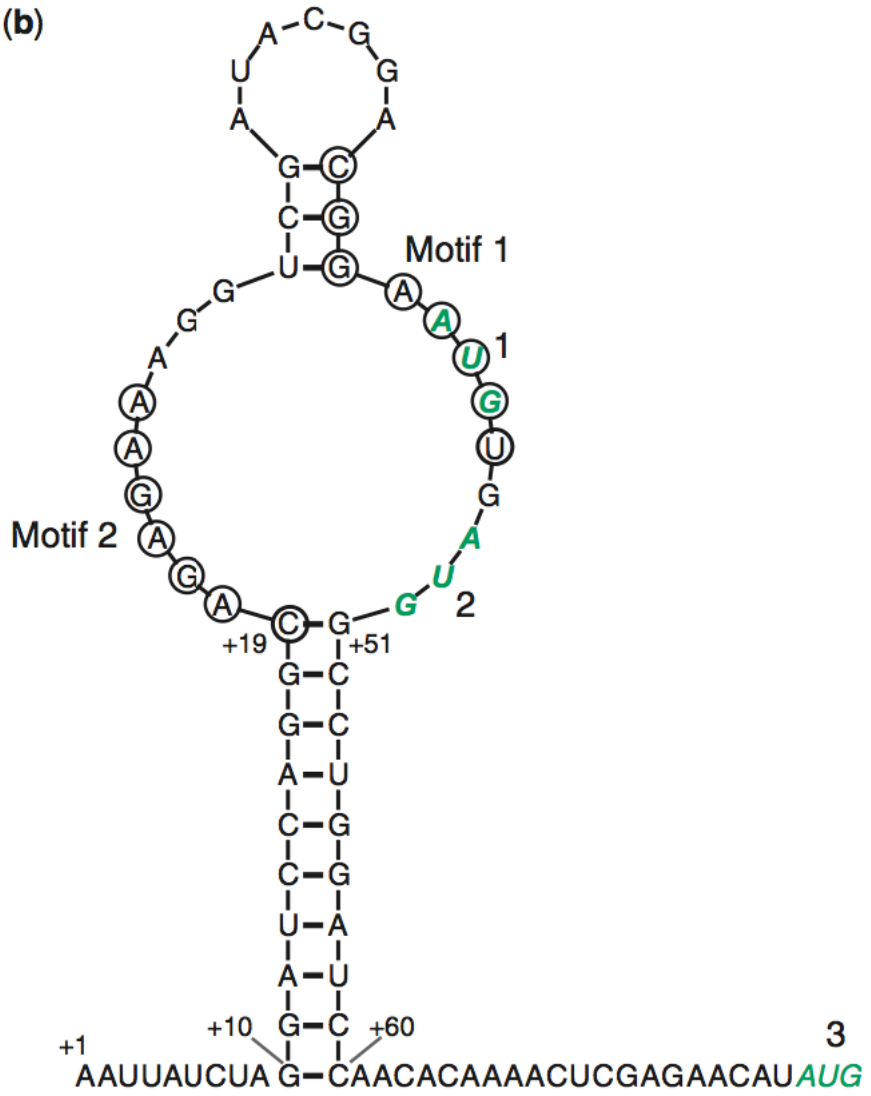

Figure 39: Figure 1B from [1]. The primary and predicted secondary structures of aptamer 5–1.2 (bases 10–60) within the 50-UTR context used in this study are shown. Residues comprising two conserved regions (Motifs 1 and 2) indispensable to TetR binding are circled. Three potential start codons, 1–3, are shown in green bold italics. Start codon 1 (within Motif 1) is out of frame, whereas 2 is in frame with 3, the downstream ORF's native start codon.

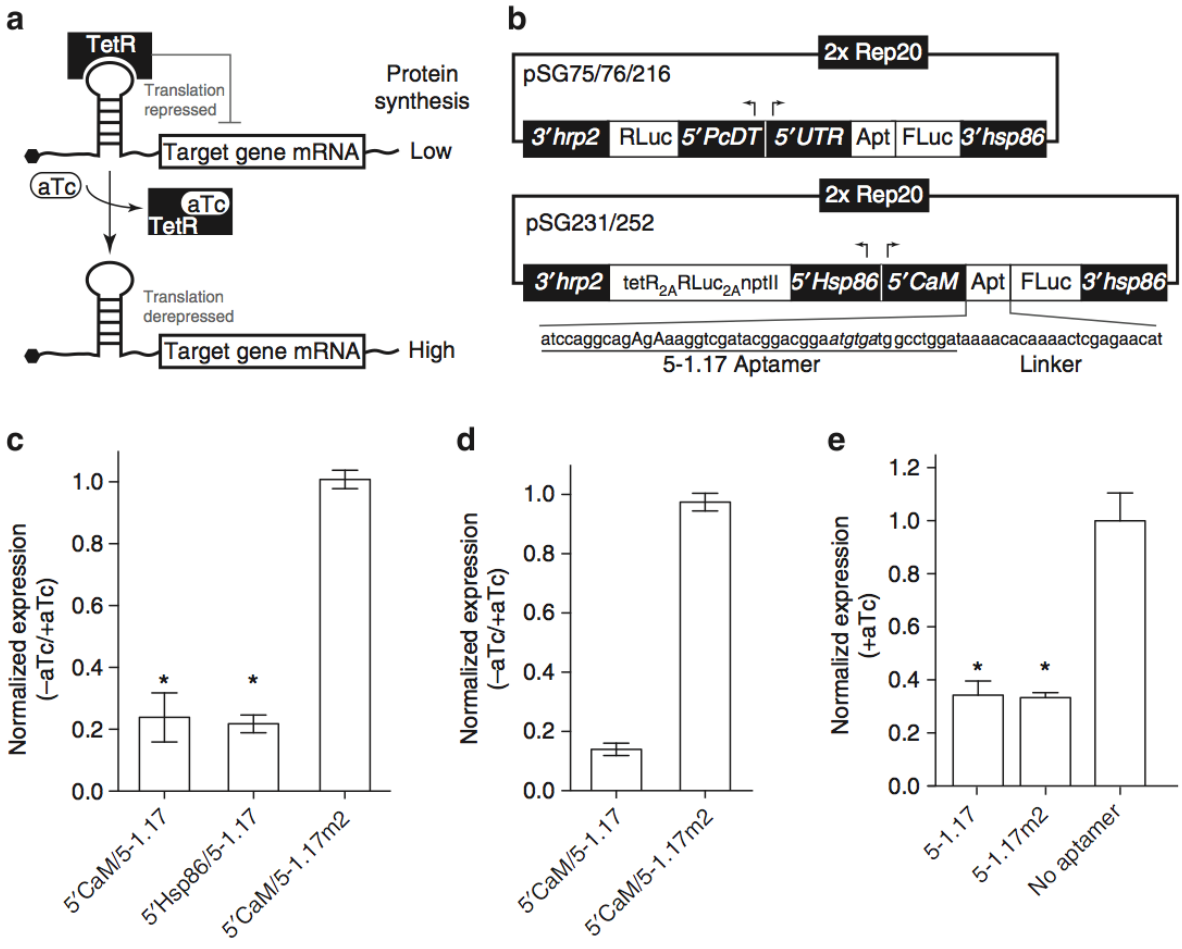

Figure 40: Figure 1 from [3]. Aptamer 5-1.17 enables aTc-dependent control of reporter gene expression. Panel A shows the schematic of aTc- and TetR-dependent regulation of translation. Panel B shows the plasmids used to screen for aTc-dependent regulation in transient transfections. Vectors pSG231 (5-1.17) and pSG252 (5-1.17m2) were used for the same purposes in stable episomal parasite lines. Either a functional (5-1.17) or mutated (5-1.17m2) aptamer was placed upstream of the FLuc reporter gene to regulate its expression. The sequence and placement context for the 5-1.17 aptamer is shown as an inset. The capitalized 'A's are mutated to 'T's to produce the non- functional 5-1.17m2. Bases in italics indicate a short upstream start/stop, and those in bold indicate a productive start codon that is kept in frame with the downstream coding sequence (CDS) of interest. A CDS may carry its own initiation codon, or not, with no effect on expression or regulation by aTc. Renilla luciferase (RLuc) is expressed constitutively, and serves as a reference during quantification. Panel C shows the aTc-inducible firefly expression following transient screening in the TetR-expressing parasite clone B10, 5-1.17, but not 5-1.17m2. Values are expressed as FLuc/RLuc (- aTc) normalized to FLuc/RLuc (+ aTc). Panel D shows the same results in stable episomal lines, 5-1.17 but not 5-1.17m2. Panel E shows that insertion of aptamer 5-1.17 downstream of the CaM 50UTR reduces its maximal FLuc expression about twofold. All data are expressed as the mean ± s.d. of two to four independent experiments. An asterisk (*) denotes a P-value of 0.002 determined by two-tailed unpaired t-test.

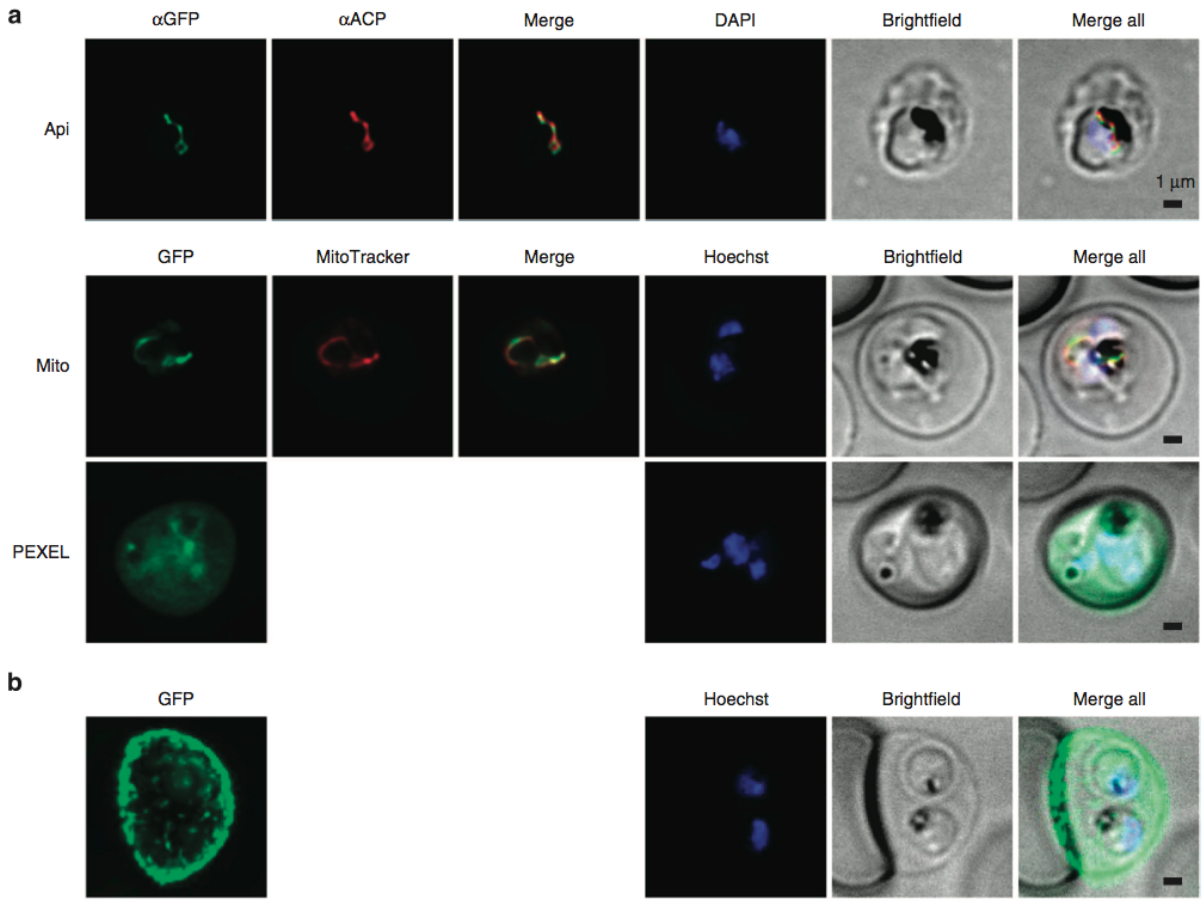

Figure 41: Figure 3 from [3]. Aptamer controlled target proteins are properly trafficked to various subcellular compartments. Panel A shows immunofluorescence and live fluorescence imaging of strains expressing chromosomally integrated GFP reporters bearing an N-terminal targeting peptide (Api = apicoplast-targeted; Mito = mitochondrion-targeted; PEXEL = protein export to erythrocyte cytoplasm). ACP = acyl carrier protein, used as an apicoplast marker. Panel B shows live fluorescence imaging of aptamer-regulated KAHRP-GFP fusion expressed from an episomal construct bearing the *P. falciparum* centromere-derived element pfCEN5–1.5.

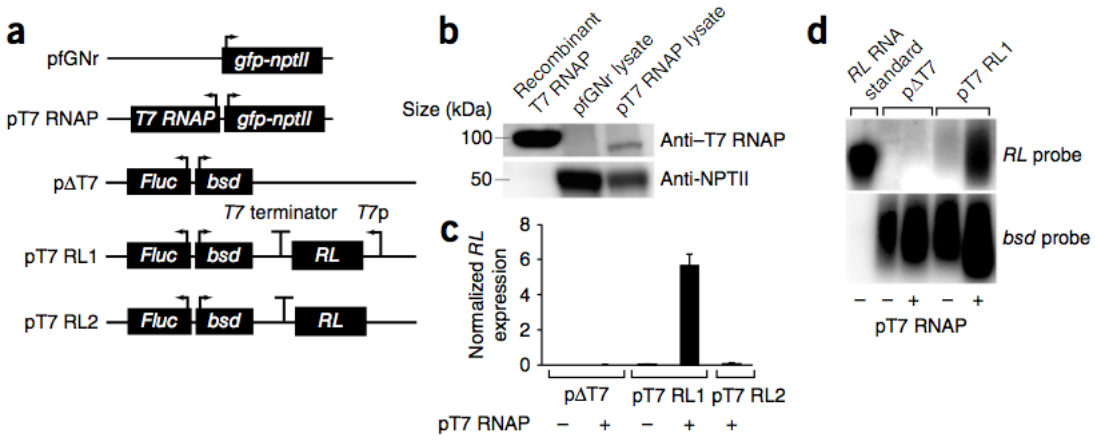

Figure 42: Figure 1A-D from [127]: Validating T7 RNAP functions in *P. falciparum*. In panel A, plasmids used to test T7 RNAP expression and activity (bsd is blasticidin-S deaminase; Fluc is firefly luciferase; gfp-nptII is green fluorescent protein–neomycin phosphoribosyl transferase II; RL is Renilla luciferase). In panel B, western blot analysis of T7 RNAP protein production in parasites shows production of T7 RNA polymerase. Blots were probed with anti–T7 RNAP and anti-NPTII (loading control) antibodies. In panel C, quantitative RT-PCR analysis of normalized RL transcript levels produced after the indicated transfections shows renilla luciferase expression only in the presence of T7 RNA polymerase. (Data are mean ± s.d.; n = 3 technical replicates). In panel D, northern blot analysis for RL transcript production, with the bsd selection marker transcript probed as a control, shows renilla luciferase RNA production in only the T7 RNA polymerase-expressing parasites.

- Western blot (Figure 47 on page 63)
- Phenotype using SEM; those parasites that do not express kahrp display a knob-less phenotype [128] (Figure 48 on page 63)

His work was directly adapted to design a system for conditional knockouts.

3.1.4 Utilizing CRISPR for conditional knockouts

Sebastian Nasamu used the linear vector system he developed as the platform for a conditional knockout scheme. The native 5'UTR was chosen as the left homologous region, and the 3' portion of the gene of interest was chosen as the right homologous region. The rest of the gene of interest was recoded, and both a TetR aptamer and HA tag were added, to provide conditional expression of the gene as well as the capability to detect the protein using western blot. Another cassette was added, expressing a resistance marker, renilla luciferase, and the TetR protein. Lox p sites were added to allow for excision by DiCre recombinase. gRNA was added outside the homology region, with the proper T7 promoter and terminator to allow for expression in the parasite. The system requires PCR of the two separate homology regions, and gblocks of both the recoded gene and the gRNA that is part of the CRISPR/Cas9 system. It is modular and straightforward, though sequencing through the native *P. falciparum* homology regions can sometimes be challenging (a challenge not limited to this setup, to be sure).

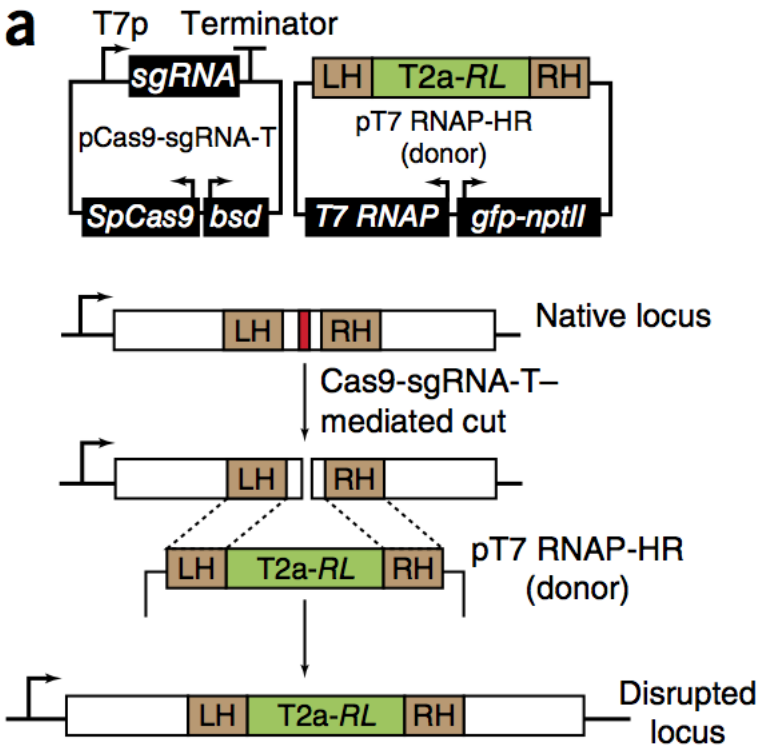

Figure 43: Figure 2A from [127]: one plasmid encodes the guide RNA for the Cas9 system (sgRNA) and Cas9 itself; another plasmid contains T7 RNA polymerase and the donor sequence. When Cas9 cuts the genome, the donor DNA is used to heal the double strand break, resulting in a disrupted locus. T2a-RL stands for T2A tag-Renilla luciferase; in this system, the 2A tag interrupts the sequence of the target gene, meaning that transcription of this gene produces a truncated target gene and renilla luciferase, by virtue of the 2A tag's ability to allow for polycistronic expression in eukaryotic transcripts [129].

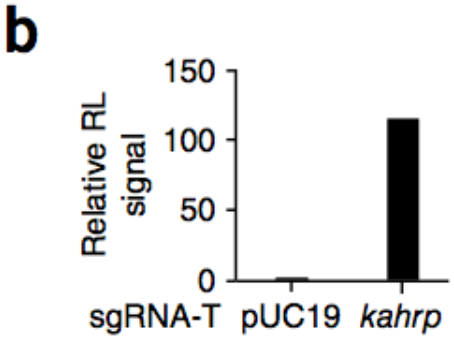

Figure 44: Figure 2B from [127]: detection of CRISPR/Cas9–mediated disruption of the *P. falciparum* kahrp locus using renilla luciferase and southern blot. Renilla luciferase expression in a parasite population when the kahrp locus is targeted by kahrp-sgRNA-T or the pUC19-sgRNA-T control in the presence of a suitable donor plasmid shows the presence of renilla luciferase only when the kahrp locus is targeted.

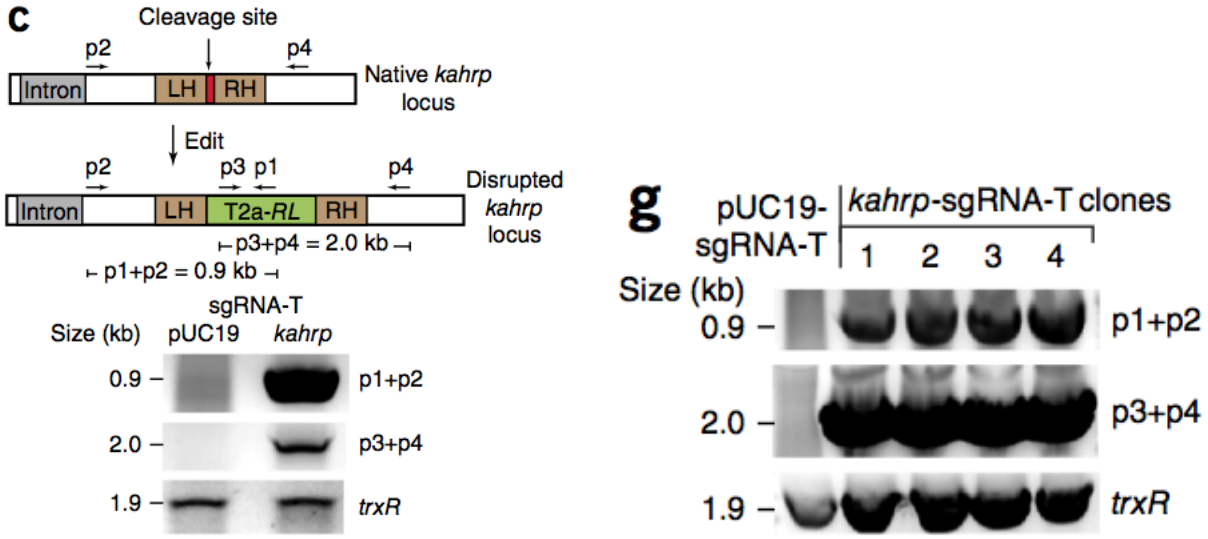

Figure 45: Figures 2C and 2G from [127]: detection of CRISPR/Cas9–mediated disruption of the *P. falciparum* kahrp locus using PCR to detect the edited locus. PCR primers (p1, p2, etc.) were used to specifically detect homology-directed repair at a target cut site in the kahrp locus. Panel C shows the population, and Panel G shows individual clones.

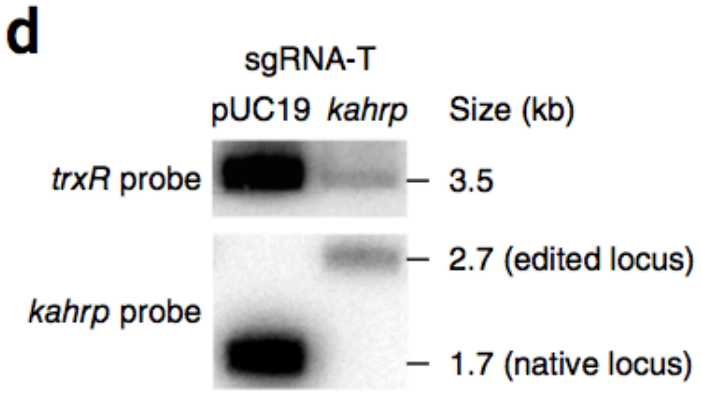

Figure 46: Figure 2D from [127]: detection of CRISPR/Cas9–mediated disruption of the *P. falciparum* kahrp locus using a southern blot. Parasite populations were obtained after transfection with the pUC19- and kahrp-sgRNA-Ts. TrxR, thioredoxin reductase, was used as a positive control.

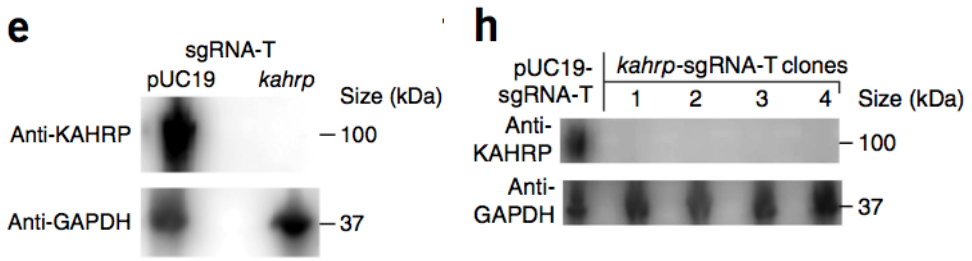

Figure 47: Figures 2E and 2H from [127]: detection of CRISPR/Cas9–mediated disruption of the *P. falciparum* kahrp locus using a western blot. Parasite populations were obtained after transfection with the pUC19- and kahrp-sgRNA-Ts. GAPDH is used as a positive control. Panel E shows the population, and Panel H shows individual clones.

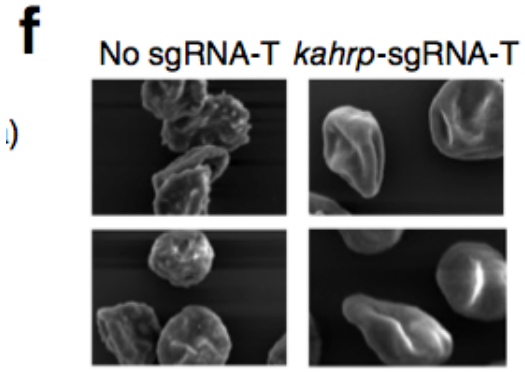

Figure 48: Figure 2F from [127]: detection of CRISPR/Cas9–mediated disruption of the *P. falciparum* kahrp locus using SEM imaging analysis of parasite populations obtained after transfection with a No sgRNA-T control and kahrp-sgRNA-T, showing loss of knobs.

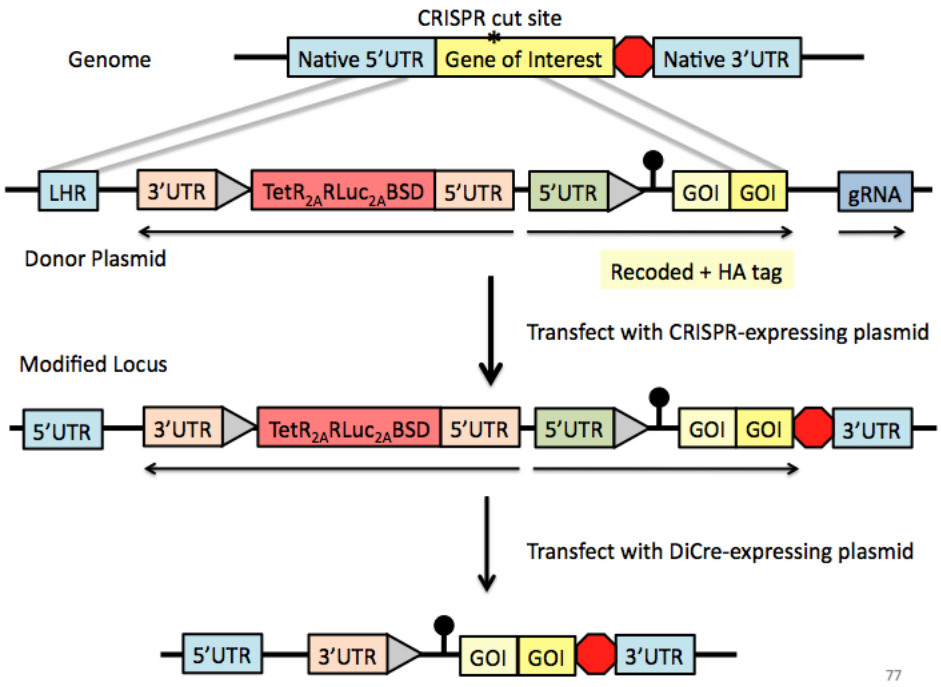

Figure 49: Representation of genome, donor plasmid, edited locus upon transfection and recombination, and final edited locus following DiCre recombinase activation.

First, in order to verify that the donor DNA would be a success, he co-transfected a plasmid expressing an already-verified zinc-finger nuclease that targeted the CRT gene [130] with the plasmid encoding the donor DNA to create a CRT conditional knockout. He has characterized both the conditional knockout for the CRT gene as well as the choline kinase gene.

3.1.5 Toolkit for functional genetics in the parasite

Now that the technique had worked for two donor vectors, expanding the test to show conditional regulation of five unrelated genes was undertaken. All five choices are considered potential drug targets. These targets were also chosen for their presence in various cellular compartments and for their potential to thoroughly test the success of the toolkit and bring to light potential improvements to make to the toolkit.

- Chloroquine Resistance Transporter (PfCRT; PF3D7_0709000)
  - Now that successful editing had been shown with the donor vector, attempting the same reaction with the CRISPR/Cas9 system would show the repeatability using a much more customizable and cheaper system.
- Choline Kinase (PfCK; PF3D7_1401800
  - Successful genotyping and phenotyping of a choline kinase conditional knock out has been accomplished.

- Thioredoxin Reductase (TrxR; PF3D7_0923800)
  - There is evidence of essentiality in the parasite: the gene could only be knocked out if a complementary copy was being expressed on an episome [131].
- Glycogen synthase kinase 3 (GSK3; PF3D7_0312400)
  - While GSK3 was originally listed under an umbrella of essential kinases that could be potential drug targets [132, 133], the gene has been successfully knocked out in our lab, as well as in rodent malaria parasite *P. berghei* [134].
- Hexose Transporter (PfHT; PF3D7_0204700)
  - This gene was first examined by heterologous expression of mRNA in Xenopus eggs, and shown to be a potential drug target [135].
  - There is evidence of essentiality in the parasite: the gene could only be knocked out if a complementary copy was being expressed on an episome [136, 137].

Note that GSK3 in this grouping is serving as the single non-essential gene. Both hexose transporter and chloroquine resistance transporter are involved with metabolite flux. Finally, choline kinase and thioredoxin reductase are the targets in this set of five that will be the most challenging to knock down fully given the fact that they are enzymes.

In addition to the gene targets, several parameters of the toolkit were tested:

- For GSK3, two separate gRNAs were used to target the Cas9 nuclease to the GSK3 gene. It is of interest to learn more about the necessary components of the gRNA targeting sequence in the parasite. While much is known about the robustness of this sequence in other systems [138], much remains unknown in the parasite.
- Co-transfections of the donor plasmid and the CRISPR-expressing plasmid were split into two populations prior to drug selection and selected with either blasticidin (corresponding to the donor plasmid) or both blasticidin and WR9920 (corresponding to the CRISPR-expressing plasmid).

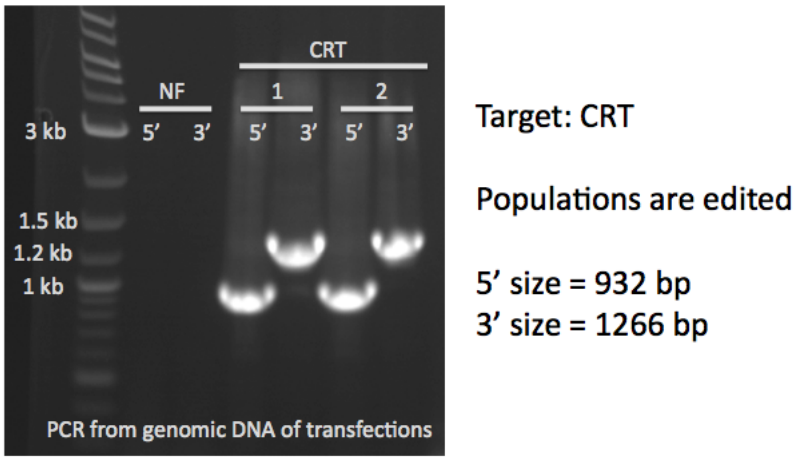

Figure 50: PCR of the 5' and 3' regions of CRT populations compared to the population and NF54attb negative control using P1 and P2 or P3 and P4, respectively.

3.2 Results

In order to define the status of the chosen targets as essential or not, first, strains were genotyped using PCR, and sequencing of PCR reactions. Southern blots are still ongoing. Western blots were used to determine levels of conditional protein expression. Next, the phenotype was assayed using growth assays, and in the case of chloroquine resistance transporter and the already-made choline kinase strain, phenotypic tests using drugs that target the genes of interest.

3.2.1 Chloroquine Resistance Transporter (CRT)

The chloroquine resistance transporter (CRT) had already been knocked out by labmate Sebastian Nasamu using a zinc finger nuclease method, but attempting to knock out the same gene with the CRISPR/Cas9 system would provide more proof of the utility of the modular and comparably cheap system. This proof was gained with positive genomic insertion as confirmed by PCR on both the 5' and 3' loci (Figure 50 on page 66). As such, the more rigorous genotyping and phenotyping was put on hold because the biological data for this strain has already been acquired. However, the population of both BSD and BSD/WR parasites has been frozen down. Sebastian Nasamu will also be including these strains in a southern blot for the manuscript to show CRISPR-based editing.

3.2.2 Thioredoxin Reductase (TrxR)

Editing with PCR: Editing was first detected in the population using PCR, followed by detection of the expected product in all six clones (Figure 51 on page 67, Figure 52 on page 68, and Figure 53 on page 68).

Southern blot and western blot analysis remain to be completed.

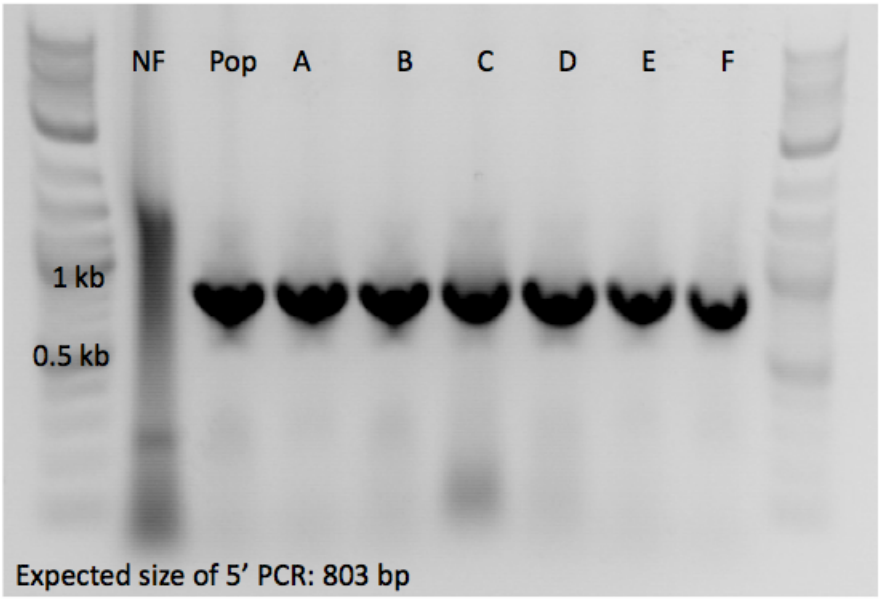

Figure 51: PCR of the 5' region of TrxR clones compared to the population and NF54attb negative control using P1 and P2.

Growth assay: Several TrxR clones were tested for essentiality by a growth assay in several different experiments, yet no growth phenotype was detected (Figure 54 on page 69, 55 on page 70).

3.2.3 Glycogen synthase kinase 3 (GSK3)

Editing with PCR: Editing was first detected in the population using PCR, followed by detection of the expected product in all twelve clones (Figure 58 on page 73, Figure 59 on page 73, and Figure 60 on page 74).

The southern blot remains to be completed.

Western blot: GSK3 was detected using an anti-HA antibody, and seen to be inducible in clones A, B, and C (Figure 61 on page 74).

Growth assay: Several GSK3 clones were tested for essentiality by a growth assay, yet no growth phenotype was detected (Figure 62 on page 75 and Figure 63 on page 76).

3.2.4 Hexose Transporter (HT)

Editing with PCR: Editing was first detected in the population using PCR (Figure 64 on page 77, Figure 65 on page 77, and Figure 66 on page 78).

The southern blot remains to be completed.

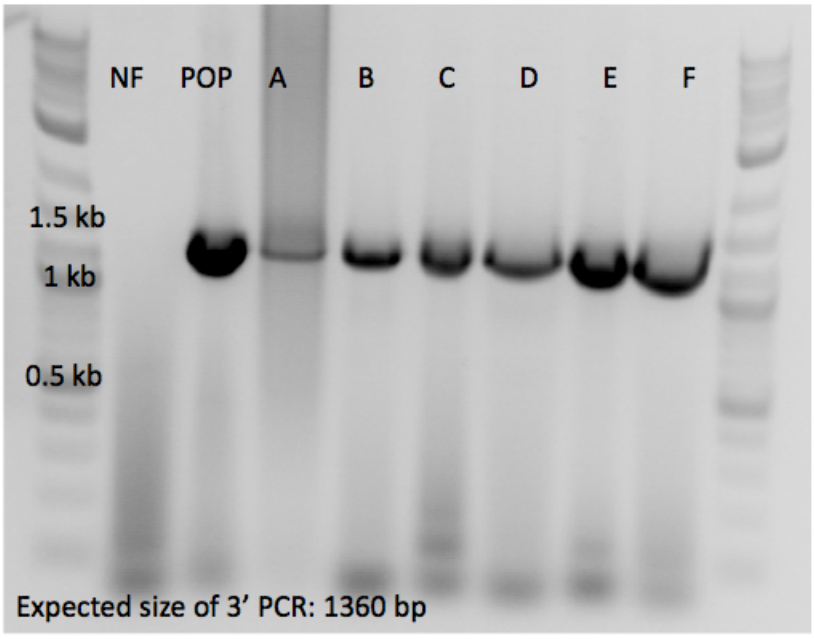

Figure 52: PCR of the 3' region of TrxR clones compared to the population and NF54attb negative control using P3 and P4.

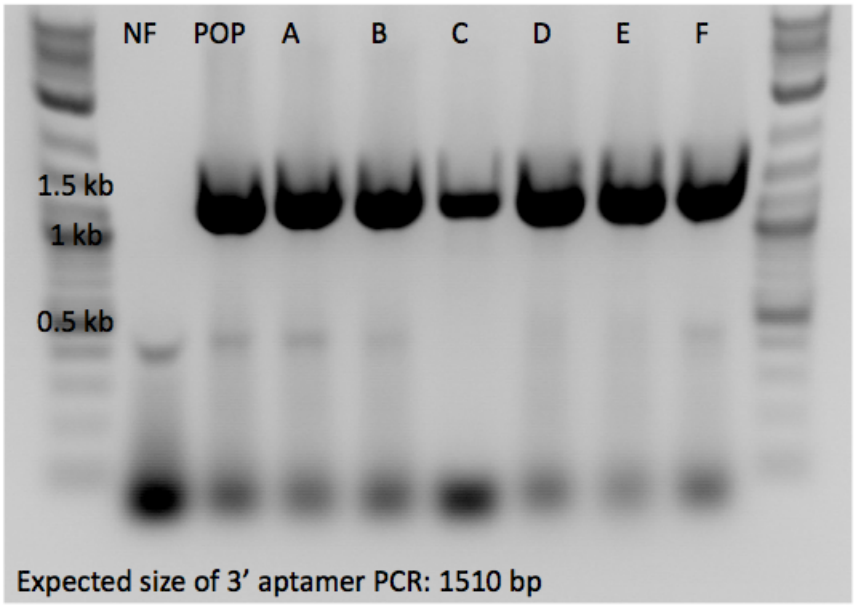

Figure 53: PCR of the 3' region of TrxR clones compared to the population and NF54attb negative control using P3 aptamer and P4.

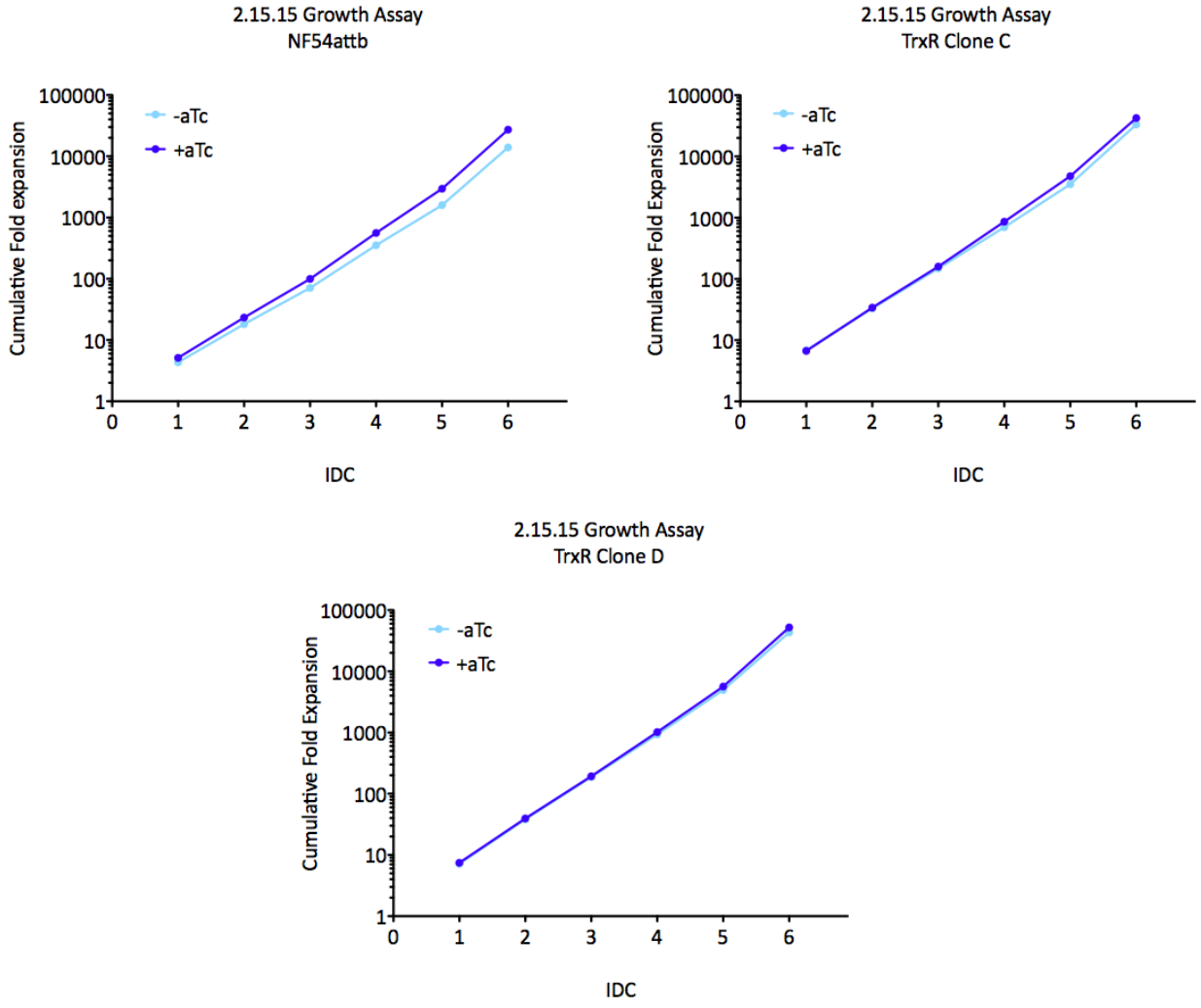

Figure 54: Phenotypic growth assay of TrxR clones plus and minus aTc compared to the NF54attb control (started on 2.15.15).

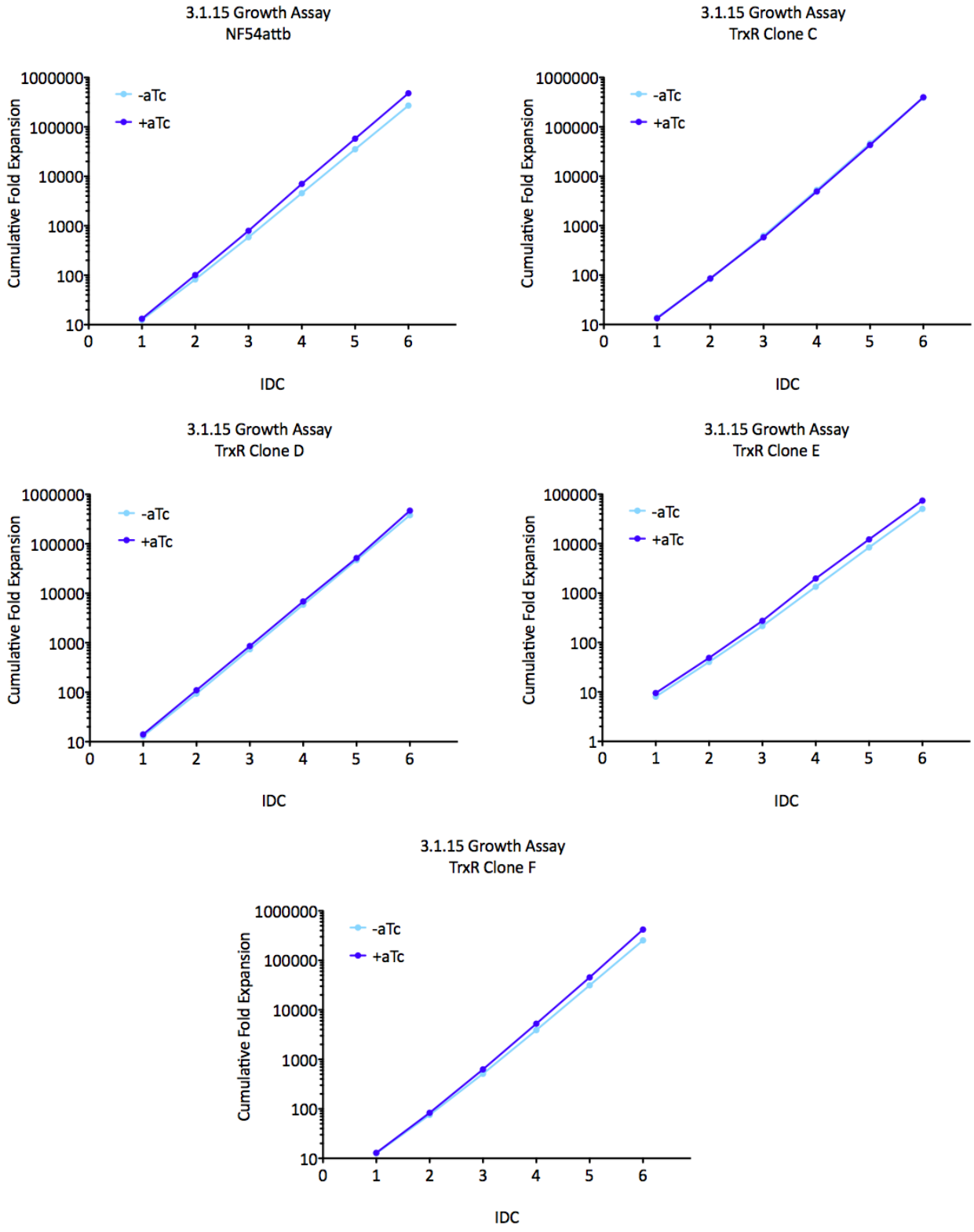

Figure 55: Phenotypic growth assay of TrxR clones plus and minus aTc compared to the NF54attb control (started on 3.1.15).

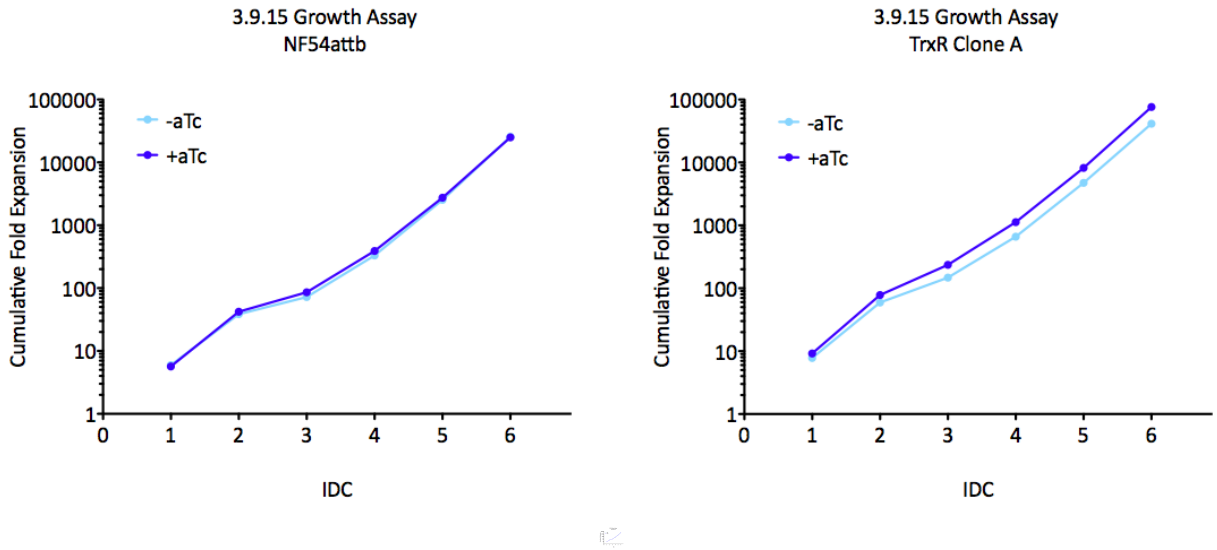

Figure 56: Phenotypic growth assay of TrxR clones plus and minus aTc compared to the NF54attb control (started on 3.9.15).

Western blot: HT was detected using an anti-HA antibody, and is inducible in clones A, B, C, and D (Figure 67 on page 78).

Growth assay: First, the HT population was tested for essentiality by a growth assay, and what resulted was a severe growth phenotype (Figure 68 on page 79 and Figure 69 on page 79). Next, clones were tested for essentiality by a growth assay, and all except one (Clone F) were found to also have a severe growth phenotype (Figure 70 on page 80 and Figure 69 on page 79). Occasionally in this system, regulation is lost either by an aptamer mutation or loss of the aptamer sequence.

3.2.5 Phenotypic Tests: Chloroquine Resistance Transporter and Choline Kinase

In order to determine whether a conditional knockout makes a parasite strain more sensitive to it's related drug, different clones of CRT and CK parasites were treated with and without aTc and with a panel of drug concentrations. Two controls were used: NF54attb is a control strain with no modifications. Each strain was also probed by the opposite strain's drug, to examine if the knockdown of a gene, whether the target or not, relates to a shift in IC50.

For both CRT and CK, there was a shift in the IC50 when the parasites were not exposed to aTc, but this shift was also seen with those parasites conditional knock out strains treated with the opposite drug in question (Figure 72 on page 82 and Figure 73 on page 83). In order to parse whether this effect is one due to biology or simply due to the range of measured shifts in expansion, this experiment will be attempted on a smaller scale testing parasitemia using a different method.

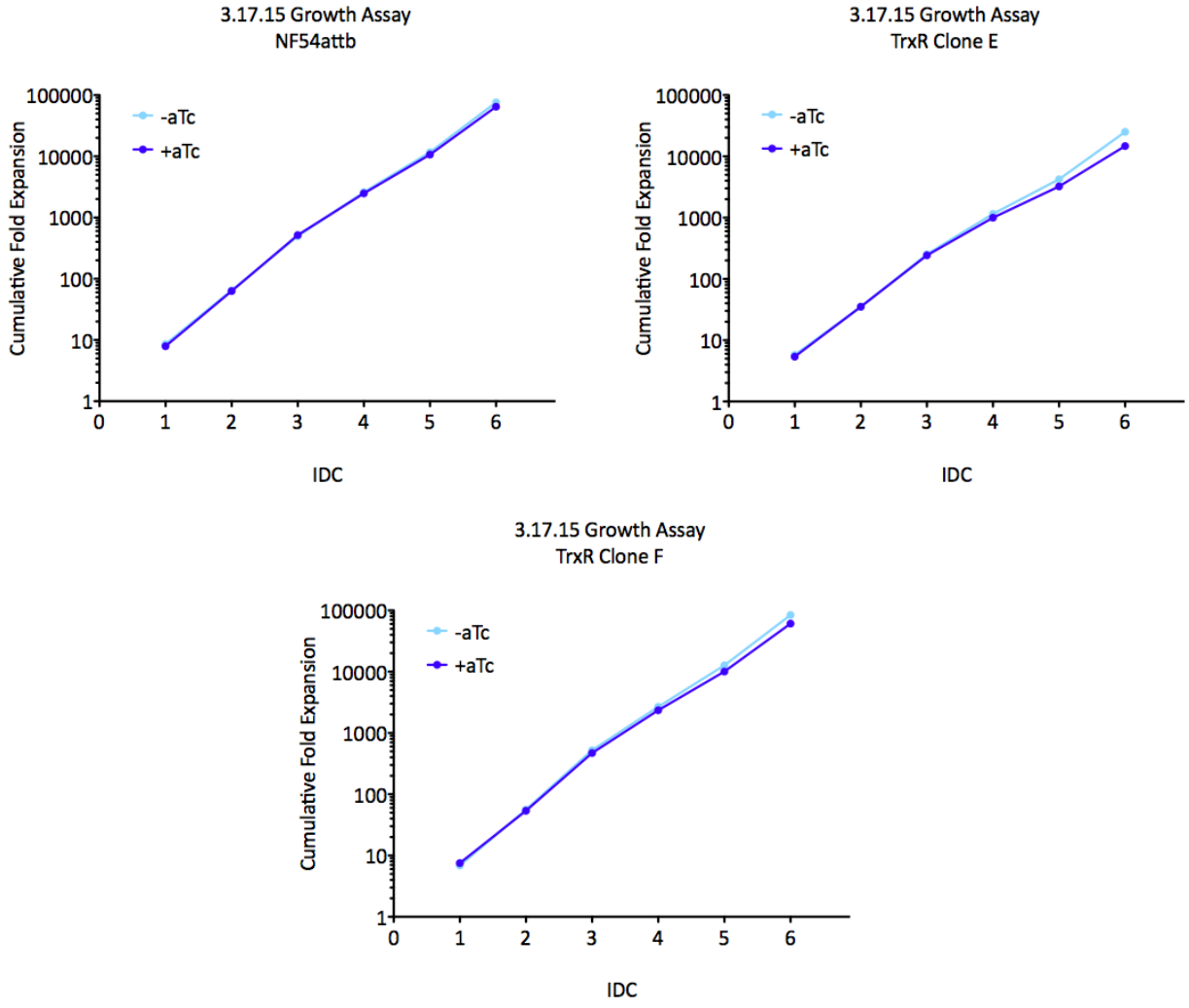

Figure 57: Phenotypic growth assay of TrxR clones plus and minus aTc compared to the NF54attb control (started on 3.17.15).

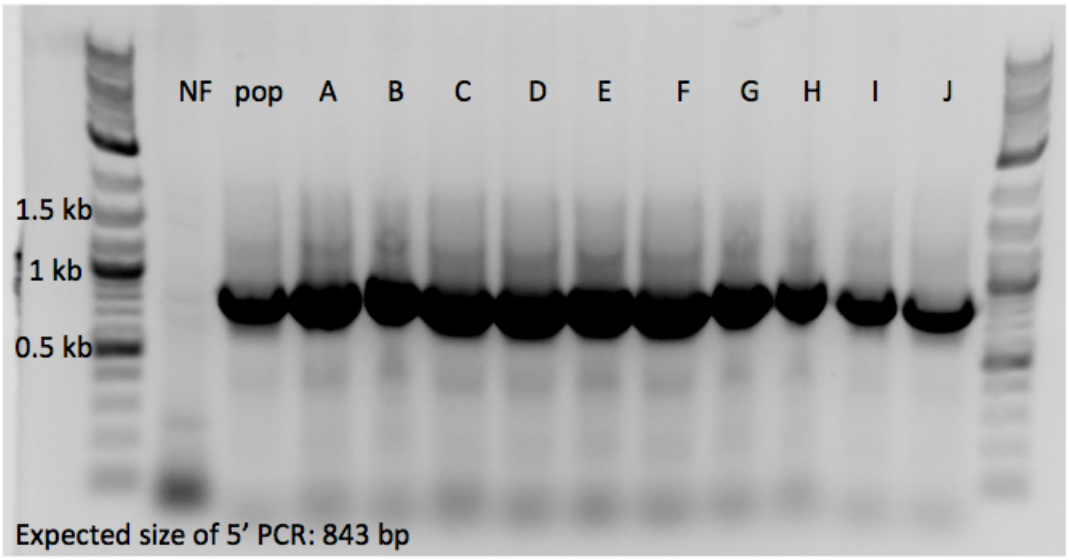

Figure 58: PCR of the 5' region of GKS3 clones compared to the population and NF54attb negative control using P1 and P2.

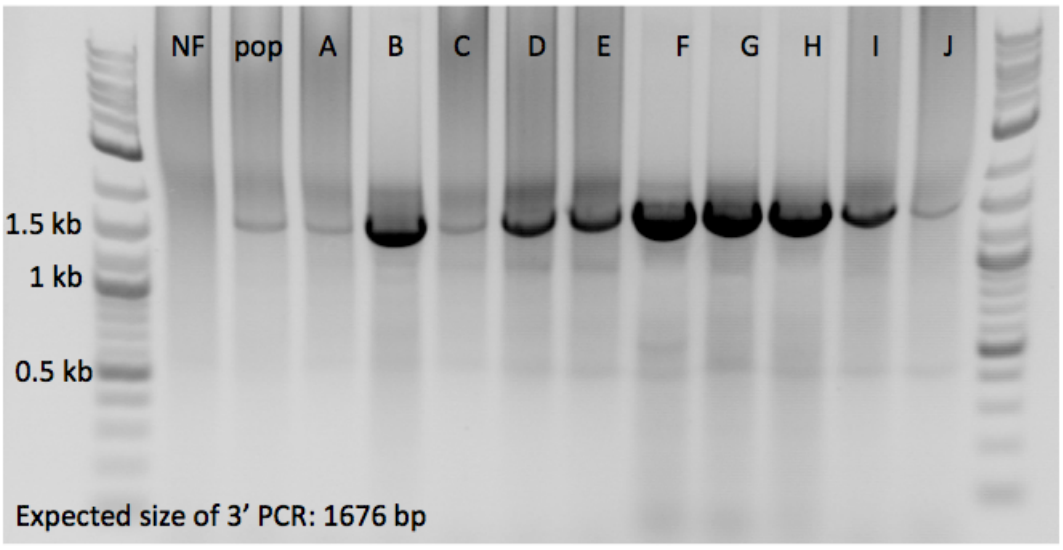

Figure 59: PCR of the 3' region of GSK3 clones compared to the population and NF54attb negative control using P3 and P4.

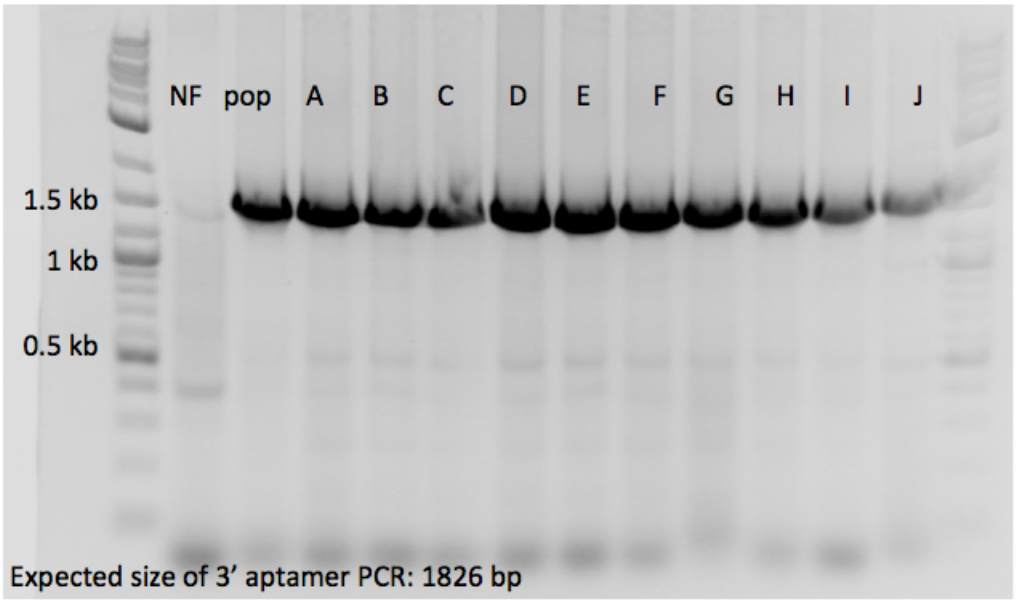

Figure 60: PCR of the 3' region of GSK3 clones compared to the population and NF54attb negative control using P3 aptamer and P4.

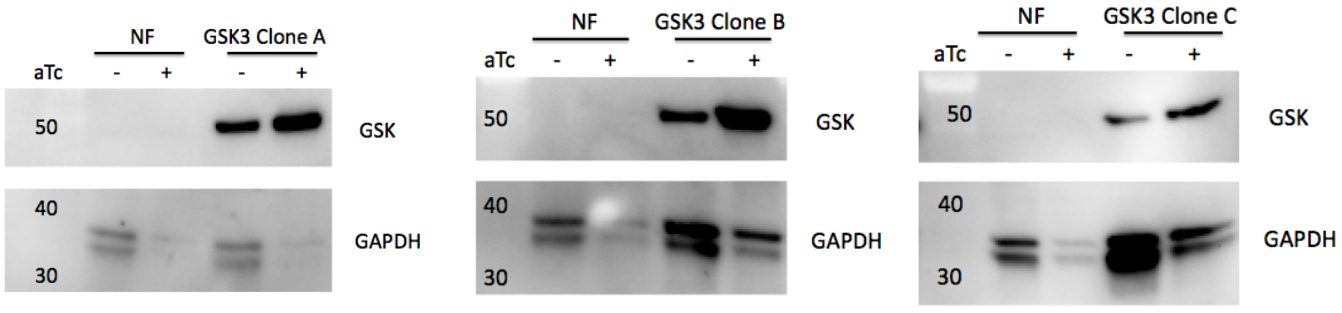

Figure 61: Western blot of GSK3 clones treated with and without aTc, detected using an anti-HA antibody.

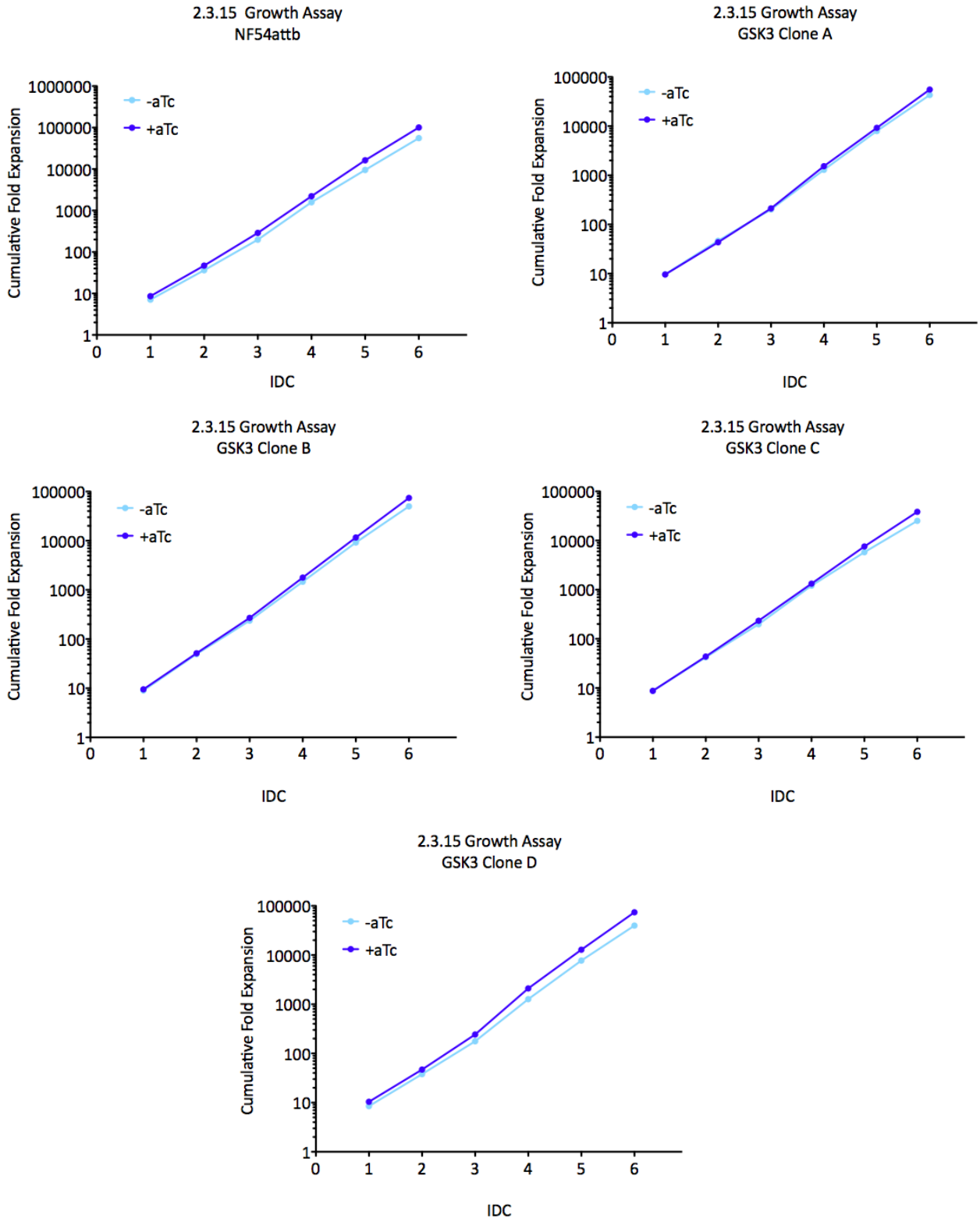

Figure 62: Phenotypic growth assay of GSK3 clones plus and minus aTc compared to the NF54attb control (started on 2.3.15).

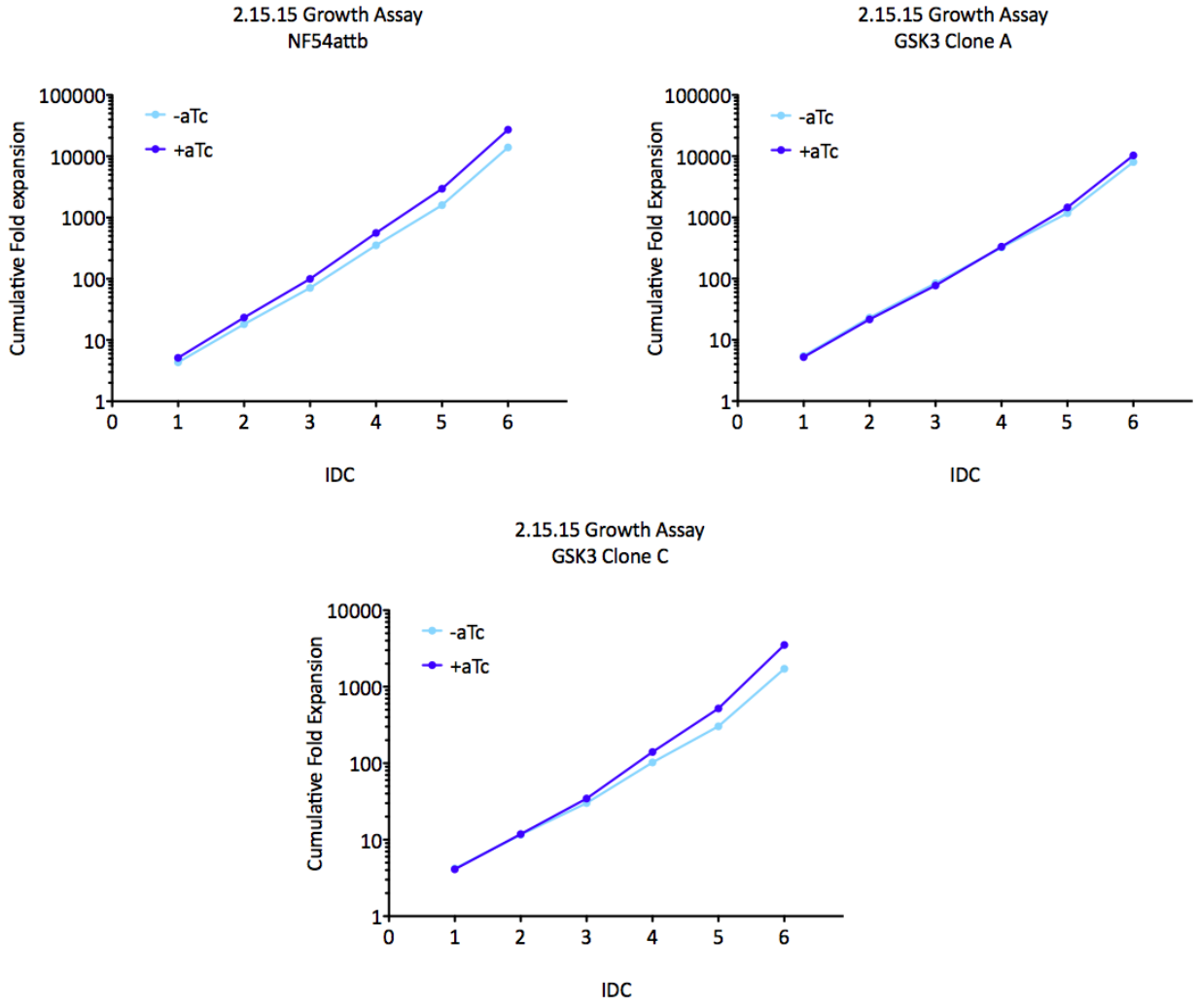

Figure 63: Phenotypic growth assay of GSK3 clones plus and minus aTc compared to the NF54attb control (started on 2.15.15).

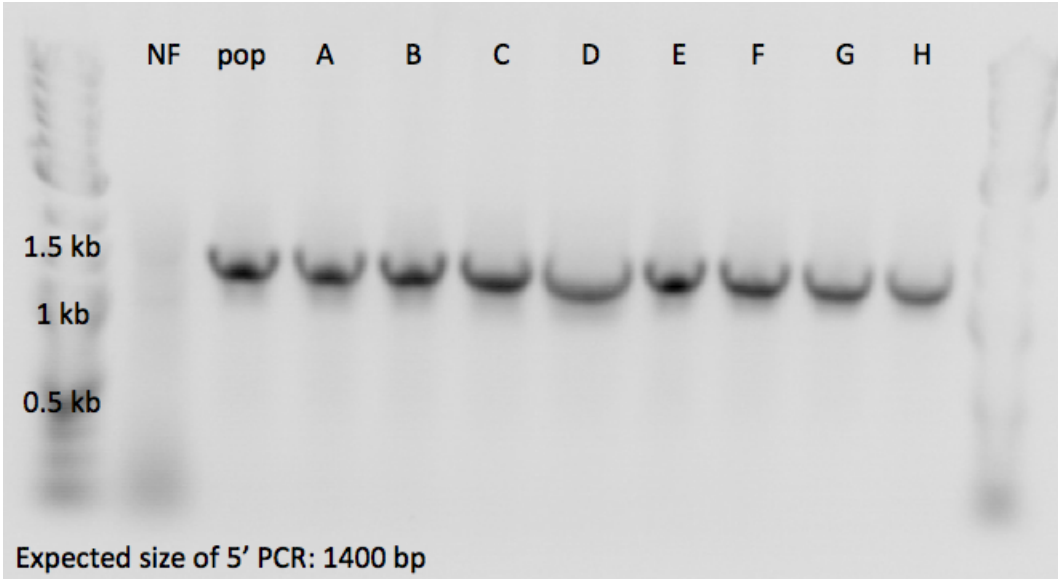

Figure 64: PCR of the 5' region of HT clones compared to the population and NF54attb negative control using P1 and P2.

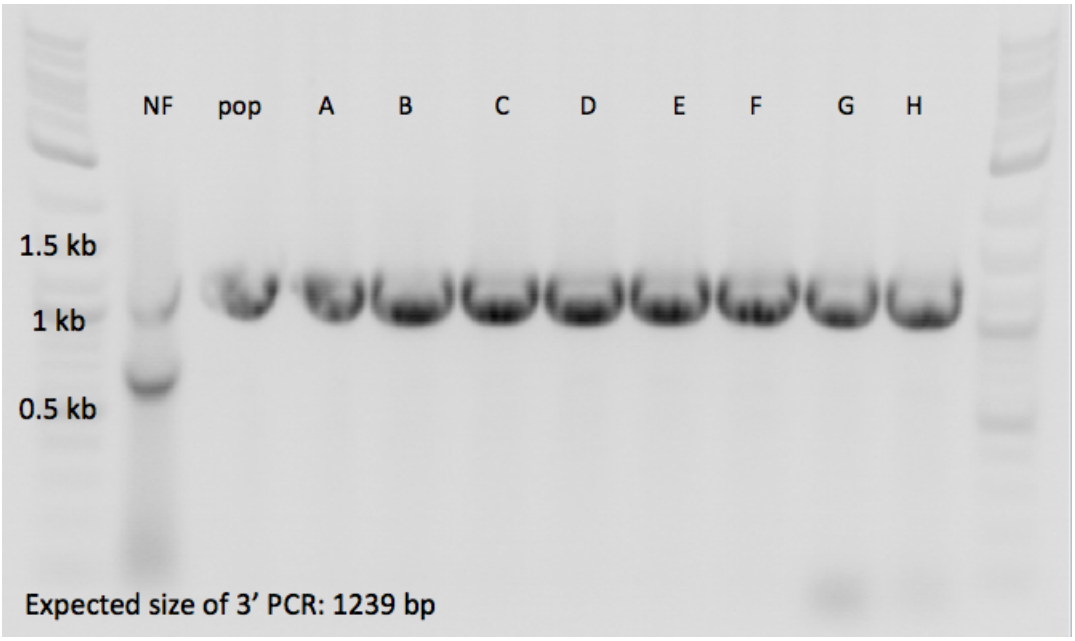

Figure 65: PCR of the 3' region of HT clones compared to the population and NF54attb negative control using P3 and P4.

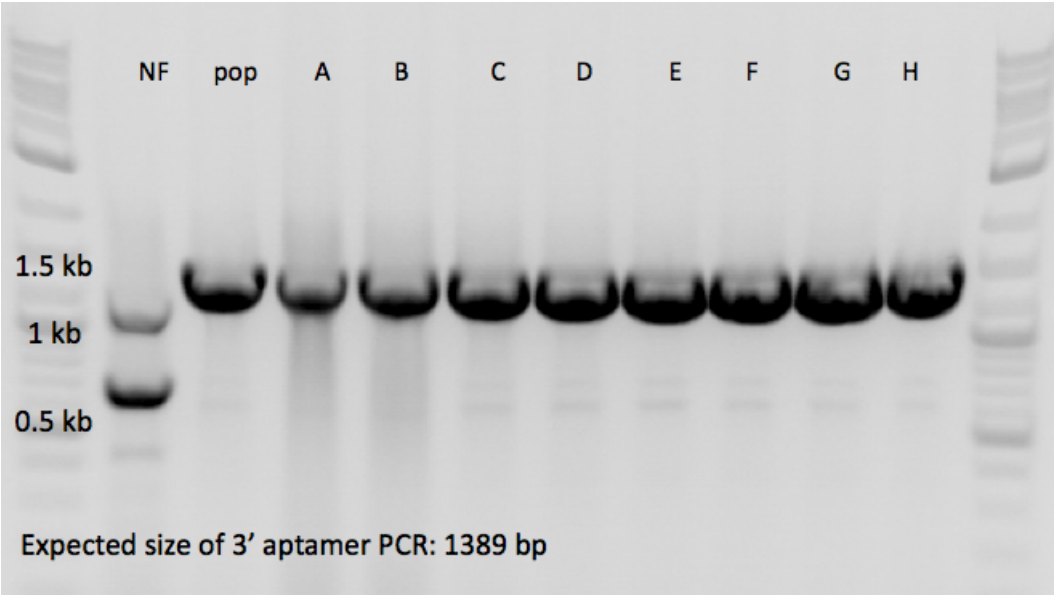

Figure 66: PCR of the 3' region of HT clones compared to the population and NF54attb negative control using P3 aptamer and P4.

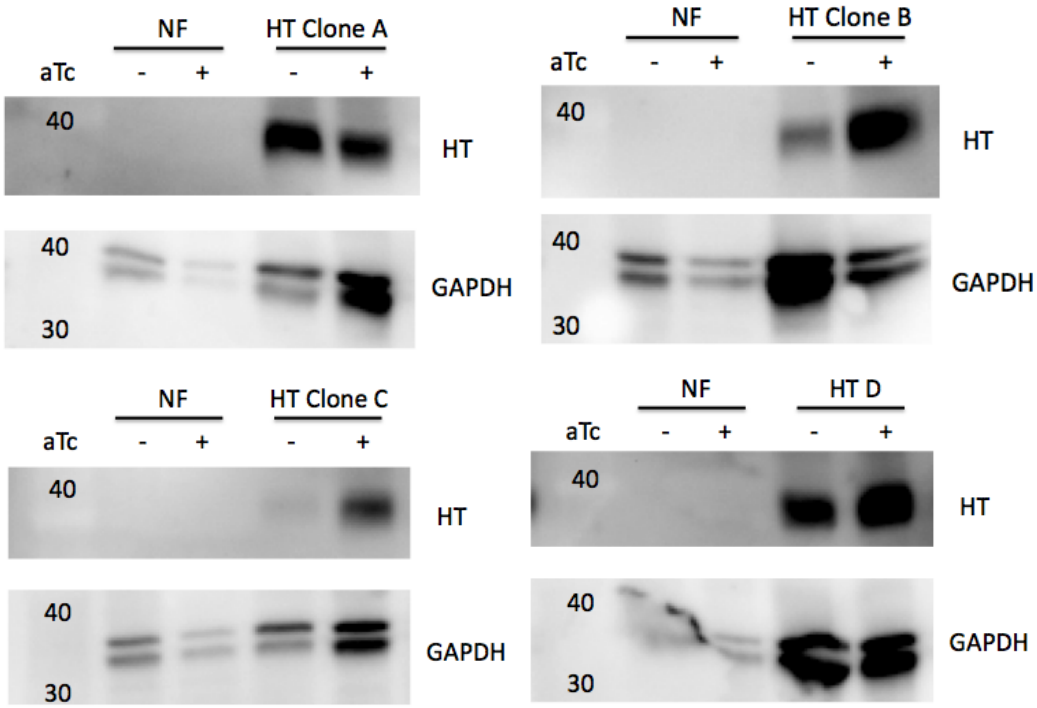

Figure 67: Western blot of HT clones treated with and without aTc, detected using an anti-HA antibody.

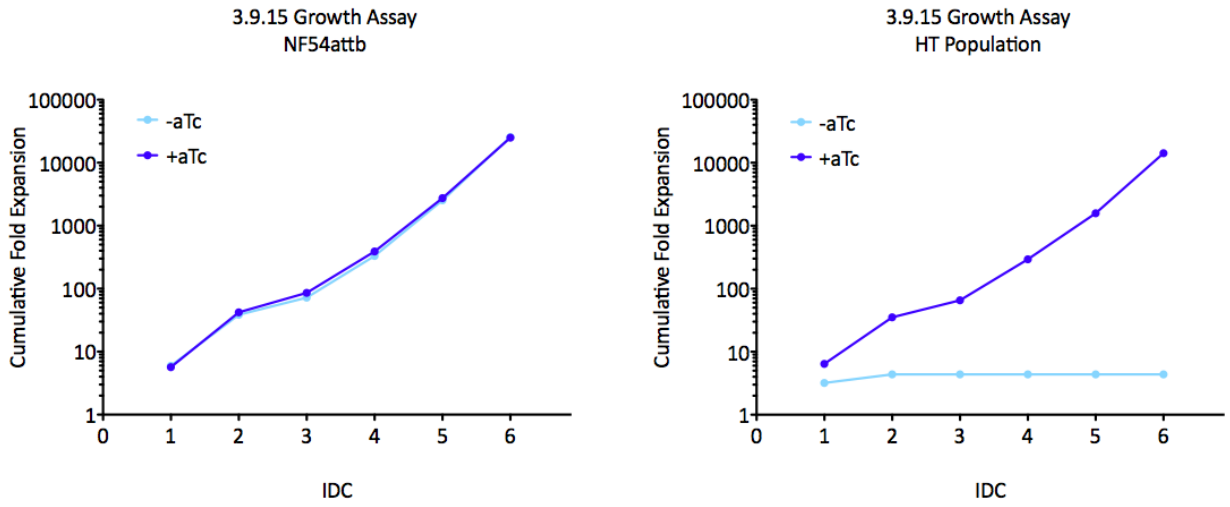

Figure 68: Phenotypic growth assay of HT population plus and minus aTc compared to the NF54attb control (started on 3.9.15).

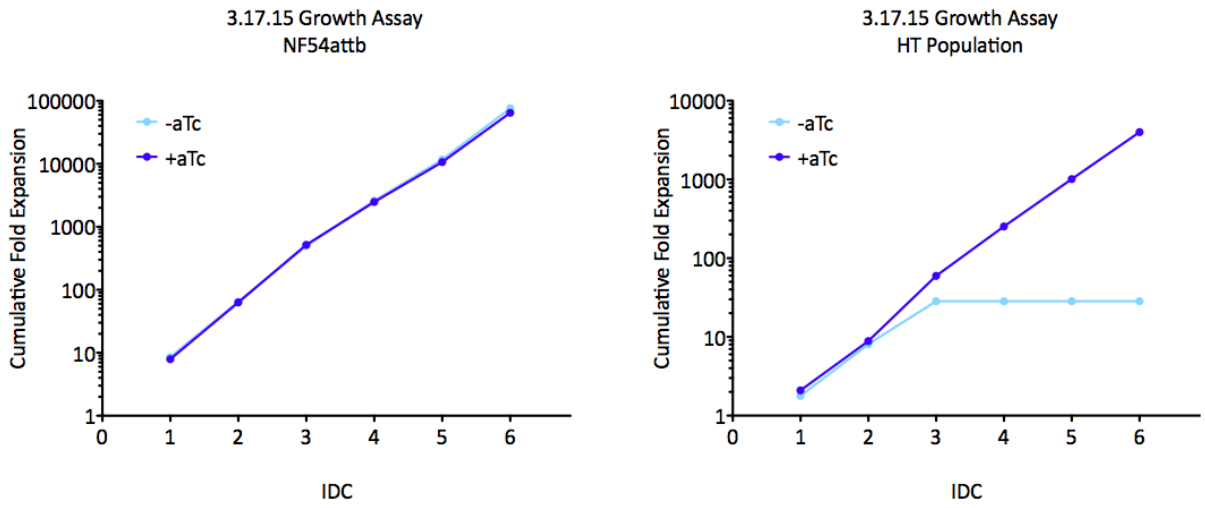

Figure 69: Phenotypic growth assay of HT population plus and minus aTc compared to the NF54attb control (started on 3.17.15).

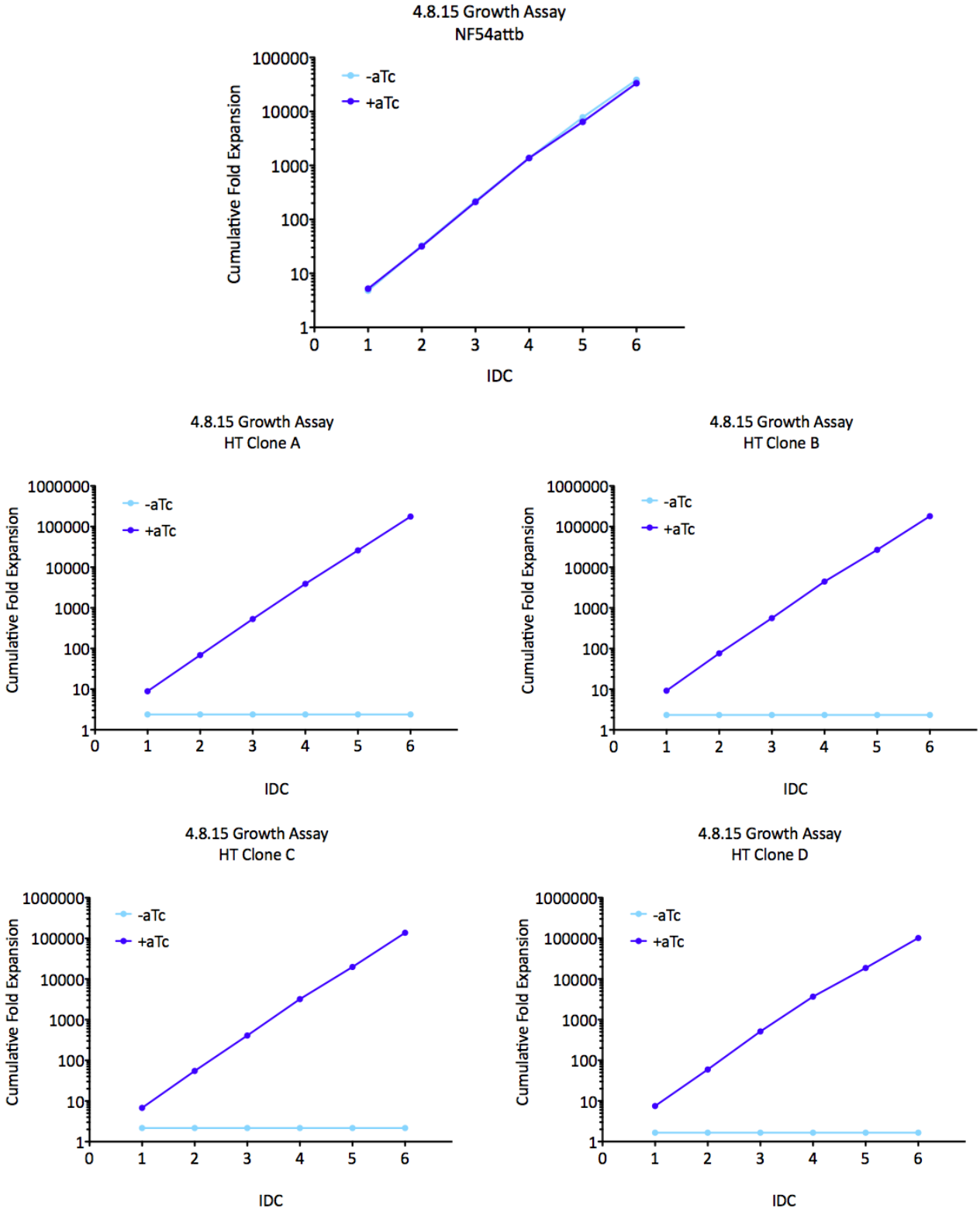

Figure 70: Phenotypic growth assay of HT clones A, B, C and D plus and minus aTc compared to the NF54attb control (started on 4.8.15).

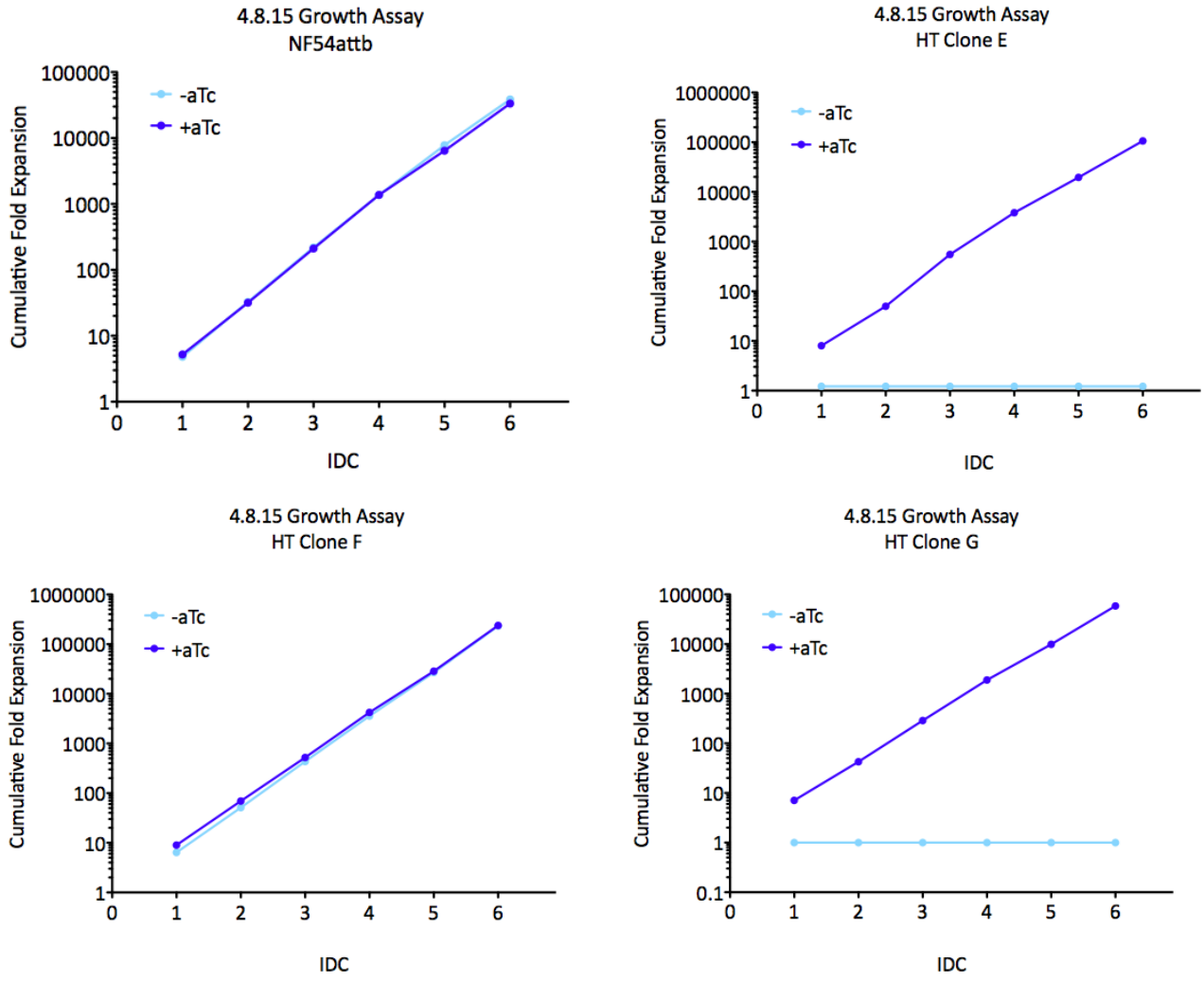

Figure 71: Phenotypic growth assay of HT clones E, F, and G plus and minus aTc compared to the NF54attb control (started on 4.8.15).

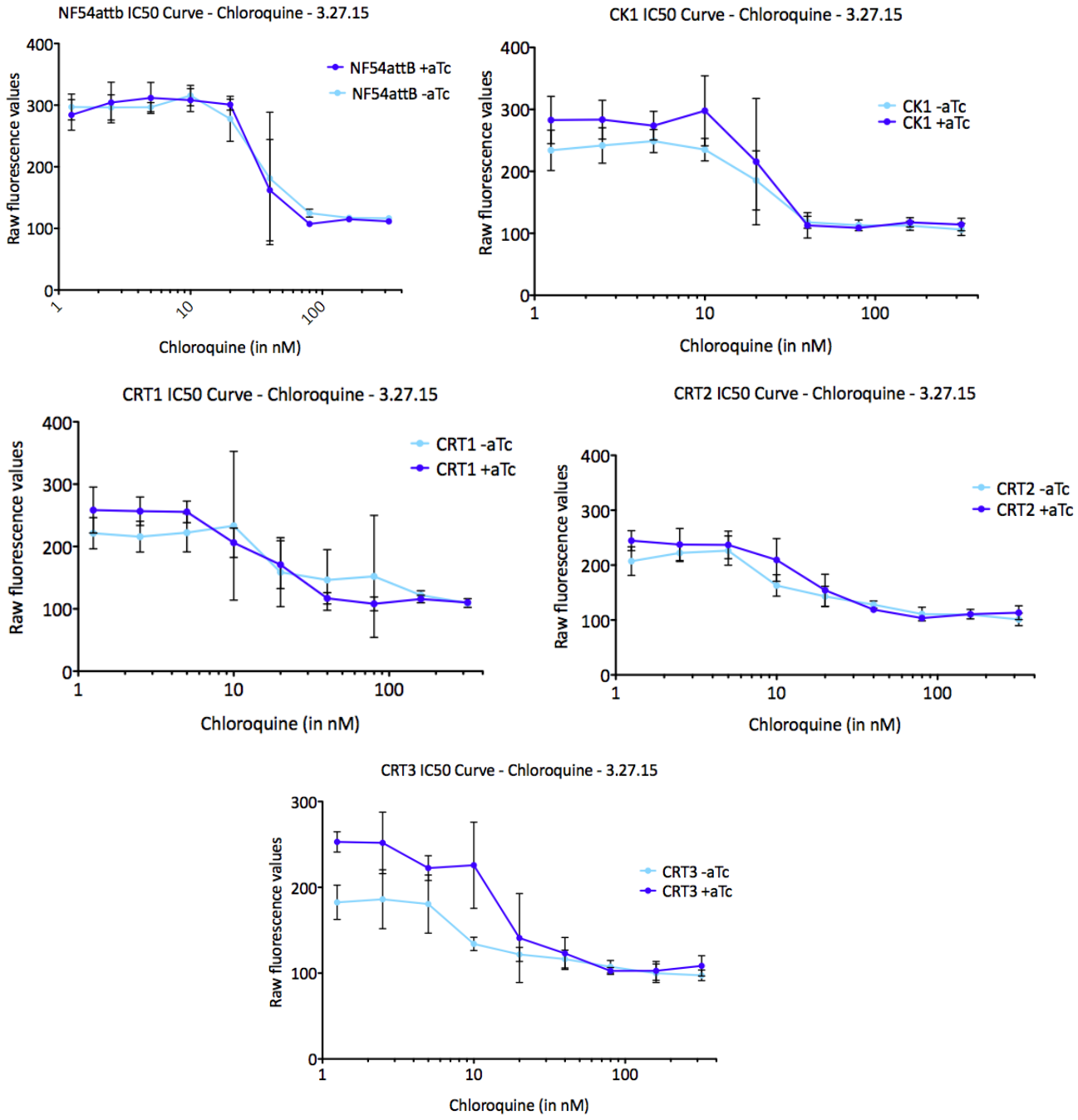

Figure 72: IC50 curves of chloroquine-challenged parasite strains +/- aTc (from experiment on 3.27.15).

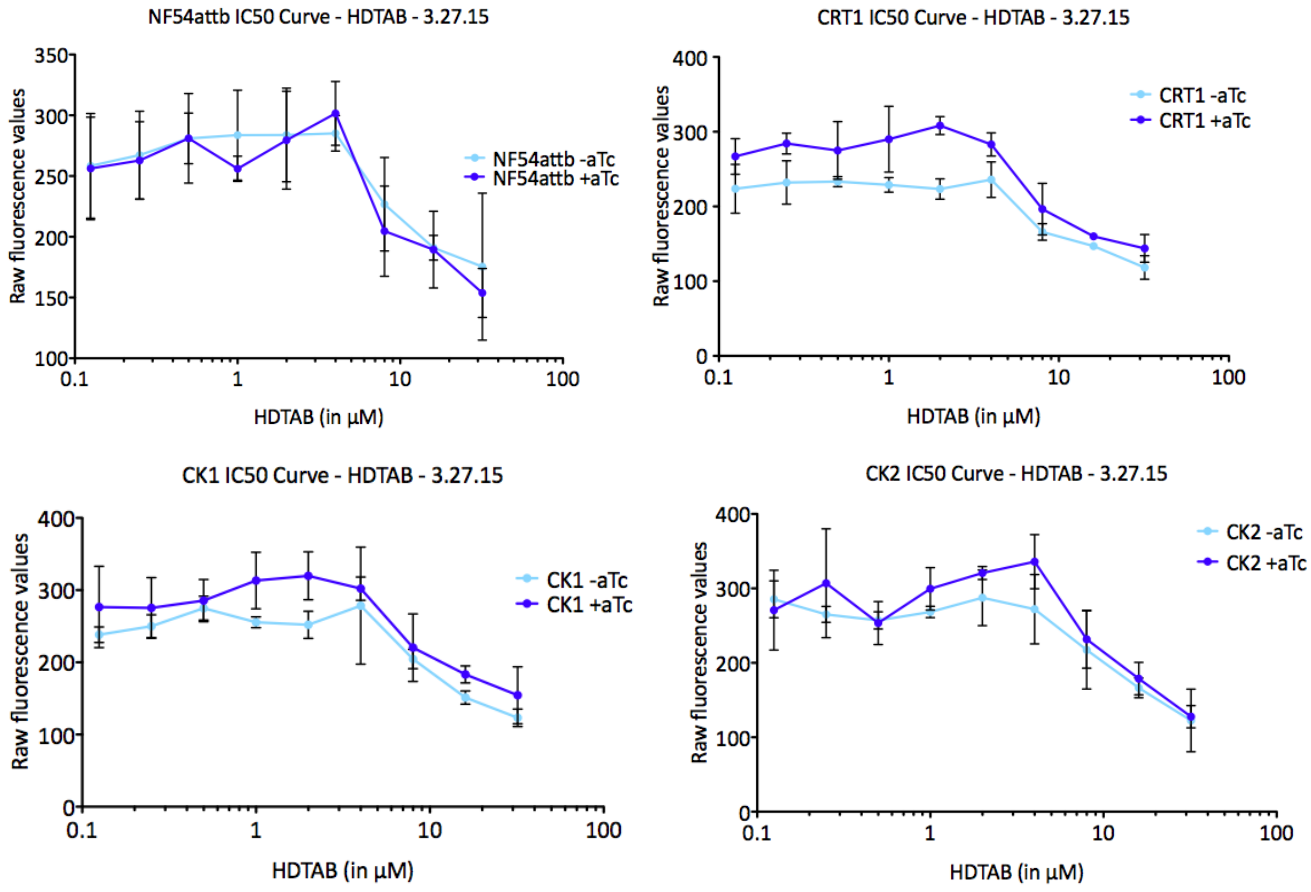

Figure 73: IC50 curves of HDTAB-challenged parasite strains +/- aTc.

3.3 Discussion

Three different genes were conditionally expressed using the TetR aptamer system in the 5' of the gene. Hexose transporter was shown to have a growth defect as expected for a putative essential gene. GSK3 was not shown to have a growth defect, as expected for a known non-essential gene. TrxR did not display a growth defect as expected, but the lack of sufficient knock down in protein production could very well be the biological reason for this outcome. In order to ensure that the 5' aptamer portion of the toolkit is able to successfully probe those genes that are unable to be targeted with either the 3' or 5'/3' aptamer systems, two things must happen:

- A small promoter library should be utilized to expand the range of expression of the gene of interest; this is especially important to address the challenges faced when conditionally expressing enzymes like TrxR and CK. Once made, these strains will conditionally express the gene of interest at different strengths.
- The DiCre recombinase portion of the toolkit needs to be further troubleshooted and expanded to allow for determination of essentiality in strains like TrxR.

Additionally, there continue to be remaining questions about the constraints of the CRISPR/Cas9 system in the malaria parasite, and many will be answered as the number of targets attempted increases:

- Does the parasite have the ability to heal and accept donor DNA that is farther away from the cut site? Could this possibly reduce design constraints?
- Are their certain guide RNAs that are unable to guide the Cas9 nuclease to the cut site due to parasite epigenetics or shielding?

The future implications of the completion of this toolkit are many: once there is a method to knock down all genes, it will be a simple matter of going through the above steps to learn more about the biology of the many unknown genes in the parasite, and identifying potential drug targets.

3.4 Methods

3.4.1 Materials

- Abcam
  - Primary antibody (mouse, anti-GAPDH)
- Agilent
  - Hemo KlenTaq polymerase
- Biodyne
  - Nylon membrane (for southern blots)
- Biorad
  - Laemmli Blue 2X
- Bulldog Bio
  - 2 mm cuvette
- Cen-Med
  - Glycerolyte-57
- EMD Millipore
  - Secondary antibody (goat anti-mouse conjugated to HRP)
- Gibco Life Technologies
  - Albumax II
  - 1X PBS, pH 7.4
- Goldbio
  - Gentamicin
- Life Technologies
  - SYBR Green I stain
- New England Biolabs (NEB)
  - Gibson master mix
  - Restriction enzymes
  - 2 log ladder

  - Protein Plus ladder
- Pierce
  - myECL Imager
  - North 2 South Imaging kit
- Promega
  - Firefly Luciferase Detection Kit
- Qiagen
  - Qiamp DNA Blood Mini Kit
- Sigma
  - Primary antibody (mouse; anti-HA tag)
  - All remaining chemicals
- ThemoScientific
  - Anhydrotetracycline hydrochloride (aTc)
  - SuperSignal Femto West Kit
- US Biological
  - RPMI 1640 Medium
- Wis-BioMed
  - C-Chip Disposable Hemocytometer

3.4.2 Culturing *Plasmodium falciparum*

The 3D7 strain of *P. falciparum* was cultured in leukocyte-free human RBCs (stored in acid-citrate-dextrose anticoagulant; from Research Blood Components, Brighton, MA) under an atmosphere of 5% O_2, 5% CO_2, and 95% N_2 at 2% hematocrit as previous described [115]. Parasites were synchronized weekly at a consistent time with 5% sorbitol (w/v) as previously reported [116] to ensure appropriate parasite ages.

To transfect parasites, uninfected red blood cells were washed twice with Wash Media (RPMI media with only RPMI and HEPES-KOH). A solution of 200 µL wash media with 50 µg plasmid DNA was added to 200 µL packed uninfected red blood cells and electroporated using a 2 mm cuvette and an 8 pulse/365 volt program. For co-transfections, 50 µg of each plasmid was used, and for transfecting more than one plasmid, the mass was scaled to add up to 50 µg. Uninfected red blood cells were incubated at 37^{o}C for 1 hour and then washed twice with warm RPMI. Half was resuspended in 4 mL media in a 12 well plate. Next, 0.5 mL

infected red blood cells taken directly from a 10 mL culture was added to the plate. Media was changed daily, and drug selection was added on day four. Transfections were monitored using renilla luciferase.

When required, parasites were lysed with a solution of 0.5% saponin, and incubated on ice for 10 minutes. The solution was centrifuged at 5000g for 5 minutes, and cells were washed several times with the saponin solution to yield a clean pellet of parasites. Pellets were frozen -80^{o}C for future analysis.

Transgenic parasites were frozen down using the glycerolyte method, as previously described [139]. Briefly, 250 µL of packed infected red blood cells at approximately 10% parasitemia during ring stage were aliquoted into cryosafe tubes. Next, 85 µL of glycerolyte was added slowly, and the solution was incubated at room temperature for five minutes. Finally, 330 µL of glycerolyte was added slowly, and the aliquot was frozen at -80^{o}C.

To create isogenic strains, populations were cloned out on 96 well plates. Briefly, parasitemia was measured by flow cytometry and hemocytometer. Cells were diluted to a concentration of 0.5 or 0.25 parasites per well at 2% HCT, and 200 µL was aliquoted into each well of a 96 well plate. At this point, the media is changed from the drug media to simply RPMI + aTc. Media was changed every third day, and cultures were split on day nine. Starting on day 12, media was changed every other day, and clones were determined by media color change. Clones were moved to a 12 well plate and brought up to a volume of 5 mL at 2% HCT, with drug added. Those clones that do not survive past the re-introduction of drug selection likely had an episomal population of the vector that was lost during the weeks on only RPMI + aTc media. Once the clones are at a high parasitemia, they were re-analyzed for genomic locus editing by PCR, and frozen using the glycerolyte method. Plates were discarded when 28 days old.

RPMI Media

- RPMI 1640 Medium (10.4 g/L)
- Hypoxanthine (30 mg/L)
- 25 mM HEPES-KOH (7.0825 g HEPES/L)
- Gentamicin (50 mg/L)
- Albumax II (5 g/L)
- Sodium bicarbonate (2 g/L)

3.4.3 Flow cytometry to determine parasitemia of *Plasmodium falciparum*

An aliquot of 200 µL of parasites at 2% HCT were added to separate wells in a 96 well u-bottom plate and stained with SYBR green 1 for 30 minutes in a 37^{o}C incubator (0.2 µL per 1 mL RPMI). Parasites were washed twice with PBS and subsequently measured for SYBR green 1 expression on a flow cytometer. Uninfected red blood cells, both stained and unstained, were used for gating purposes.

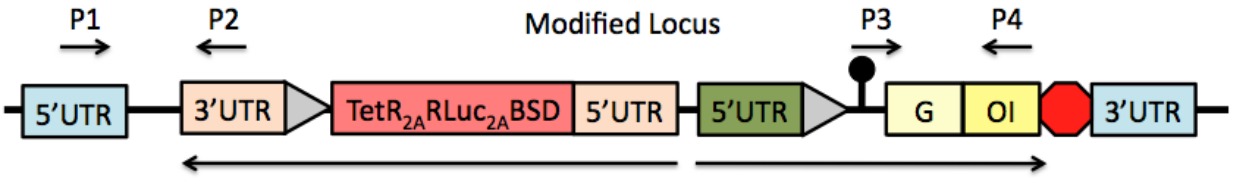

Figure 74: Representation of vectors and location of primers utilized for PCR and sequencing. The shared primer P2 is located between the left homologous region and the non-native 3' UTR for the resistance cassette, and the shared primer P3 is in the HA tag Primers 3 and 4 are located in the genome just beyond each homology region (in the non-recoded portion of the gene of interest).

3.4.4 Renilla luciferase assays to determine renilla luciferase expression

Every fourth day of a transfection, cultures were split 1:2; new blood was added to the culture maintained on the plate, and the culture that was removed was aliquoted into individual eppendorfs, and pelleted at 300g for three minutes. The supernatant was removed, and lysis buffer was applied. The solution was incubated at room temperature for 10 minutes to lyse the cell membranes, vortexed, and the renilla luciferase substrate was added in the dark. Individual renilla luciferase counts were determined using a luminometer.

3.4.5 Vector Design

Plasmids were designed by Sebastian Nasamu using the online application Benchling. Primers were ordered from IDT and sequencing was done by Genewiz. In order to detect editing of the genomic locus, a set of primers was designed. Each construct shared two primers, P2 and P3, and had two unique primers, P1 and P4 (Table 1 on page 89). Primers P1 and P2 allowed for inspection of the 5' insertion, and primers 3 and 4 allowed for inspection of the 3' locus. These primers are specific for genomic editing, and no products result from testing the original vector. After PCR products are run on a gel, they were gel-extracted and the sequence analyzed by Genewiz. An addition version of P3 designated "P3 aptamer" to examine the 3' locus was utilized to ensure the correct placement and sequencing of the 5' aptamer sequence (Figure 74 on page 88).

3.4.6 Genomic DNA Extraction

In order to test populations or clones of parasites, gDNA was analyzed by PCR. During transfections, the lysed parasites measured in luciferase assays were utilized as the raw material to be converted into gDNA using the Qiagen Qiamp Blood Mini Kit. In those populations that were visible by Giemsa stain, saponin-lysed parasites were resuspended in PBS and then processed in the same way using the Qiagen kit. Traditional methods were utilized for PCR of genomic DNA.

	Primer Sequence (5' to 3')
P2	cttcgcatctgggcagatgatgtc
P3	agctacccatacgatgttccag
P3 aptamer	
Chloroquine resistance transporter (CRT) - P1	gactttcgattgttcattctgtttattg
Chloroquine resistance transporter (CRT) - P4	agacaagaagtgaacaattggaaaaaggatacc
Thioredoxin reductase (TrxR) - P1	tattgaatggtaaggtttataatggaa
Thioredoxin reductase (TrxR) - P4	ctgggacattttcagctacgtctcctacagc
Glycogen synthase kinase 3 (GSK3) - P1	tataccatcatatttacaatatcgtgagtat
Glycogen synthase kinase 3 (GSK3) - P4	caaaagttgaacagctctggtagc
Hexose transporter (HT) - P1	cataatttgcgtacatagtaacctcataaaaaac
Hexose transporter (HT) - P4	cataacaaacgttgctacaatggaaag

Table 1: Primer sequences to detect editing of the genomic locus.

3.4.7 Growth Assay

Parasites were treated as described in Table 2 on page 91 to determine if there was a phenotypic growth phenotype with the removal of aTc (and hence, the removal of the expression of the gene of interest).

Fold expansion was calculated by dividing the final parasitemia as measured by flow by the starting parasitemia as measured by flow. An average was taken of the fold expansion in four replicate wells and this value was denoted the average fold expansion for a given IDC. To analyze the growth phenotype, the cumulative fold expansion was calculated by multiplying the values from the prior IDC. For example, if the average fold expansion of IDC 1 was 4 and the average fold expansion of IDC 2 was 2, the cumulative fold expansion of IDC 1 would be 4, and the cumulative fold expansion of IDC 2 would be 8. This allows for a clear separation of growth phenotypes.

3.4.8 Western Blot

Parasites were split into flasks of parasites with and without aTc, and harvested by saponin lysis after 2-4 IDCs. They were frozen at -80 prior to use. Parasite pellets were lysed at a ratio of approximately 1-2 µL parasites to 30 µL 1X Laemmli solution (a mixture of 475 µL water, 475 µL Laemmli Blue 2x and 50 µL beta-mercaptoethanol) and boiled at 95^{o}C for five minutes. The lysates spun down briefly to pellet the insoluble fraction and loaded into precast gels and run for approximately 40 minutes at 250 volts in a 1X SDS buffer. After separation by SDS-PAGE, gels were transferred to a PVDF membrane using an overnight wet transfer at 25 volts. Blots were blocked with 5% milk in TBST for three hours, followed by a three hour incubation with the primary antibody in 1% milk in TBST. Blots were washed three times with TBST and then incubated with a horseradish peroxidase-coupled secondary antibody for one hour. Blots were washed three times with TBST, and incubated with a 1:1 solution of SuperSignal West Femto substrate before image capture using a myECL Imager.

3.4.9 Southern Blot

The schematics of genomic and edited loci are provided for TrxR as an example (Figure 75 on page 92). Though not completed for this document, it is representative of the procedure with which to determine genomic locus editing.

The probe was amplified from genomic DNA using PCR and run on a gel to ensure size fidelity (Table 3 on page 93). The probe was gel extracted and biotinylated. Briefly, a solution of with a probe concentration of 100 ng was diluted into a total volume of 24 µL in a PCR tube. Next, a 10 µL volume of random heptamers was added, and the solution incubated at 99^{o}C for five minutes. The PCR tube was flash frozen in liquid nitrogen for five minutes, and then thawed to 4^{o}C. A mixture with dNTPs containing biotin-11-dUTP is added, as well as reaction buffer and Klenow. The reaction was incubated for one hour at 37^{o}C, and inactivated using EDTA. Probe was stored at -20^{o}C when not in use.

Equal amounts of genomic DNA from the NF54attb control, the population samples, or individual clones was digested overnight with the appropriate enzymes and run out on a non-EtBr 1% agarose gel. The DNA

Day	
1	Synchronize parasites.
2	Split parasites to approximately 2% parasitemia.
3	Determine exact parasitemia using flow cytometry. Split parasites down to 0.5% parasitemia and add blood to a final hematocrit of 1%. Add parasites to plate, four replicates per condition. Add media plus or minus aTc to plates, and place in the incubator.
4	Determine starting parasitemia of IDC 1.
5	Leave parasites in the incubator.
6	Determine final parasitemia of IDC 1. Split parasites down to approximately 1% parasitemia, add blood to a final hematocrit of 1%, and add appropriate media. Determine starting parasitemia of IDC 2.
7	Leave parasites in the incubator.
8	Determine final parasitemia of IDC 2. Split parasites down to approximately 1% parasitemia, add blood to a final hematocrit of 1%, and add appropriate media. Determine starting parasitemia of IDC 3.
9	Leave parasites in the incubator.
10	Determine final parasitemia of IDC 3. Split parasites down to approximately 1% parasitemia, add blood to a final hematocrit of 1%, and add appropriate media. Determine starting parasitemia of IDC 4.
11	Leave parasites in the incubator.
12	Determine final parasitemia of IDC 4. Split parasites down to approximately 1% parasitemia, add blood to a final hematocrit of 1%, and add appropriate media. Determine starting parasitemia of IDC 5.
13	Leave parasites in the incubator.
14	Determine final parasitemia of IDC 5. Split parasites down to approximately 1% parasitemia, add blood to a final hematocrit of 1%, and add appropriate media. Determine starting parasitemia of IDC 6.
15	Leave parasites in the incubator.
16	Determine final parasitemia of IDC 6.

Table 2: Description of growth assay to test essentiality of genes of interest.

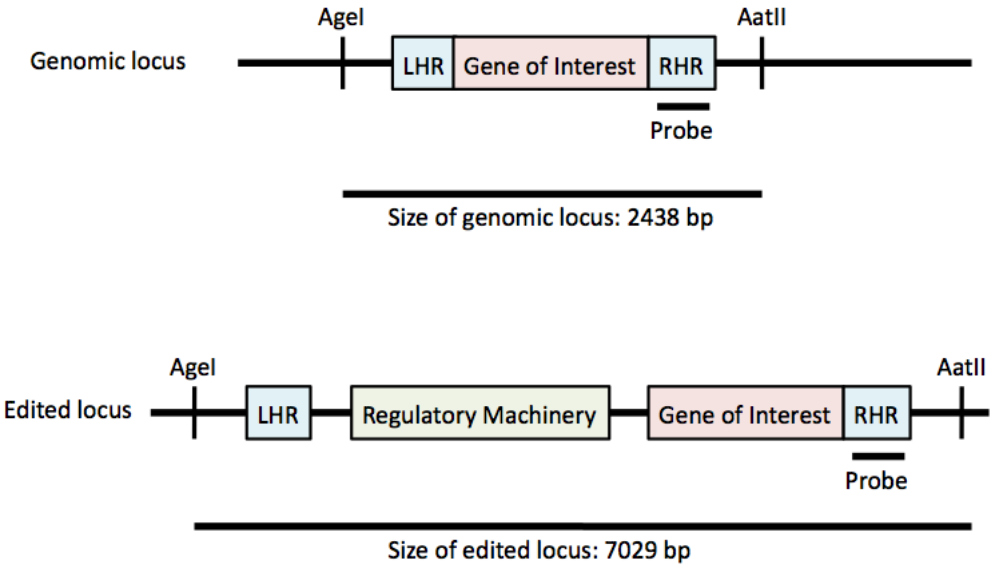

Figure 75: Schematic of genomic locus and edited locus for southern blot detection of thioredoxin reductase (TrxR). Present is the probe location in the right homologous region (the 3' part of the gene) and restriction sites for digestion. If the population of expressing plasmid is episomal, the size that will be seen on the blot is 14.6 kb.

was transferred to a Biodyne Plus positively charged membrane using a downward transfer capillary stack for two hours. The blot was neutralized and UV-fixed by a Stratalinker at 1200 joules. At this point, the blot could be stored indefinitely at room temperature in the dark.

To prepare the blot for hybridization, it was curled into a hybridization tube (DNA side facing in) and incubated for two hours in a hybridization oven at 55^{o}C. Meanwhile, 10 µL biotinylated probe was mixed with 190 µL 10 mM EDTA and heated at 99^{o}C for five minutes, and cooled to 4^{o}C. The probe was pipetted into the hybridization solution and hybridized overnight in the hybridization oven at 55^{o}C.

The next day, the hybridization buffer was carefully decanted and the blot was washed and prepared for imaging using the Pierce North 2 South kit. Image capture was performed using a myECL imager.

3.4.10 Phenotypic Test: IC50 Curves

Isogenic strains of the conditional knockouts for chloroquine resistance transporter and choline kinase were tested for their ability to withstand drug killing by their respective drugs in the presence or absence of aTC (and therefore their protein target). Chloroquine was tested against the chloroquine resistance transporter conditional knockouts, with one of the CK clones and NF54attb as controls. HDTAB was tested against the choline kinase knockouts, with one of the CRT clones and NF54attb as controls.

On day one, cultures were split into a plus aTc and minus aTc condition at between 5-10% parasitemia. Media was changed as normal for one IDC in order to provide a starting point without the expression of

	Primer Sequence (5' to 3')
Thioredoxin reductase (TrxR) - 5'	aagaaattagttacaactgtacaatctcacatacgttcat
Thioredoxin reductase (TrxR) - 3'	cttcgctgatgagtttctgttgcgcccgggacaatcaatgtctccttttcttccaatagc
Glycogen synthase kinase 3 (GSK3) - 5'	ccaatttttcgggacagtcaagtgtggatcagctagtta
Glycogen synthase kinase 3 (GSK3) - 3'	ctgatgagtttctgttgcgcccgggacaaatgcatggatctcgtagttcatcaaaaaagg
Hexose transporter (HT) - 5'	ggcttatgtttttatttccttctgtcatatcattaatagg
Hexose transporter (HT) - 3'	gctgatgagtttctgttgcgcccgggacaataaataagcaactaaaactcctacacatcc

Table 3: Primer sequences for southern probes.

the gene of interest. On day three, parasites were synchronized and then measured using flow cytometry. The parasites were diluted to 2% parasitemia at 1% HCT. Stocks of gene of interest inhibitors were made: chloroquine at 2.56 mM (0.0132 g/10 mL RPMI) and gexadecyltrimethylammonium bromide (HDTAB) at 256 mM (0.933 g/10 mL DMSO). The highest concentrations on the plate, 2.56 µM for chloroquine, and 256 µM for HDTAB, was made by a 1:1000 dilution of the stock into RPMI. A 96 well plate was set up with 100 µL RPMI in all columns but the first column, in which 200 µL of the diluted drug solution was aliquoted, and the last column, to which 200 µl RPMI alone was added (drug concentration of zero). A 1:2 dilution series was accomplished by taking 100 µL from column A and adding it to column B. 100 µL was then taken from column B and aliquoted into column C, and so on. Next, 100 µL of the 2% parasitemia at 2% HCT was added to each well on the plate. This results in a final pyrimethamine series from 0 to 125 µM, and a parasite concentration of 1% at 0.5% HCT, a known concentration that allows untreated parasites to thrive through the end of the current IDC and one additional IDC. Plates were put back into the incubator and left undisturbed. On day six, 50 µL of resuspended parasites were aliquoted onto a black plate, and were lysed with 50 µL parasite lysis buffer (20 mM Tris at pH 7.5, 5 mM EDTA, 0.008% saponin, and 0.08% Triton-X 100) that also contained SYBR green 1. Parasites were allowed to lyse overnight in the dark, and SYBR was measured the next day with an excitation value of 485 nm and an emission value of 530 nm.

4 Creation of a mutator strain to study drug resistance in *Plasmodium falciparum*

4.1 Introduction

Drug resistant malaria has arisen against every antimalarial employed against the disease [14]. Learning more about resistance is given top priority by the World Health Organization. Determining resistance potential of new drugs and drug combinations before they are released into clinical use is desirable, and once there is a method to test resistance potential, it can be an important component of the drug development process. However, studying drug resistance in the laboratory is hampered by many factors [15].

First, while there have been drug resistant strains selected *in vitro* for almost 40 years, the process remains time-consuming and unpredictable. Artemisinin is currently the first choice for treatment, and is now used in the form of artemisinin-combination therapy, since parasites resistant to artemisinin are now commonplace. Yet, until 2014, artemisinin-resistant parasites had not been created *in vitro*. Indeed, in 2012, a review of the molecular markers of resistant malaria began their section of artemisinin with the sentence:

> The search for molecular markers for artemisinin resistance via a genetic approach of selecting for resistance and identifying mutations that might be causal for resistance has been severely hampered by the difficulties in selecting stably resistant lines in vitro [140].

There is a very telling sentence in that particular manuscript that perfectly summarizes the time-consuming nature of selecting drug resistant parasites *in vitro*:

> The artemisinin-resistant F32-ART5 parasite line was selected by culturing the artemisinin-sensitive F32-Tanzania clone under a dose-escalating regimen of artemisinin for 5 years [141].

Second, connecting a phenotype to a genotype is particularly challenging, meaning that while chloroquine resistance was first identified in the field in 1965, connecting the resistance phenotype to mutations in PfCRT, the chloroquine resistance transporter, took much longer, and the mechanism of resistance is still not well understood [142].

Third, choosing a strain with which to attempt to induce drug resistance is challenging. It is difficult to recreate the genetically diverse population of parasites found in the wild in a laboratory setting. Utilizing a single isogenic strain, whether it is a recent isolate from the field or one that has been passaged many times *in vitro*, cannot capture the great variety of parasites intermixing in both the mosquito vector and the human host. While patient isolates have been used successfully, these strains are not isogenic or well-characterized. Indeed, these isolates are often possess more than one parasite strain, and as such, it is more difficult to accurately judge and characterize drug susceptibility prior to inducing drug resistance [140].

Laboratory strains that have been passaged for long lengths of time are often better understood, yet their capacity to produce mutants successfully *in vitro* is unreliable. Strains that are classified as having "accelerated resistance to multiple drug strains" (AMRDs) have been used to assess the development of resistance

to new antimalarials, yet these are still time-consuming experiments that do not necessarily offer a complete assessment of the likelihood of a drug's resistance potential once it is used in the field [143]. For example, the HB3 parasite strain is susceptible to all antimalarials except pyrimethamine, and when on chloroquine pressure for 30 months, the resulting strains were only slightly more resistant than the wild type strain [144]. Yet, high mefloquine pressure on the W2 strain, a parasite line resistant to many antimalarials including a low concentration of mefloquine, resulted in no parasites capable of withstanding the higher mefloquine concentration [145, 146].

It takes 10 to 20 years to develop a new drug for the treatment of malaria, and unfortunately, the development of drug resistance against newer drugs like atovaquone is happening on a time scale of 1 year, in contrast to the 15 years it took for parasites to become resistant to chloroquine [147]. Ultimately, the combination of the time it takes to develop a new antimalarial and the time with which resistant parasites are found has created an untenable environment within which to fight the disease. Truly, it is essential to remember that the cost of antimalarial resistance is very high. The development of drug resistance does not just affect the individual patient's ability to respond to treatment. It fundamentally shifts the population of parasites in the field, the spread of which increases the burden of disease in many ways, as well-displayed by the World Health Organization's Global Report on Antimalarial Drug Efficacy and Drug Resistance [148] (Figure 76 on page 96). More must be done to mitigate these effects.

4.1.1 Creating Drug Resistant Strains in the Laboratory

The first drug resistant strain created in vitro was reported in 1978. Nguyen-Dinh et al slowly increased the concentration of chloroquine over a period of time to yield mutants that were able to tolerate three times the normally lethal concentration [159]. Thus began the challenge to create and characterize drug resistant lines to both learn about drug resistance mechanisms, both before and after anti-malarials are released for clinical use. Nzila et al reviewed the literature on creating drug resistant mutants in vitro in 2010, and their summary is listed and expanded in Table 4 on page 97 and Table 5 on page 98 to include references through 2015 [15].

With such challenges present and such a wide variety of methodologies with inconsistent results, it is worthwhile to consider other tactics in creating drug resistant mutants.

4.1.2 DNA Repair Mutant Parasite Strains

The development of drug resistance is caused by genomic instability, to which there are many contributing factors: the fidelity of replication and DNA repair, cell cycle genes, ubiquination, nucleus architecture, chromatin dynamics, presence or absence of certain inorganic nutrients (enzyme co-factors), and hypoxia/oxidative stress. While it is known that in *P. falciparum*, clindamycin-resistant mutants possess subtelomeric instability [176], the main focus of research in development of drug resistance and genomic instability in the parasite has been related to DNA repair.

In other organisms, from bacteria [177] to other parasites [178] to human cancer cells [179], defects in DNA repair are linked to increased mutation rates. In particular, one mouse study has shown that interfering with DNA repair creates parasites with a high mutation rate:

BOX 2. EFFECTS OF ANTIMALARIAL DRUG RESISTANCE ON GLOBAL MALARIA CONTROL	
Disease burden	• The appearance of chloroquine resistance in Africa led to an increase in hospital admissions (Zucker et al., 1996). • Increasing mortality trends were found at community level (Trape et al., 1998; Korenromp et al., 2003). • Ineffective treatment causes anaemia and low birth weight (Björkman, 2002) and renders the health of children and adults infected with *P. falciparum* or *P. vivax* more fragile (Tjitra et al., 2008). • Resistance to antimalarial drugs was implicated, at least partially, in malaria epidemics (Warsame et al., 1990). • Resistance to antimalarial drugs is associated with increased transmission (Price & Nosten, 2001).
Economic cost	• Resistance to antimalarial drugs has increased the global cost of controlling the disease, including the cost of new drug development (Phillips & Phillips-Howard, 1996). • Therapeutic failure requires consultation at a health facility for further diagnosis and treatment, resulting in loss of working days for adults, absence from school for children and increased cost to the health system (Talisuna, Bloland & D'Alessandro, 2004).
Changes to distribution of malaria species	• The proportion of *P. falciparum* malaria has changed, such as an increase with respect to *P. vivax* (Dash et al., 2008).
Access to high-quality treatment	• Ineffective treatment in the public sector due to resistance could lead to greater reliance of patients on the unregulated private sector, which in turn could increase the use of monotherapies or substandard and counterfeit medicines and increase the risk for drug resistance.

Figure 76: Taken directly from the World Health Organization's Global Report on Antimalarial Drug Efficacy and Drug Resistance[148]. Those papers cited in the chart are cited in the bibliography [149, 150, 151, 152, 153, 154, 155, 156, 157, 158].

Drug	Strain	Drug Resistance Profile of Strain Prior to Testing	Ri (IC50)	Time Required to Select Resistance	Stability	Reference
Chloroquine	FCR3	Chloroquine and cycloguanil	–	4 months	1 month	[159]
Chloroquine	FAC8	Chloroquine	2.34 (83 ng/mL)	–	1 month	[160]
Chloroquine	HBE	Pyrimethamine	1.64 (28 ng/mL)	30 months	–	[144]
Chloroquine	106/01	Chloroquine	12 (37 nM)	2 months	–	[161]
Melfoquine	FCK	Chloroquine	16 (8 nmol/L)	3 months	–	[162]
Melfoquine	Smith	Chloroquine, pyrimethamine and sulfadoxine	3.4 (3.5 µg/L)	–	–	[163]
Melfoquine	Camp	Chloroquine	2.4 (4.9-12 µg/L)	–	6 months	[163]
Melfoquine	W2	Chloroquine, pyrimethamine and sulfadoxine	4.6 (4.5 nM)	22.4 months	12 months	[164]
Melfoquine	K1	Chloroquine, pyrimethamine and sulfadoxine	4.07 (22.4 ng/mL)	–	–	[146]
Melfoquine	W2mef	Chloroquine, pyrimethamine, sulfadoxine, and mefloquine	1.41 (58.88 ng/mL)	–	–	[146]
Melfoquine	W2mef	Chloroquine, pyrimethamine, sulfadoxine, and mefloquine	1.07 (15.2 ng/mL)	18 months	–	[145]
HFT	T9.96	Chloroquine	3.3 (6.6-22 nM)	6 months	6 months	[165]
HFT	K1	Chloroquine, pyrimethamine and sulfadoxine	9 (2.2 nM)	2 months	–	[165]
Pyrimethamine	FCR3	Chloroquine and cycloguanil	– (15 nM)	7 months	–	[166]
5-fluoro-orotate	W2	Chloroquine, pyrimethamine and sulfadoxine	100 (2 nM)	2 months	–	[167]
5-fluoro-orotate	FCR3	Chloroquine and cycloguanil	–	2 months	–	[167]
Atovaquone	W2	Chloroquine, pyrimethamine and sulfadoxine	30 (3 nM)	2 months	–	[167]

Table 4: The table from Nzila et al. [15] summarizing work creating resistant strains in vitro was revised and expanded to include references through 2015. Ri is the resistance index (the ratio of the IC50 of the selected parasite line to the IC50 of the parent strain prior to drug pressure). Stability refers to the time that the cultures retain resistance when the drug pressure is removed.

Drug	Strain	Drug Resistance Profile of Strain Prior to Testing	Ri (IC50)	Time Required to Select Resistance	Stability	Reference
Atovaquone	K1	Chloroquine, pyrimethamine and sulfadoxine	837 (13.6 nM)	–	$<$ 3 months	[168]
BMS-3888891	Dd2	Chloroquine, pyrimethamine, sulfadoxine and quinine	12 (10 nM)	2.66 months	–	[169]
N-89	FCR3	Chloroquine and cycloguanil	10 (25 nM)	24 months	–	[170]
Azithromycin	Dd2	Chloroquine, pyrimethamine, sulfadoxine and quinine	15.3 (124 nM)	0.7 months	–	[171]
Azithromycin	7G8	Chloroquine and pyrimethamine	17.5 (228 nM)	0.7 months	–	[171]
Lumefantrine	V1S	Chloroquine	15.0 (32 nM)	16 months	2 weeks	[172]
PfDHODH Inhibitors	3D7/Dd2	none / Chloroquine, pyrimethamine, sulfadoxine and quinine	Varied depending on mutation, see extensive list of values in cited paper	30-100 days	–	[173]
Artemisinin	F32	–	IC50 not used as measurement (used ring stage survival assays)	5 years	–	[141]
Artelinic acid	W2	Chloroquine, pyrimethamine and sulfadoxine	5.5 (23.3 nM)	28 months	–	[174]
Artelinic acid	TM91C235	–	3.0 (33.7 nM)	28 months	–	[174]
Artelinic acid	D6	none	3.8 (34 nM)	28 months	–	[174]
Fosmidomycin	Dd2	Chloroquine, pyrimethamine, sulfadoxine and quinine	8 (2200 nM)	6 weeks	–	[175]

Table 5: The table from Nzila et al. [15] summarizing work creating resistant strains in vitro was revised and expanded to include references through 2015. Ri is the resistance index (the ratio of the IC50 of the selected parasite line to the IC50 of the parent strain prior to drug pressure). Stability refers to the time that the cultures retain resistance when the drug pressure is removed.

- Honma et al found that the rodent malaria parasite *P. berghei* expressing a defective DNA polymerase δ had defective proofreading 3' to 5' exonuclease activity and had an 85 fold higher mutation rate in comparison to parasites expressing a wild type polymerase when parasites were passaged in mice [180].

4.1.3 Antimalarial Resistant Strains Developing from DNA Repair Mutant Parasite Strains

Bacterial strains with defects in DNA repair are classified as mutators, and they have been found to increase the frequency of drug resistance by up to 1000 times the frequency with which it would occur in non-mutator cells [177]. In the field of antibiotics, hypermutators have been used to assist in the characterization of new potential drugs and the development of drug resistance [181, 182, 183].

Importantly, development of drug resistance has been linked to parasite strains that are DNA repair mutants:

- Castellini et al investigated the characteristics of several accelerated resistance to multiple drugs (ARMD) strains of *P. falciparum* and found that some have defective DNA mismatch repair, while several non-ARMD strains were proficient in DNA mismatch repair [184].
- Bethke et al found that *P. berghei* parasites passaged in mosquitoes with a disrupted PbMSHR2-2 locus had an elevated frequency of resistance after drug pressure was applied compared to a wild type control, though their particular studies did not show any increase in the development of drug resistance when the parasites were passaged in mice alone [185].
- Trotta et al found that two strains with known drug resistance profiles had much lower rates of DNA repair when irradiated with UV light (D6 is resistant to mefloquine and W2 is an ARMD strain) [186].

Thus, one particular strategy that could overcome the limitations of isolated strains is to develop a DNA repair mutant in the parasite, and examine the resulting strain for a mutator phenotype. Indeed, this was one of the recommendations of Nzila et al [15]: create a DNA repair mutant strain to be the basis for testing drug resistance.

4.1.4 Potential Target: Uracil DNA Glycosylase

Plasmodium falciparum lysates were tested for their ability to remove uracil from DNA, and were found to be positive for uracil DNA glycosylase activity [187]. Additionally, malaria parasite relatives trypanosomes that have uracil DNA glycosylase knocked out present a mutator phenotype [178]. There is redundancy in DNA repair enzymes, so it is unlikely that UDG is an essential gene.

However, several attempts to knock out the endogenous uracil DNA glycosylase failed, as did an attempt with the CRISPR/Cas9 system developed by Jeffrey Wagner (note: this attempt was made as a traditional knockout, not as a conditional knockout). In additional, recently published evidence suggests that the *Plasmodium falciparum* uracil DNA glycosylase could be essential [188]. This data is not direct and conclusive evidence that the gene is essential, but the fact that a chemical compound inhibits endogenous uracil DNA glycosylase activity in lysates as well as inhibits parasite growth could mean that knocking out this gene will be difficult, as we saw.

4.1.5 Potential Mutator Strain Technique: Expression of a Gain of Function DNA Repair Mutant

Another common way to create a DNA repair mutant is by expressing a gain of function mutant to disrupt the careful balance of DNA repair pathways [189]. In particular, several DNA glycosylase mutants have been developed, and their ability to remove other bases from the genome is well-documented in yeast [190, 191]. Expressing this particular gene in the parasite could create a well-defined strain upon which to test drugs for their mutator potential. Even better, this gene could be conditionally expressed or under several different promoters to change the mutator characteristics to offer up a test set for new drugs with a titrated mutator capability.

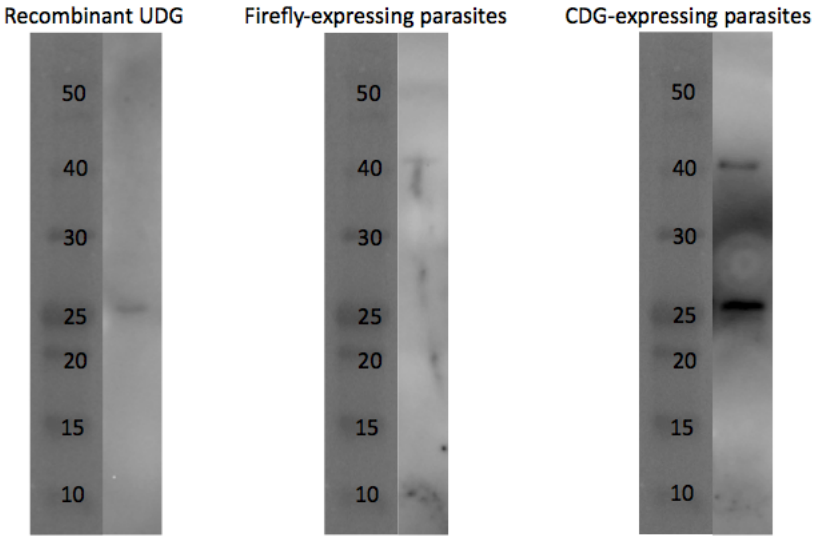

Figure 77: The primary antibody for this western blot is from Abcam and recognizes a motif from uracil DNA glycosylase, a motif shared by cytosine DNA glycosylase. Lane 1 was loaded with recombinant human UDG from New England Biolabs (size: 25.7 KDa). Lane 2 was loaded with firefly luciferase-expressing parasites. Lane 3 was loaded with cytosine DNA glycosylase-expressing parasites. Cytosine DNA glycosylase is 25.8 KDa. The putative *Plasmodium falciparum* uracil DNA glycosylase (UDG) is 37.46 KDa.

4.2 Results

4.2.1 Successful Expression of Cytosine DNA Glycosylase (CDG) in *Plasmodium falciparum*

Parasites were transfected with the circular plasmid encoding the gene for cytosine DNA glycosylase (CDG). Once parasites recovered, a population was brought up and tested for expression of the gene using a western blot (Figure 77 on page 101). The gain of function mutant CDG was detected using an antibody originally designed for an epitope of uracil DNA glycosylase.

In order to gauge functionality of the expressed CDG, a TUNEL assay was attempted to detect abasic sites, with and a preliminary result showed that CDG-expressing parasites had an increased number of abasic sites (data not shown). However, later assays proved to have unreliable results with control cells, making it difficult to make strong conclusions about the data. Before functionality of the enzyme can be concluded, this assay will require further troubleshooting.

4.2.2 Experimental design: efficiently define mutator phenotype characteristics

There are many methods to characterize and define the mutator status of a given population of interest. These include health assays [192, 193], gene reversion tests [194] and probing the population with selected mutagens [195, 196, 197]. As this strain is being designed for use with anti-malarials, utilizing these drugs for the initial test is appropriate.

There are several variables to keep in mind when choosing an anti-malarial. First, the drug must be accessible, both in terms of cost and procurement.

Second, it must have already been used to successfully make a resistant strain in the laboratory. While one potential end use of this mutator strain is to address the challenges of drugs where mutants have not been made in the laboratory, a proof of concept with an already-studied drug is prudent.

In this case, pyrimethamine was an obvious choice. It is well-studied, inexpensive, and easy to buy [166, 15]. Furthermore, when the most commonly cited mutations are examined, one stands out as resulting from a mutation from a GCA codon (alanine) to a GTA codon (valine), consistent with the mechanism of action of cytosine DNA glycosylase [191].

Third, the drug concentration must be chosen. The ideal drug concentration is one that kills all of the parental strain yet allows resistant parasites present in the population to thrive (Figure 78 on page 103). This range is difficult to determine without empirical evidence, since the particular IC50 of the resistant line that will be created is unknown at the start of the experiment. Notably, not all parasites that are resistant to the same drug have the same mechanism of action, meaning the IC50 of these strains can vary significantly [145, 146, 198]. Drug resistant lines have been created by application of a great variety of drug concentrations, but for the purposes of this experiment, exceeding the IC100 value should allow for isolation of resistant parasites in a shorter time frame. Additionally, drug resistant parasites have been created in vitro using sub-lethal doses and a step-up method that slowly increases the drug concentration over time [15].

Fourth, the application style must be decided. There are many options, and no true gold standard exists. Instead, there is a varied set of protocols that have allowed for the creation of drug resistant lines in vitro in the past [199]. An experiment that makes use of an initial bolus of drug followed by removing said drug can be effective, but there can be non-resistant escapes using this method, especially given the fact that different drugs affect the parasite at different stages in the life cycle. These can be avoided by designing an assay that relies on drug cycling: essentially, you add an initial amount of drug, remove it, and then at designated intervals, add the drug back in to ensure all the present parasites in the population are resistant. However, the most rigorous method for creating drug resistant parasites requires a constant administration of a drug. Again, the concentration of drug administered is crucial here: if the concentration is too low, non-resistant parasites will persist. If the concentration is too high, even resistant parasites will all be killed.

Finally, a means to assess the mutator status must be determined. In all cases, the response of a putative mutator strain is compared to a non-mutator strain. Deep sequencing to search for mutations would be ideal, but it is expensive and time-consuming. More targeted sequencing of a few select genes can also be useful, and the *Plasmodium falciparum* gene dihydrofolate reductase (DHFR) is standard choice in the field. A standard methodology in other organisms is a reversion test [194]. However, this option is less feasible since creating a transgenic strain of *Plasmodium falciparum* can be an incredibly time intensive task. [200].

One way to assess mutator strains is to make two flasks of parasites: one control, one putative mutator. In this case, it would be firefly luciferase-expressing parasites as the control strain, and cytosine DNA glycosylase-expressing parasites as the putative mutator strain. The strains are both treated with the same concentration of a different drug, and the time that it takes to develop resistant parasites is a numerical

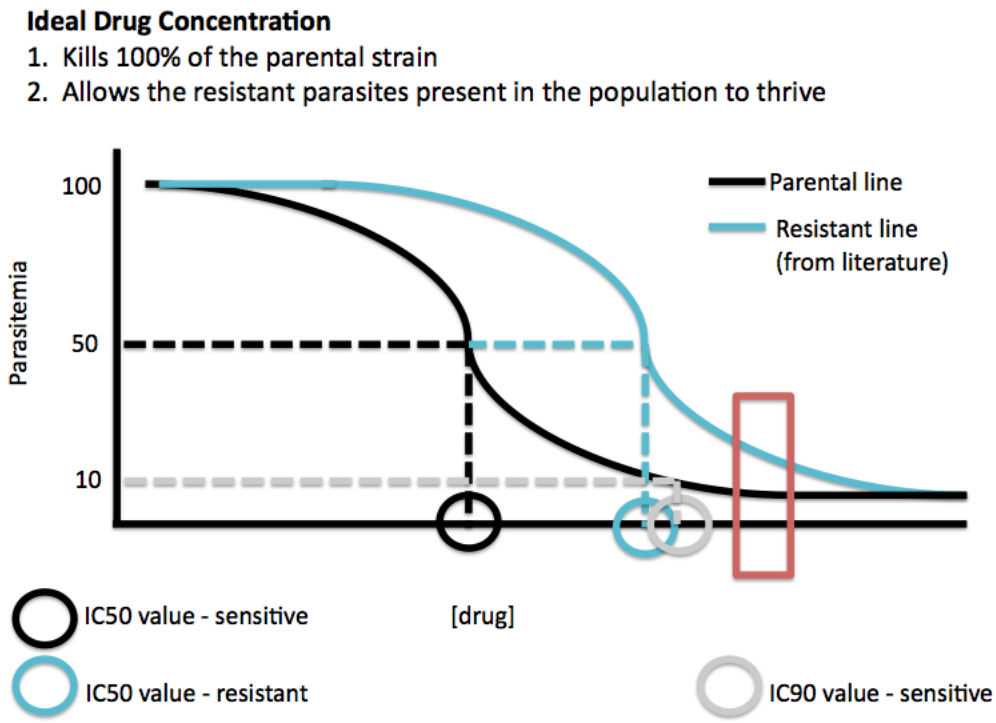

Figure 78: Determining the appropriate drug concentration for application requires knowledge of the IC50 of the parental line as well as resistant lines from the literature.

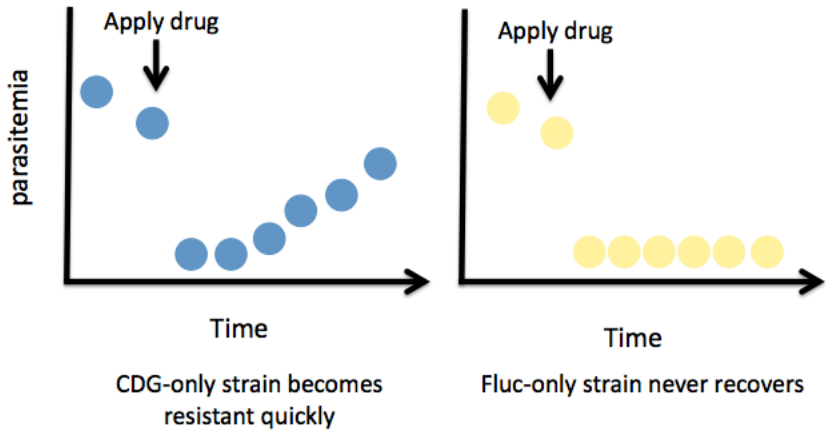

Figure 79: Assessing mutator strains with two separate flasks of parasites, one control (Fluc-only) and one putative mutator (CDG-only). In this hypothetical instance, the Fluc-only strain never recovers, while the CDG-only strain becomes resistant. Another possible scenario could be the recovery of the Fluc-only strain, but in a longer time frame.

yet ultimately qualitative measurement of mutator status (Figure 79 on page 104). Of note: this type of experiment does not account for small variations in the individual culture flasks. Things like absolutely hematocrit (the percentage of red blood cells) and mixing of the cells to expose them to drug can be attempted to be controlled, but the only way to ensure that an experimental set is treated exactly the same is to have the strains together in the same flask.

This would result in a competition assay: essentially, the mutator strain would directly compete against the control strain under drug pressure in the same flask. Therefore, the dynamics of the population as it shifts over time could be utilized as a more quantitative and precise assessment of mutator status. A panel of different starting concentrations of parasite strains could also be used to further define the characteristics of the putative mutator strain (Figure 80 on page 105).

The last component of experiment is ensuring that the population dynamics are measurable. In this case, the control strain expresses firefly luciferase, an enzyme with an easily-measurable output using a commercially available kit-based luminometer assay. Before continuing with the experiment, the raw data for firefly luciferase must be measured and correlated to absolute parasitemia counts, as measured by flow cytometry.

4.2.3 Correlating Firefly Luciferase Results to Parasitemia

In order to properly and efficiently measure the percentage of a given population that expresses firefly luciferase, a dilution series of firefly luciferase-expressing parasites was made and measured both on the flow cytometer using SYBR-green staining and a firefly luciferase detection kit (Figure 81 on page 105). This provided an equation by which to estimate the number of parasites that match up with a given raw value of luciferase.

Next, mixtures of firefly luciferase-expressing and CDG-expressing parasites were measured for firefly luciferase activity and their parasitemia was measured using flow cytometry. At this point, the parasitemia

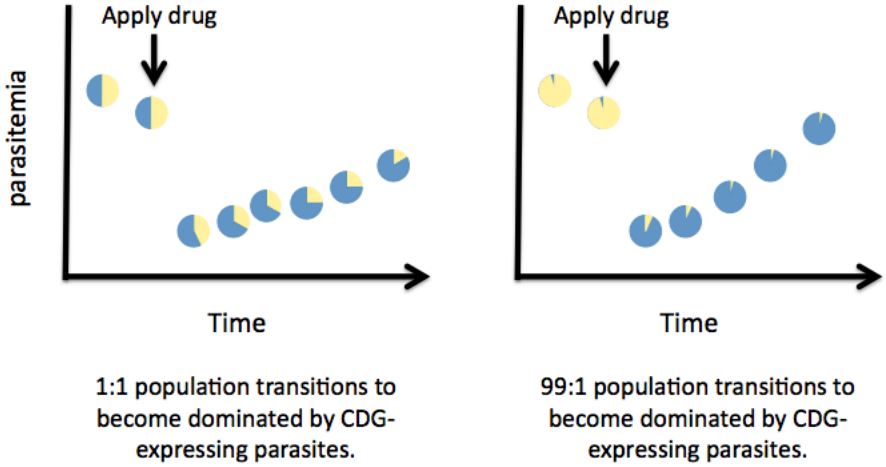

Figure 80: Assessing mutator strains with flasks of mixed populations. Strains are mixed in known concentrations as determined by flow cytometry, and then drug is added. With this setup, the dynamics in the population serve as a more quantitative readout in defining mutator status.

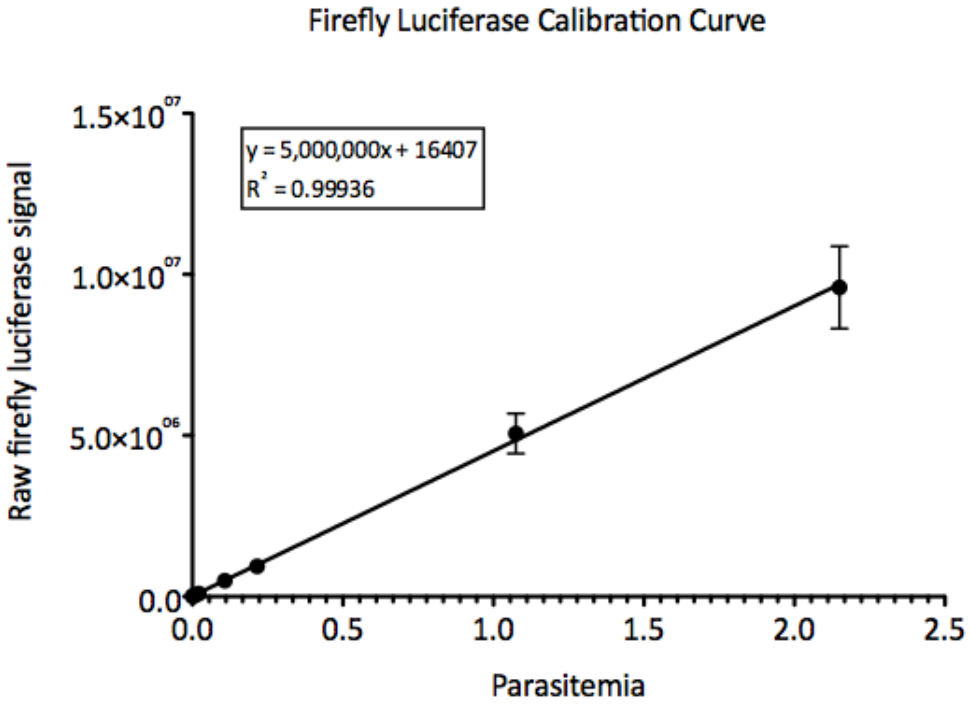

Figure 81: Calibration curve of firefly-expressing parasites.

of firefly-expressing parasites in the mixture was back-calculated based on the calibration curve (Figure 81 on page 105) and compared to the actual parasitemia of firefly luciferase-expressing parasites (Figure 82 on page 107).

The success of this test means that the percentage of a mixed population that expresses firefly luciferase can be tracked over time and used to determine the population dynamics of a strain.

4.2.4 Determining IC50 Value of Pyrimethamine

The IC50 value of pyrimethamine is known for pyrimethamine-sensitive strains in the literature, yet, confirming the drug's capability to kill the strains in this experiment and confirming the IC50 is important before proceeding with the initial drug challenge experiment. When parasites were treated with different concentrations of pyrimethamine, the IC50 fell into the expected range, approximately 20-30 nM (Figure 83 on page 108).

4.2.5 Initial Pyrimethamine Challenge

The drug challenge assay designed above was implemented.

- Drug of choice: pyrimethamine
- Drug concentration: 320 nM (10-16X IC50 value of 20 nM)
- Drug application: consistent
- Measuring mutator status: competition assay with firefly luciferase as readout to determine population dynamics

Parasites were kept on pyrimethamine for 12 weeks, and checked via smear every four days for emergence of resistant parasites. However, none were observed.

4.2.6 Designing a Second Drug Challenge

As no resistant parasites came up after the initial pyrimethamine challenge, changing the pyrimethamine concentration from 100 to 300 nM pyrimethamine could potentially yield resistant parasites.

Another option is to look into alternative drug options. A much larger panel of anti-malarials was interrogated to see if the common mutations that led to drug resistance could have been caused by the removal of a native cytosine. Certainly, these are not the only possible mutations that could arise, but as a starting point, it is reasonable to first interrogate those drugs whose mutations match the mechanism of action.

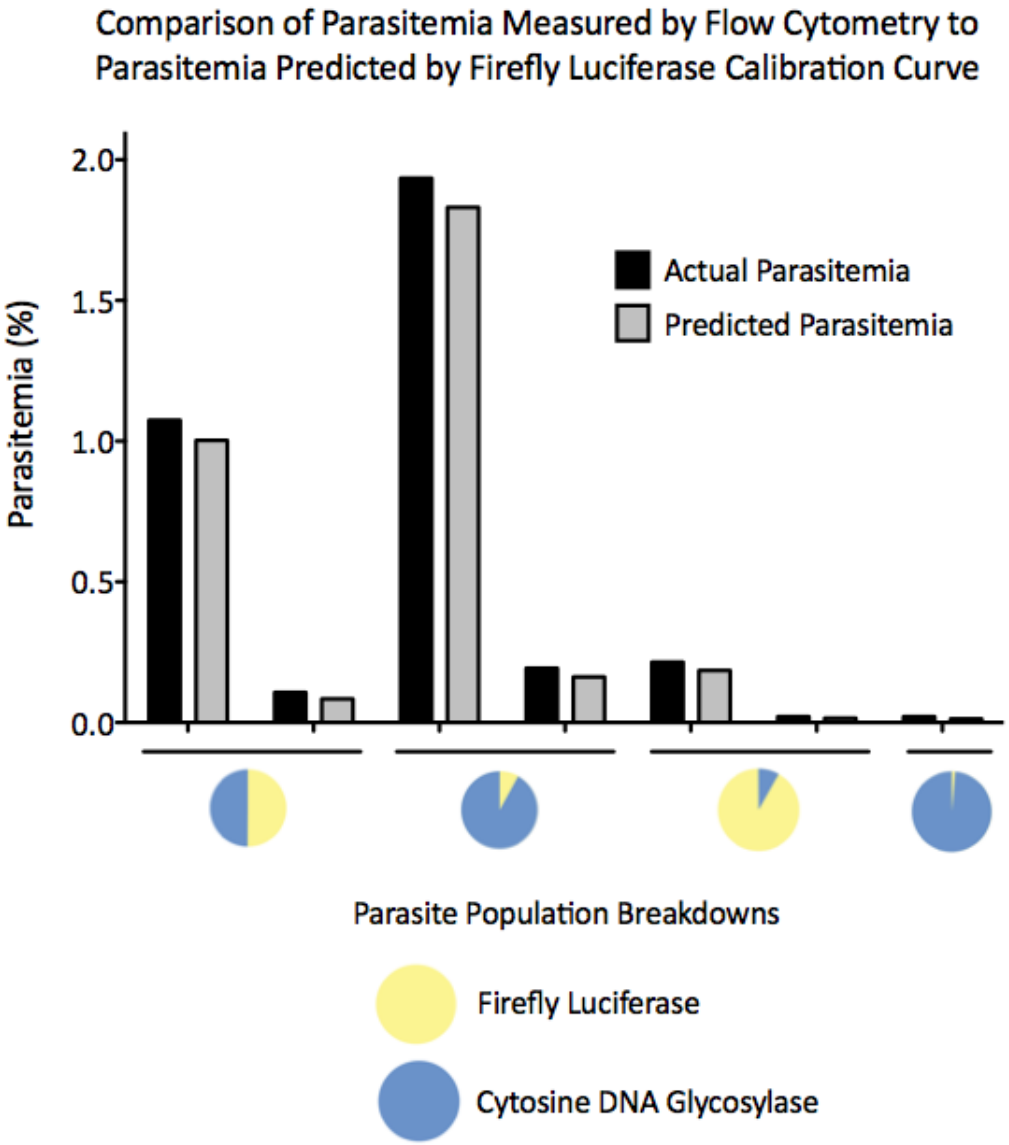

Figure 82: The predicted parasitemia of firefly-expressing parasites compared to the actual parasitemia in a mixed population. When analyzed by an unpaired T test, the P value is 0.913.

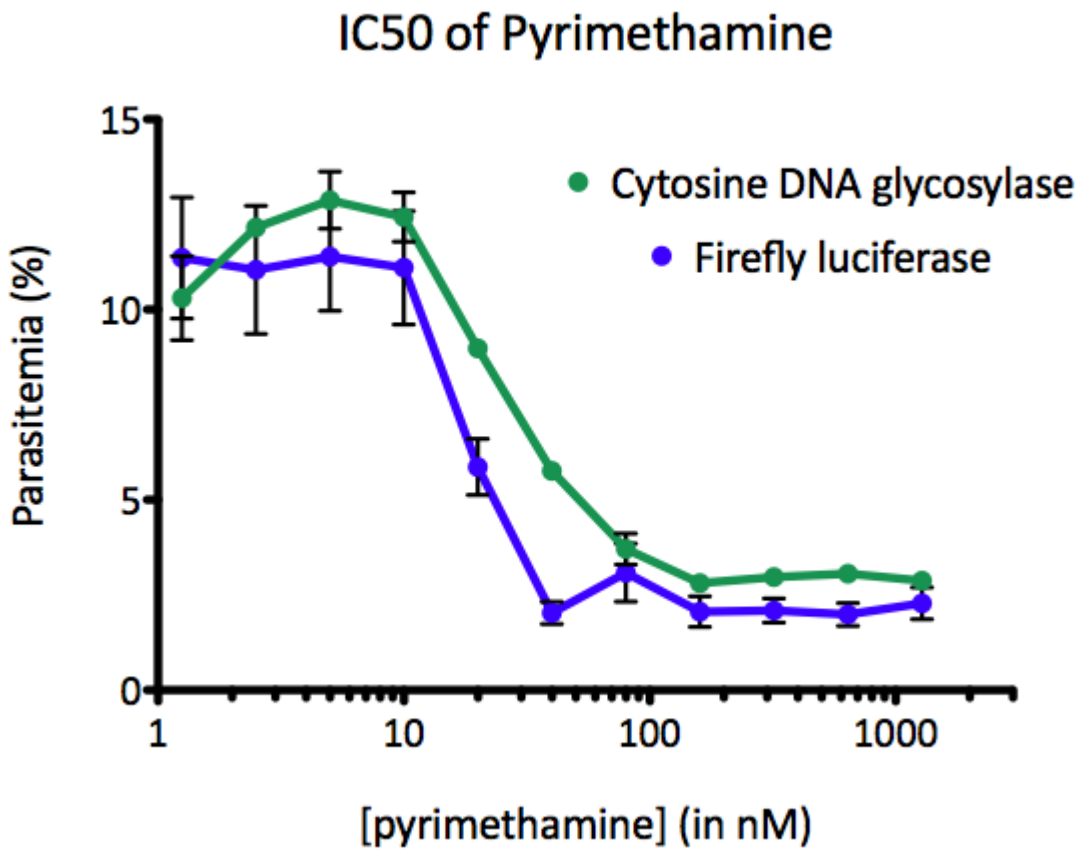

Figure 83: The IC50 value of pyrimethamine as applied to the strains used in these experiments

Common mutations that lead to drug resistance

- Mupirocin [201]
  - Gene target is apicoplast isoleucyl-tRNA synthetase (on the apicoplast chromosome)
  - Base pair 4034 is changed from cytosine to thymine (amino acid 1233 is changed from proline to serine)
- Thiaisoleucine [201]
  - Gene target is cytoplasmic isoleucyl-tRNA synthetase
  - Base pair 2430 is changed from adenine to thymine (amino acid 810 is changed from leucine to phenylalanine)
- Atovaquone (in *Plasmodium yoelii*, a rodent malaria parasite) [202]
  - Gene target is mitochondrial cytochrome b
  - Three lines have two separate concurrent changes: base pair 811 is changed from thymine to guanine (amino acid 271 is changed from leucine to valine) and base pair 815 is changed from alanine to guanine (amino acid 272 is changed from lysine to arginine)
  - Three lines have one mutation: base pair 774 is changed from adenine to guanine (amino acid 258 is changed from isoleucine to methionine)
  - Two lines have one mutation: base pair 803 is changed from adenine to guanine (amino acid 268 is changed from tyrosine to cysteine)
  - One line has one mutation: base pair 799 is changed from thymine to adenine (amino acid 267 is changed from threonine to isoleucine)
- Azithromycin [171]
  - Gene target is apicoplast encoded *P. falciparum* ribosomal protein L4 (PfRpl4)
  - Base pair 227 is changed from guanine to thymine (amino acid 76 is changed from glycine to valine)
- Chloroquine [161, 140, 203]
  - Gene target is *P. falciparum* chloroquine resistance transporter (PfCRT)
  - Eight common mutations, though amino acid 76 changes are deemed required for resistance
    - Amino acid 76 is changed from lysine to threonine
    - Amino acid 220 is changed from alanine to serine
    - Amino acid 326 is changed from asparagine to serine
    - Amino acid 356 is changed from isoleucine to threonine
    - Amino acid 371 is changed from arginine to isoleucine
    - Amino acid 76 is changed from lysine to alanine

    - Amino acid 198 is changed from glutamic acid to lysine
    - Amino acid 271 is changed from glutamine to glutamic acid

- Fosmidomycin [175]
  - Gene target of *P. falciparum* 1-deoxy-D-xylulose 5-phosphate reductoisomerase (Pfdxr)
  - Gene is amplified

- Sulfadoxine [204]
  - Gene target is hydroxymethyldihydropterin pyrophosphokinase: dihydropteroate synthase (H2Pte synthase)
  - Base pair 1310 is changed from cytosine to guanine (amino acid 437 is changed from alanine to glycine)
  - Base pair 1743 is changed from cytosine to guanine (amino acid 581 is changed from alanine to glycine)
  - Base pair 1837 is changed from guanine to thymine or adenine (amino acid 613 is changed from alanine to serine or threonine)
  - Base pair 1306 is changed from thymine to guanine (amino acid 436 is changed from serine to alanine)
  - Base pair 1307 is changed from cytosine to thymine (amino acid 436 is changed from serine to phenylalanine)

- Mefloquine [205]
  - Gene target is *P. falciparum* multidrug resistance protein-1(PfMDR1)
  - Gene is amplified

- Amodiaquine [206]
  - Gene target is *P. falciparum* chloroquine resistance transporter (PfCRT)
    - Base pair 227 is changed from adenine to cytosine (amino acid 76 is changed from lysine to threonine)
  - Gene target is *P. falciparum* multidrug resistance protein-1(PfMDR1)
    - Base pair 256 is changed from guanine to thymine (amino acid 86 is changed from asparagine to tyrosine)

- Clindamycin [176]
  - Gene target is apicoplast 23S rRNA
  - Base pair 4210 is changed from to adenine to cytosine

- Cycloguanil [198, **?**]
  - Gene target is dihydrofolate reductase (DHFR)

  - Amino acid 16 is changed from alanine to valine
  - Amino acid 108 is changed from serine to threonine

- Lumefantrine [140]
  - Gene target is *P. falciparum* multidrug resistance protein-1(PfMDR1)
  - Gene is amplified

- Pyrimethamine [207]
  - Gene target is dihydrofolate reductase (DHFR)
  - Base pair 47 is changed from cytosine to thymine (amino acid 16 is changed from alanine to valine)
  - Base pair 152 is changed from adenine to thymine (amino acid 51 is changed from asparagine to isoleucine)
  - Base pair 175 is changed from thymine to cytosine (amino acid 59 is changed from cysteine to arginine)
  - Base pair 323 is changed from guanine to adenine (amino acid 108 is changed from serine to asparagine)
  - Base pair 323 is changed from guanine to cytosine (amino acid 108 is changed from serine to threonine)
  - Base pair 490 is changed from adenine to thymine (amino acid 164 is changed from isoleucine to leucine)

Those drugs which have common mutations of a cytosine to another nucleotide would be good options for another drug challenge.

4.3 Discussion

Mutant cytosine DNA glycosylase was successfully expressed in the malaria parasite, though the functionality remains undetermined.

The first drug challenge with pyrimethamine yielded no parasites. Additional trials are required to define the mutator status of this strain.

4.3.1 Next steps

The first step is to determine the functionality of the CDG enzyme as expressed in the malaria parasite, either by troubleshooting the TUNEL assay or utilizing different methods to look at DNA damage in the parasite.

Once confirmed, the next step will be to re-challenge the mutator strain cytosine DNA glycosylase with another drug, either pyrimethamine or one of the others described.

The final step to show this strain's utility in the lab would be to utilize it against drugs already in use in the field and classify them for their resistance potential, and comparing this to the time between the first use of the drug and the first noted emergence of resistance.

Once determined, this mutator strain could be used to test a wide variety of scenarios:

- anti-malarials in the Malaria Box [208]
- other compounds in development for malaria treatment
- drug combinations, whether already in use or not

Much remains to be done both in the field epidemiologically and in the lab in order to address the pressing public health need of overcoming drug resistance. Further development and characterization of a lab-based method to measure resistance potential could help address this challenge.

4.4 Methods

4.4.1 Materials

- Abcam
  - Uracil DNA glycosylase antibody (ab23926); rabbit (primary antibody)
- Agilent
  - Hemo KlenTaq polymerase
- ApoDirect
  - TUNEL Assay
- Biorad
  - Laemmli Blue 2X
- Bulldog Bio
  - 2 mm cuvette
- Gibco Life Technologies
  - Albumax II
  - 1X PBS, pH 7.4
- Goldbio
  - Gentamicin
- Life Technologies
  - SYBR Green I stain
- Promega
  - Firefly luciferase kit
  - Secondary antibody (goat anti-rabbit conjugated to horseradish peroxidase)
- New England Biolabs (NEB)
  - Recombinant Uracil DNA glycosylase (UDG)
  - Gibson master mix
  - Restriction enzymes
  - 2 log ladder
  - Protein Plus ladder

- Pierce
  - myECL Imager
- Promega
  - Firefly Luciferase Detection Kit
- ThemoScientific
  - SuperSignal Femto West Kit
- Sigma and Research Products International (RPI)
  - All remaining chemicals
- US Biological
  - RPMI 1640 Medium

4.4.2 Culturing *Plasmodium falciparum*

The 3D7 strain of *P. falciparum* was cultured in leukocyte-free human RBCs (stored in acid-citrate-dextrose anticoagulant; from Research Blood Components, Brighton, MA) under an atmosphere of 5% O_2, 5% CO_2, and 95% N_2 at 2% hematocrit as previous described [115]. Parasites were synchronized weekly at a consistent time with 5% sorbitol (w/v) as previously reported [116] to ensure appropriate parasite ages.

When required, parasites were lysed with a solution of 0.5% saponin, and incubated on ice for 10 minutes. The solution was centrifuged at 5000g for 5 minutes, and cells were washed several times with the saponin solution to yield a clean pellet of parasites. Pellets were frozen -80^{o}C for future analysis.

To transfect parasites, uninfected red blood cells were washed twice with Wash Media (RPMI media with only RPMI and HEPES-KOH). A solution of 200 µL wash media with 50 µg plasmid DNA was added to 200 µL packed uninfected red blood cells and electroporated using a 2 mm cuvette and an 8 pulse/365 volt program. For co-transfections, 50 µg of each plasmid was used, and for transfecting more than one plasmid, the mass was scaled to add up to 50 µg. For example, if pCRISPR was being co-transfected with two separate donor vectors, the reaction contained 50 µg pCRISPR, 25 µg of donor vector one, and 25 µg of donor vector two. Uninfected red blood cells were incubated at 37^{o}C for 1 hour and then washed twice with warm RPMI. Half was resuspended in 4 mL media in a 12 well plate. Next, 0.5 mL infected red blood cells taken directly from a 10 mL culture was added to the plate. Media was changed daily, and drug selection was added on day four. Transfections were monitored using firefly luciferase.

Transgenic parasites were frozen down using the glycerolyte method, as previously described [139]. Briefly, 250 µL of packed infected red blood cells at approximately 10% parasitemia during ring stage were aliquoted into cryosafe tubes. Next, 85 µL of glycerolyte was added slowly, and the solution was incubated at room temperature for five minutes. Finally, 330 µL of glycerolyte was added slowly, and the aliquot was frozen at -80^{o}C.

RPMI Media

- RPMI 1640 Medium (10.4 g/L)
- Hypoxanthine (30 mg/L)
- 25 mM HEPES-KOH (7.0825 g HEPES/L)
- Gentamicin (50 mg/L)
- Albumax II (5 g/L)
- Sodium bicarbonate (2 g/L)

4.4.3 Flow cytometry to determine parasitemia of *Plasmodium falciparum*

An aliquot of 200 µL of parasites at 2% HCT were added to separate wells in a 96 well u-bottom plate and stained with SYBR green 1 for 30 minutes in a 37^{o}C incubator (0.2 µL per 1 mL RPMI). Parasites were washed twice with PBS and subsequently measured for SYBR green 1 expression on a flow cytometer. Uninfected red blood cells, both stained and unstained, were used for gating purposes.

4.4.4 Firefly luciferase assays to determine firefly luciferase expression

Solutions of infected red blood cells were made at an appropriate parasitemia at 2% hematocrit. One mL of each solution was aliquoted into individual eppendorfs, and samples were pelleted at 300g for three minutes. The supernatant was removed, and lysis buffer was applied. The solution was incubated at room temperature for 10 minutes to lyse the cell membranes, vortexed, and the firefly luciferase substrate was added in the dark. Individual firefly luciferase counts were determined using a luminometer.

4.4.5 Cloning Plasmid to Express Cytosine DNA Glycosylase

The base vector and control in this experiment is pfYC120, a vector that express the resistance marker bsd for Blasticidin S resistance in the "A" cassette, and firefly luciferase in the "B" cassette (strain JCN 875 in the Niles lab database; Figure 84 on page 116) [123].

The source DNA for cytosine DNA glycosylase was provided by Shawn Finney-Manchester of the Maheshri Lab at MIT, and was originally made by the Krokan Lab in 1996 [190]. The cytosine DNA glycosylase gene was amplified from the PRS415-GAL1pr-CDG plasmid using two primers (forward = CTTAAATATATACACACACCTAAAACTTACAAAGTATCCTAGGATGTTTGGAGAGAGCTG; reverse = TTTAATCTATTATTAAATAAATTTAATGGGGTACCCGCGGCAGCTCCTTCCAGTCAATGG). The plasmid was cut with AvrII and SacII to release the firefly luciferase gene, and the PCR product and cut vector were incubated with the NEB Gibson master mix for 1 hour at 50^{o}C and then transformed into *E. coli*. Colonies were miniprepped, and underwent test digests prior to Sanger sequencing (Genewiz). Once sequence confirmation was acquired, the strain was banked (strain 1808 in the Niles lab database).

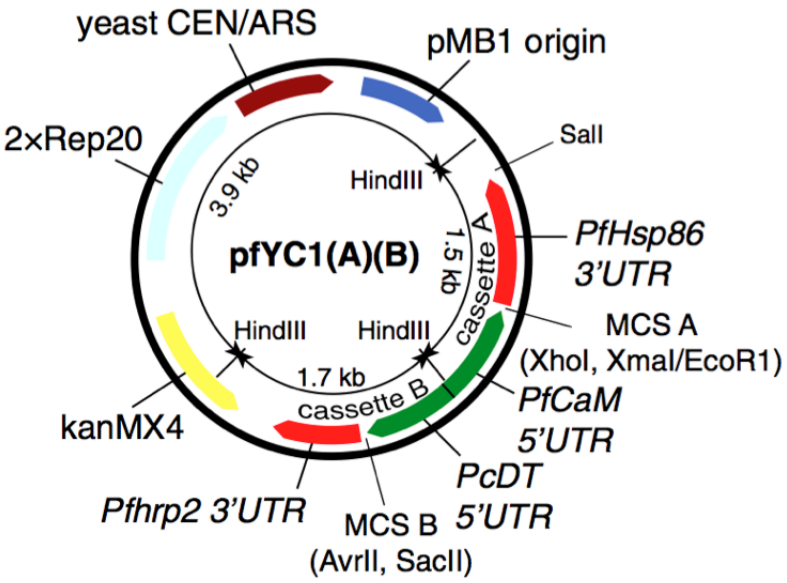

Figure 84: Plasmid map for pfYC1(A)(B) series plasmids. The control firefly-expressing vector in these experiments has bsd in cassette A, and firefly luciferase in cassette B. The CDG-expressing vector replaces the firefly luciferase with CDG in cassette B [123].

4.4.6 Western Blot

Parasites were grown to 10% parasitemia and lysed using a saponin solution (0.5 g/L) and were frozen at -80 prior to use. Parasite pellets were lysed with a mixture of 450 µL water, 450 µL Laemeli Blue 2x and 50 µL beta-mercaptoethanol and boiled at 95ºC for five minutes. The lysates spun down briefly to pellet the insoluble fraction and loaded into precast gels and run for approximately 40 minutes at 250 volts in a 1X SDS buffer. After separation by SDS-PAGE, gels were transferred to a PVDF membrane using an overnight wet transfer at 25 volts. Blots were blocked with 5% milk in TBST for three hours, followed by a three hour incubation with the primary antibody in 1% milk in TBST. Blots were washed three times with TBST and then incubated with a horseradish peroxidase-coupled secondary antibody for one hour. Blots were washed three times with TBST, and incubated with a 1:1 solution of SuperSignal West Femto substrate before image capture using a myECL Imager.

4.4.7 Determining IC50 of Pyrimethamine

On day one, parasites starting at approximately 10-15% parasitemia were double-synchronized to ensure that parasites in the experiment were in the same stage of the intra-erythrocytic development cycle (IDC). As this process kills off a large proportion of the population, parasites may not need to be split on day two, yet their parasitemia should be gauged via smear to ensure that on day three the parasitemia is approximately 10%. On day three, the parasitemia was measured using flow cytometry. The parasites were diluted to 2% parasitemia at 2% HCT. A stock of pyrimethamine was made at the concentration of 2.56 mM (6.4 mg/10 mL DMSO) and the highest concentration on the plate, 2.56 µM was made by a 1:1000 dilution of

the pyrimethamine stock into RPMI. A 96 well plate was set up with 100 µL RPMI in all columns but the first column, in which 200 µL of the 2.56 µM pyrimethamine in RPMI was aliquoted, and the last column, to which 200 µl RPMI alone was added (pyrimethamine concentration of zero). A 1:2 dilution series of the 2.56 µM pyrimethamine in RPMI solution was accomplished by taking 100 µL from column A and adding it to column B. 100 µL was then taken from column B and aliquoted into column C, and so on. Thus, before adding parasites, a dilution series from 2.56 µM to 0 was spread across the plate. Next, 100 µL of the 2% parasitemia at 2% HCT was added to each well on the plate. This results in a final pyrimethamine series from 0 to 125 µM, and a parasite concentration of 1% at 1% HCT, a known concentration that allows untreated parasites to thrive through the end of the current IDC and one additional IDC. On day six, the parasitemia in each well was measured using flow cytometry.

4.4.8 Correlating Firefly Luciferase Results to Parasitemia

First, the parasitemia of firefly luciferase-expressing parasites was determined using flow cytometry. The strain was diluted and blood was added to create a solution of 2% parasitemia at 2% HCT. A dilution series was made, and blood was added to maintain hematocrit. Samples were measured again using flow cytometry and using the luminometer to determine firefly luciferase activity. The raw luciferase values were plotted to their corresponding parasitemia, and a trend line was added. The equation to back-calculate the parasitemia of firefly-expressing parasites was saved for use in a test set.

Next, a test set to determine whether the calibration curve could be utilized to determine the firefly luciferase parasitemia in mixed samples was made. First, the parasitemia of parasite strains expressing firefly luciferase and CDG was measured using flow cytometry. Strains were diluted and blood was added to create solutions of 2% parasitemia at 2% HCT. Before continuing, 200 µL samples were retested on the flow cytometer to confirm parasitemia. Next, five different ratios of parasites were mixed and the parasites were diluted in a 1:10 dilution series to determine the range of detection using firefly luciferase (Table 6 on page 118).

Blood was added to keep each sample at 2% HCT. These fifteen different solutions were aliquoted into individual eppendorfs, and firefly luciferase activity was measured.

4.4.9 Initial Drug Challenge

Parasitemia was measured using flow cytometry, and strains were diluted and blood was added to create solutions of 2% parasitemia at 2% HCT. Strains were mixed into several different ratios, and the parasitemia of each was re-measured using flow cytometry Table 7 on page 118. Several aliquots were frozen down for possible future firefly luciferase assays. Next, the parasites were spun down and the supernatant was removed. Parasites being treated with drug were resuspended with 320 nM pyrimethamine in RPMI (12.5 µL in 100 mL RPMI) and dispensed into 10 mL flasks. Two flasks contained a 1:1 ratio of the parasite strains as controls to ensure that the media conditions are capable of supporting parasite survival, and for future health assays. The media was changed in flasks daily, with the pyrimethamine and RPMI solution made fresh each day. Cultures were split 1:2 every four days as is done in a parasite transfection, the optimal timing to both ensure that a small population survives yet has healthy and new blood to invade.

Sample Parasitemia	Sample Ratio (Fluc:CDG)
2%	50:50
0.2%	50:50
0.02%	50:50
2%	90:10
0.2%	90:10
0.02%	90:10
2%	10:90
0.2%	10:90
0.02%	10:90
2%	1:99
0.2%	1:99
0.02%	1:99
2%	0.5:99.5
0.2%	0.5:99.5
0.02%	0.5:99.5

Table 6: Ratios of parasite strains and their corresponding parasitemias.

Sample Name	Sample Ratio (Fluc:CDG)
Firefly luciferase A	100:0
Firefly luciferase B	100:0
Cytosine DNA glycosylase A	0:100
Cytosine DNA glycosylase B	0:100
1:1 ratio A	50:50
1:1 ratio B	50:50
9:1 ratio A	90:10
9:1 ratio B	90:10
99:1 ratio A	99:1
99:1 ratio B	99:1
1:1 ratio A (no drug)	50:50
1:1 ratio B (no drug)	50:50

Table 7: Sample names for initial drug challenge and their corresponding ratios.

5 Conclusion

It is necessary to better prevent and treat malaria worldwide, and even more is required to fully eradicate the disease. Yet, with the development of tools in the laboratory to address many of the complications surrounding the problems of prevention and treatment, we will be one step closer to addressing this public health crisis.

First, I have addressed the interactions of the parasite with the human host at the level of nitrite in the immune system and mechanical interactions within a space similar to the host microvasculature. While the main conclusion here is that the relationship between the parasite and host is complex and requires further investigation, that in itself is a conclusion that leads toward better understanding such relationships.

Second, I helped build on tools developed by the lab to engineer and contribute to a toolkit that allows for the testing of the many genes of unknown function within the parasite to find new potential drug targets. With 50% of genes in the parasite having no known homology to any other genes, this rich pool of potential drug targets can now be manipulated and elucidated in a modular, efficient, and straightforward way.

Finally, I engineered a mutator strain that could potentially allow for the testing of resistance potential in the parasite, as well as assist in determining the mechanisms of action for the development of resistance in drugs already used in the clinic.

While all three are technologies still in various states of refinement at the completion of this project, they show the potential for biological engineering to directly address a global health problem while investigating biology at the most fundamental level.

References

[1] Brian J Belmont and Jacquin C Niles. Engineering a direct and inducible protein-rna interaction to regulate rna biology. *ACS Chem Biol*, 5(9):851–61, Sep 2010.

[2] Brian J Belmont. Engineered mrna regulation using an inducible protein-rna aptamer interaction. pages 1–131, Feb 2013.

[3] Stephen J Goldfless, Jeffrey C Wagner, and Jacquin C Niles. Versatile control of plasmodium falciparum gene expression with an inducible protein-rna interaction. *Nat Commun*, 5:5329, Jan 2014.

[4] World Health Organization. World malaria report 2011. pages 1–91, Dec 2011.

[5] Paul R Gilson and Brendan S Crabb. Morphology and kinetics of the three distinct phases of red blood cell invasion by plasmodium falciparum merozoites. *Int J Parasitol*, 39(1):91–6, Jan 2009.

[6] The malERA Consultative Group on Basic Science and Enabling Technologies. A research agenda for malaria eradication: Basic science and enabling technologies. *PLoS medicine*, 8(1):e1000399, Jan 2011.

[7] Drew C Mackellar, Matthew T O'Neill, Ahmed S I Aly, John B Sacci, Alan F Cowman, and Stefan H I Kappe. Plasmodium falciparum etramp10.3 is an essential parasitophorous vacuole and exported protein in blood stages. *Eukaryotic Cell*, 9(5):784–94, May 2010.

[8] Alexis Kaushansky, Sebastian A Mikolajczak, Marissa Vignali, and Stefan H I Kappe. Of men in mice: the success and promise of humanized mouse models for human malaria parasite infections. *Cell Microbiol*, Feb 2014.

[9] Malcolm J Gardner, Neil Hall, Eula Fung, Owen White, Matthew Berriman, Richard W Hyman, Jane M Carlton, Arnab Pain, Karen E Nelson, Sharen Bowman, Ian T Paulsen, Keith James, Jonathan A Eisen, Kim Rutherford, Steven L Salzberg, Alister Craig, Sue Kyes, Man-Suen Chan, Vishvanath Nene, Shamira J Shallom, Bernard Suh, Jeremy Peterson, Sam Angiuoli, Mihaela Pertea, Jonathan Allen, Jeremy Selengut, Daniel Haft, Michael W Mather, Akhil B Vaidya, David M A Martin, Alan H Fairlamb, Martin J Fraunholz, David S Roos, Stuart A Ralph, Geoffrey I McFadden, Leda M Cummings, G Mani Subramanian, Chris Mungall, J Craig Venter, Daniel J Carucci, Stephen L Hoffman, Chris Newbold, Ronald W Davis, Claire M Fraser, and Bart Barrell. Genome sequence of the human malaria parasite plasmodium falciparum. *Nature*, 419(6906):498–511, Oct 2002.

[10] C B Mamoun, R Truong, I Gluzman, N S Akopyants, A Oksman, and D E Goldberg. Transfer of genes into plasmodium falciparum by polyamidoamine dendrimers. *Mol Biochem Parasitol*, 103(1):117–21, Sep 1999.

[11] Sandra Hasenkamp, Karen T Russell, and Paul Horrocks. Comparison of the absolute and relative efficiencies of electroporation-based transfection protocols for plasmodium falciparum. *Malaria Journal*, 11:210, Jan 2012.

[12] Anusha M Gopalakrishnan, Anup K Kundu, Tarun K Mandal, and Nirbhay Kumar. Novel nanosomes for gene delivery to plasmodium falciparum-infected red blood cells. *Sci Rep*, 3:1534, Jan 2013.

[13] Marcel Deponte, Heinrich C Hoppe, Marcus C S Lee, Alexander G Maier, Dave Richard, Melanie Rug, Tobias Spielmann, and Jude M Przyborski. Wherever i may roam: protein and membrane trafficking in p. falciparum-infected red blood cells. *Mol Biochem Parasitol*, 186(2):95–116, Dec 2012.

[14] Philip J Rosenthal. The interplay between drug resistance and fitness in malaria parasites. *Molecular Microbiology*, 89(6):1025–38, Sep 2013.

[15] Alexis Nzila and Leah Mwai. In vitro selection of plasmodium falciparum drug-resistant parasite lines. *Journal of Antimicrobial Chemotherapy*, 65(3):390–8, Mar 2010.

[16] Narla Mohandas and Xiuli An. Malaria and human red blood cells. *Med Microbiol Immunol*, 201(4):593–8, Nov 2012.

[17] B M Cooke, N Mohandas, and R L Coppel. The malaria-infected red blood cell: structural and functional changes. *Advances in Parasitology*, 50:1–86, Jan 2001.

[18] Sanjay A Desai. Why do malaria parasites increase host erythrocyte permeability? *Trends in Parasitology*, 30(3):151–159, Mar 2014.

[19] M Aikawa, I J Udeinya, J Rabbege, M Dayan, J H Leech, R J Howard, and L H Miller. Structural alteration of the membrane of erythrocytes infected with plasmodium falciparum. *J Protozool*, 32(3):424–9, Aug 1985.

[20] M Aikawa, C L Hsieh, and L H Miller. Ultrastructural changes of the erythrocyte membrane in ovale-type malarial parasites. *J Parasitol*, 63(1):152–4, Feb 1977.

[21] Eriko Nagao, Takayuki Arie, David W Dorward, Rick M Fairhurst, and James A Dvorak. The avian malaria parasite plasmodium gallinaceum causes marked structural changes on the surface of its host erythrocyte. *J Struct Biol*, 162(3):460–7, Jun 2008.

[22] Brian M Cooke, Narla Mohandas, and Ross L Coppel. Malaria and the red blood cell membrane. *Semin Hematol*, 41(2):173–88, Apr 2004.

[23] Zhangli Peng, Xuejin Li, Igor V Pivkin, Ming Dao, George E Karniadakis, and Subra Suresh. Lipid bilayer and cytoskeletal interactions in a red blood cell. *Proceedings of the National Academy of Sciences*, 110(33):13356–61, Aug 2013.

[24] Teresa Tiffert and Virgilio L Lew. Dynamic morphology and cytoskeletal protein changes during spontaneous inside-out vesiculation of red blood cell membranes. *Pflugers Arch - Eur J Physiol*, Mar 2014.

[25] Xinhong Pei, Xiuli An, Xinhua Guo, Michal Tarnawski, Ross Coppel, and Narla Mohandas. Structural and functional studies of interaction between plasmodium falciparum knob-associated histidine-rich protein (kahrp) and erythrocyte spectrin. *J Biol Chem*, 280(35):31166–71, Sep 2005.

[26] Xinhong Pei, Xinhua Guo, Ross Coppel, Souvik Bhattacharjee, Kasturi Haldar, Walter Gratzer, Narla Mohandas, and Xiuli An. The ring-infected erythrocyte surface antigen (resa) of plasmodium falciparum stabilizes spectrin tetramers and suppresses further invasion. *Blood*, 110(3):1036–42, Aug 2007.

[27] Xinhong Pei, Xinhua Guo, Ross Coppel, Narla Mohandas, and Xiuli An. Plasmodium falciparum erythrocyte membrane protein 3 (pfemp3) destabilizes erythrocyte membrane skeleton. *J Biol Chem*, 282(37):26754–8, Sep 2007.

[28] Brian M Cooke, Donna W Buckingham, Fiona K Glenister, Kate M Fernandez, Lawrence H Bannister, Matthias Marti, Narla Mohandas, and Ross L Coppel. A maurer's cleft-associated protein is essential for expression of the major malaria virulence antigen on the surface of infected red blood cells. *J Cell Biol*, 172(6):899–908, Mar 2006.

[29] Brian M Cooke, Narla Mohandas, Alan F Cowman, and Ross L Coppel. Cellular adhesive phenomena in apicomplexan parasites of red blood cells. *Vet Parasitol*, 132(3-4):273–95, Sep 2005.

[30] Inès Vigan-Womas, Micheline Guillotte, Cécile Le Scanf, Sébastien Igonet, Stéphane Petres, Alexandre Juillerat, Cyril Badaut, Farida Nato, Achim Schneider, Anne Lavergne, Hugues Contamin, Adama Tall, Laurence Baril, Graham A Bentley, and Odile Mercereau-Puijalon. An in vivo and in vitro model of plasmodium falciparum rosetting and autoagglutination mediated by varo, a group a var gene encoding a frequent serotype. *Infect Immun*, 76(12):5565–80, Dec 2008.

[31] Rick M Fairhurst, Cameron D Bess, and Michael A Krause. Abnormal pfemp1/knob display on plasmodium falciparum-infected erythrocytes containing hemoglobin variants: fresh insights into malaria pathogenesis and protection. *Microbes Infect*, 14(10):851–62, Aug 2012.

[32] A C Allison and E M Eugui. The role of cell-mediated immune responses in resistance to malaria, with special reference to oxidant stress. *Annu Rev Immunol*, 1:361–92, Jan 1983.

[33] Reina E Mebius and Georg Kraal. Structure and function of the spleen. *Nat Rev Immunol*, 5(8):606–16, Aug 2005.

[34] Sha Huang, Anburaj Amaladoss, Min Liu, Huichao Chen, Rou Zhang, Peter R Preiser, Ming Dao, and Jongyoon Han. In vivo splenic clearance correlates with in vitro deformability of red blood cells from plasmodium yoelii-infected mice. *Infect Immun*, 82(6):2532–41, Jun 2014.

[35] Pierre A Buffet, Geneviève Milon, Valentine Brousse, Jean-Michel Correas, Bertrand Dousset, Anne Couvelard, Reza Kianmanesh, Olivier Farges, Alain Sauvanet, François Paye, Marie-Noëlle Ungeheuer, Catherine Ottone, Huot Khun, Laurence Fiette, Ghislaine Guigon, Michel Huerre, Odile Mercereau-Puijalon, and Peter H David. Ex vivo perfusion of human spleens maintains clearing and processing functions. *Blood*, 107(9):3745–52, May 2006.

[36] Hernando A del Portillo, Mireia Ferrer, Thibaut Brugat, Lorena Martin-Jaular, Jean Langhorne, and Marcus V G Lacerda. The role of the spleen in malaria. *Cell Microbiol*, 14(3):343–55, Mar 2012.

[37] Anna Bachmann, Claudia Esser, Michaela Petter, Sabine Predehl, Vera von Kalckreuth, Stefan Schmiedel, Iris Bruchhaus, and Egbert Tannich. Absence of erythrocyte sequestration and lack of multicopy gene family expression in plasmodium falciparum from a splenectomized malaria patient. *PLoS ONE*, 4(10):e7459, Jan 2009.

[38] S Suresh, J Spatz, J P Mills, A Micoulet, M Dao, C T Lim, M Beil, and T Seufferlein. Connections between single-cell biomechanics and human disease states: gastrointestinal cancer and malaria. *Acta Biomater*, 1(1):15–30, Jan 2005.

[39] I Bakaltcheva, S Leslie, V MacDonald, B Spargo, and A Rudolph. Reversible cross-linking and co treatment as an approach in red cell stabilization. *Cryobiology*, 40(4):343–59, Jun 2000.

[40] C W Haest, D Kamp, G Plasa, and B Deuticke. Intra- and intermolecular cross-linking of membrane proteins in intact erythrocytes and ghosts by sh-oxidizing agents. *Biochim Biophys Acta*, 469(2):226–30, Sep 1977.

[41] L H Bannister, J M Hopkins, R E Fowler, S Krishna, and G H Mitchell. A brief illustrated guide to the ultrastructure of plasmodium falciparum asexual blood stages. *Parasitol Today (Regul Ed)*, 16(10):427–33, Oct 2000.

[42] J P Mills, M Diez-Silva, D J Quinn, M Dao, M J Lang, K S W Tan, C T Lim, G Milon, P H David, O Mercereau-Puijalon, S Bonnefoy, and S Suresh. Effect of plasmodial resa protein on deformability of human red blood cells harboring plasmodium falciparum. *Proc Natl Acad Sci USA*, 104(22):9213–7, May 2007.

[43] Apurba Paul, Rani Pallavi, Utpal S Tatu, and Vasant Natarajan. The bystander effect in optically trapped red blood cells due to plasmodium falciparum infection. *Transactions of the Royal Society of Tropical Medicine and Hygiene*, 107(4):220–3, Apr 2013.

[44] Sha Huang, Andreas Undisz, Monica Diez-Silva, Hansen Bow, Ming Dao, and Jongyoon Han. Dynamic deformability of plasmodium falciparum-infected erythrocytes exposed to artesunate in vitro. *Integr Biol (Camb)*, 5(2):414–22, Feb 2013.

[45] YongKeun Park, Monica Diez-Silva, Gabriel Popescu, George Lykotrafitis, Wonshik Choi, Michael S Feld, and Subra Suresh. Refractive index maps and membrane dynamics of human red blood cells parasitized by plasmodium falciparum. *Proc Natl Acad Sci USA*, 105(37):13730–5, Sep 2008.

[46] Melek Bor-Kucukatay, Rosalinda B Wenby, Herbert J Meiselman, and Oguz K Baskurt. Effects of nitric oxide on red blood cell deformability. *Am J Physiol Heart Circ Physiol*, 284(5):H1577–84, May 2003.

[47] Ting Ye, Nhan Phan-Thien, Boo Cheong Khoo, and Chwee Teck Lim. Stretching and relaxation of malaria-infected red blood cells. *Biophys J*, 105(5):1103–9, Sep 2013.

[48] Danielle I Stanisic, Alyssa E Barry, and Michael F Good. Escaping the immune system: How the malaria parasite makes vaccine development a challenge. *Trends in Parasitology*, 29(12):612–22, Dec 2013.

[49] Mario Recker, Caroline O Buckee, Andrew Serazin, Sue Kyes, Robert Pinches, Zóe Christodoulou, Amy L Springer, Sunetra Gupta, and Chris I Newbold. Antigenic variation in plasmodium falciparum malaria involves a highly structured switching pattern. *PLoS Pathog*, 7(3):e1001306, Mar 2011.

[50] Kami Kim. Malaria var gene expression: Keeping up with the neighbors. *Cell Host Microbe*, 11(1):1–2, Jan 2012.

[51] George M Warimwe, Mario Recker, Esther W Kiragu, Caroline O Buckee, Juliana Wambua, Jennifer N Musyoki, Kevin Marsh, and Peter C Bull. Plasmodium falciparum var gene expression homogeneity as a marker of the host-parasite relationship under different levels of naturally acquired immunity to malaria. *PLoS ONE*, 8(7):e70467, Jan 2013.

[52] David J Pombo, Gregor Lawrence, Chakrit Hirunpetcharat, Christine Rzepczyk, Michelle Bryden, Nicole Cloonan, Karen Anderson, Yuvadee Mahakunkijcharoen, Laura B Martin, Danny Wilson, Salenna Elliott, Suzanne Elliott, Damon P Eisen, J Brice Weinberg, Allan Saul, and Michael F Good. Immunity to malaria after administration of ultra-low doses of red cells infected with plasmodium falciparum. *Lancet*, 360(9333):610–7, Aug 2002.

[53] Julius Clemence Hafalla, Olivier Silvie, and Kai Matuschewski. Cell biology and immunology of malaria. *Immunol Rev*, 240(1):297–316, Mar 2011.

[54] Magdalena Plebanski, Carolyn M Hannan, Shahriar Behboudi, Katie L Flanagan, Vasso Apostolopoulos, Robert E Sinden, and Adrian V S Hill. Direct processing and presentation of antigen from malaria sporozoites by professional antigen-presenting cells in the induction of cd8 t-cell responses. *Immunol Cell Biol*, 83(3):307–12, Jun 2005.

[55] M C Seguin, F W Klotz, I Schneider, J P Weir, M Goodbary, M Slayter, J J Raney, J U Aniagolu, and S J Green. Induction of nitric oxide synthase protects against malaria in mice exposed to irradiated plasmodium berghei infected mosquitoes: involvement of interferon gamma and cd8+ t cells. *J Exp Med*, 180(1):353–8, Jul 1994.

[56] A K Nussler, L Rénia, V Pasquetto, F Miltgen, H Matile, and D Mazier. In vivo induction of the nitric oxide pathway in hepatocytes after injection with irradiated malaria sporozoites, malaria blood parasites or adjuvants. *Eur J Immunol*, 23(4):882–7, Apr 1993.

[57] A W Taylor-Robinson, R S Phillips, A Severn, S Moncada, and F Y Liew. The role of th1 and th2 cells in a rodent malaria infection. *Science*, 260(5116):1931–4, Jun 1993.

[58] Caroline Lin Lin Chua, Graham Brown, John A Hamilton, Stephen Rogerson, and Philippe Boeuf. Monocytes and macrophages in malaria: protection or pathology? *Trends in Parasitology*, 29(1):26–34, Jan 2013.

[59] A D Urquhart. Putative pathophysiological interactions of cytokines and phagocytic cells in severe human falciparum malaria. *Clin Infect Dis*, 19(1):117–31, Jul 1994.

[60] Lisa J Ioannidis, Catherine Q Nie, and Diana S Hansen. The role of chemokines in severe malaria: more than meets the eye. *Parasitology*, pages 1–12, Dec 2013.

[61] C F Ockenhouse, S Schulman, and H L Shear. Induction of crisis forms in the human malaria parasite plasmodium falciparum by gamma-interferon-activated, monocyte-derived macrophages. *J Immunol*, 133(3):1601–8, Sep 1984.

[62] Maritza Jaramillo, D Channe Gowda, Danuta Radzioch, and Martin Olivier. Hemozoin increases ifn-gamma-inducible macrophage nitric oxide generation through extracellular signal-regulated kinase- and nf-kappa b-dependent pathways. *J Immunol*, 171(8):4243–53, Oct 2003.

[63] Martin Olivier, Kristin Van Den Ham, Marina Tiemi Shio, Fikregabrail Aberra Kassa, and Sophie Fougeray. Malarial pigment hemozoin and the innate inflammatory response. *Front. Immunol.*, 5:25, Jan 2014.

[64] Irene Gramaglia, Peter Sobolewski, Diana Meays, Ramiro Contreras, John P Nolan, John A Frangos, Marcos Intaglietta, and Henri C Van Der Heyde. Low nitric oxide bioavailability contributes to the genesis of experimental cerebral malaria. *Nat Med*, 12(12):1417–22, Dec 2006.

[65] Ian A Clark, Alison C Budd, Lisa M Alleva, and William B Cowden. Human malarial disease: a consequence of inflammatory cytokine release. *Malar J*, 5:85, Jan 2006.

[66] Ian A Clark, Lisa M Alleva, Alison C Budd, and William B Cowden. Understanding the role of inflammatory cytokines in malaria and related diseases. *Travel Med Infect Dis*, 6(1-2):67–81, Jan 2008.

[67] I A Clark, K A Rockett, and W B Cowden. Proposed link between cytokines, nitric oxide and human cerebral malaria. *Parasitol Today (Regul Ed)*, 7(8):205–7, Aug 1991.

[68] Aubrey J Cunnington, Eleanor M Riley, and Michael Walther. Stuck in a rut? reconsidering the role of parasite sequestration in severe malaria syndromes. *Trends in Parasitology*, 29(12):585–92, Dec 2013.

[69] Louis Schofield. Intravascular infiltrates and organ-specific inflammation in malaria pathogenesis. *Immunol Cell Biol*, 85(2):130–7, Jan 2007.

[70] Gordon A Awandare, Prakasha Kempaiah, Daniel O Ochiel, Paolo Piazza, Christopher C Keller, and Douglas J Perkins. Mechanisms of erythropoiesis inhibition by malarial pigment and malaria-induced proinflammatory mediators in an in vitro model. *Am J Hematol*, 86(2):155–62, Feb 2011.

[71] Silke C Mueller, Reinhard März, Manfred Schmolz, and Bernd Drewelow. Intraindividual long term stability and response corridors of cytokines in healthy volunteers detected by a standardized whole-blood culture system for bed-side application. *BMC Med Res Methodol*, 12:112, Jan 2012.

[72] Isabel G Azcárate, Patricia Marín-García, Alí N Kamali, Susana Pérez-Benavente, Antonio Puyet, Amalia Diez, and José M Bautista. Differential immune response associated to malaria outcome is detectable in peripheral blood following plasmodium yoelii infection in mice. *PLoS ONE*, 9(1):e85664, Jan 2014.

[73] M M Stevenson, M F Tam, S F Wolf, and A Sher. Il-12-induced protection against blood-stage plasmodium chabaudi as requires ifn-gamma and tnf-alpha and occurs via a nitric oxide-dependent mechanism. *J Immunol*, 155(5):2545–56, Sep 1995.

[74] Pallavi Lonkar and Peter C Dedon. Reactive species and dna damage in chronic inflammation: reconciling chemical mechanisms and biological fates. *Int J Cancer*, 128(9):1999–2009, May 2011.

[75] Peter C Dedon and Steven R Tannenbaum. Reactive nitrogen species in the chemical biology of inflammation. *Arch Biochem Biophys*, 423(1):12–22, Mar 2004.

[76] Rob van Zwieten, Arthur J Verhoeven, and Dirk Roos. Inborn defects in the antioxidant systems of human red blood cells. *Free Radic Biol Med*, 67C:377–386, Dec 2013.

[77] L Jia, C Bonaventura, J Bonaventura, and J S Stamler. S-nitrosohaemoglobin: a dynamic activity of blood involved in vascular control. *Nature*, 380(6571):221–6, Mar 1996.

[78] Petra Kleinbongard, Rainer Schulz, Tienush Rassaf, Thomas Lauer, André Dejam, Thomas Jax, Intan Kumara, Putrika Gharini, Svetlana Kabanova, Burcin Ozüyaman, Hans-Georg Schnürch, Axel Gödecke, Artur-A Weber, Mirko Robenek, Horst Robenek, Wilhelm Bloch, Peter Rösen, and Malte Kelm. Red blood cells express a functional endothelial nitric oxide synthase. *Blood*, 107(7):2943–51, Apr 2006.

[79] Rohitas Deshmukh and Vishal Trivedi. Pro-stimulatory role of methemoglobin in inflammation through hemin oxidation and polymerization. *Inflamm Allergy Drug Targets*, 12(1):68–78, Feb 2013.

[80] Mildred M Pelletier, Petra Kleinbongard, Lorna Ringwood, Rania Hito, Christian J Hunter, Alan N Schechter, Mark T Gladwin, and André Dejam. The measurement of blood and plasma nitrite by chemiluminescence: pitfalls and solutions. *Free Radic Biol Med*, 41(4):541–8, Aug 2006.

[81] André Dejam, Christian J Hunter, Mildred M Pelletier, Lewis L Hsu, Roberto F Machado, Sruti Shiva, Gordon G Power, Malte Kelm, Mark T Gladwin, and Alan N Schechter. Erythrocytes are the major intravascular storage sites of nitrite in human blood. *Blood*, 106(2):734–9, Jul 2005.

[82] K A Rockett, M M Awburn, W B Cowden, and I A Clark. Killing of plasmodium falciparum in vitro by nitric oxide derivatives. *Infect Immun*, 59(9):3280–3, Sep 1991.

[83] H Atamna and H Ginsburg. Origin of reactive oxygen species in erythrocytes infected with plasmodium falciparum. *Mol Biochem Parasitol*, 61(2):231–41, Oct 1993.

[84] O I Iribhogbe, E O Agbaje, I A Oreagba, O O Aina, and A D Ota. Oxidative stress and micronutrient therapy in malaria: an in vivo study in plasmodium berghei infected mice. *Pak J Biol Sci*, 16(4):160–7, Feb 2013.

[85] Murtala Bindawa Isah and Mohammed Auwal Ibrahim. The role of antioxidants treatment on the pathogenesis of malarial infections: a review. *Parasitol Res*, 113(3):801–9, Mar 2014.

[86] F Mohring, J Pretzel, E Jortzik, and K Becker. The redox systems of plasmodium falciparum and plasmodium vivax: Comparison, in silico analyses and inhibitor studies. *Curr Med Chem*, 21(15):1728–56, Jan 2014.

[87] Sylke Müller. Redox and antioxidant systems of the malaria parasite plasmodium falciparum. *Molecular Microbiology*, 53(5):1291–305, Sep 2004.

[88] Gustavo Salinas. An update on redox biology of parasites. *Antioxidants & Redox Signaling*, 19(7):661–4, Sep 2013.

[89] Françoise Nepveu and Francesco Turrini. Targeting the redox metabolism of plasmodium falciparum. *Future Med Chem*, 5(16):1993–2006, Oct 2013.

[90] L R Brunet. Nitric oxide in parasitic infections. *Int Immunopharmacol*, 1(8):1457–67, Aug 2001.

[91] P G Kremsner, S Winkler, E Wildling, J Prada, U Bienzle, W Graninger, and A K Nüssler. High plasma levels of nitrogen oxides are associated with severe disease and correlate with rapid parasitological and clinical cure in plasmodium falciparum malaria. *Trans R Soc Trop Med Hyg*, 90(1):44–7, Jan 1996.

[92] A K Nussler, W Eling, and PG Kremsner. Patients with plasmodium falciparum malaria and plasmodium vivax malaria show increased nitrite and nitrate plasma levels. *J Infect Dis*, 169(6):1418–9, Jun 1994.

[93] Onésia Cristina Oliveira-Lima, Danielle Bernardes, Mauro Cunha Xavier Pinto, Rosa Maria Esteves Arantes, and Juliana Carvalho-Tavares. Mice lacking inducible nitric oxide synthase develop exacerbated hepatic inflammatory responses induced by plasmodium berghei nk65 infection. *Microbes Infect*, 15(13):903–10, Nov 2013.

[94] Leonardo José De Moura Carvalho, Aline Da Silva Moreira, Cláudio Tadeu Daniel-Ribeiro, and Yuri Chaves Martins. Vascular dysfunction as a target for adjuvant therapy in cerebral malaria. *Mem. Inst. Oswaldo Cruz*, 109(5):577–88, Aug 2014.

[95] Viktória Jeney, Susana Ramos, Marie-Louise Bergman, Ingo Bechmann, Jasmin Tischer, Ana Ferreira, Virginia Oliveira-Marques, Chris J Janse, Sofia Rebelo, Silvia Cardoso, and Miguel P Soares. Control of disease tolerance to malaria by nitric oxide and carbon monoxide. *CellReports*, 8(1):126–36, Jul 2014.

[96] Lihui Wang, Claire Delahunty, Judith Helena Prieto, Stefan Rahlfs, Esther Jortzik, John R Yates, and Katja Becker. Protein s-nitrosylation in plasmodium falciparum. *Antioxidants & Redox Signaling*, Feb 2014.

[97] K A Rockett, M M Awburn, E J Rockett, W B Cowden, and I A Clark. Possible role of nitric oxide in malarial immunosuppression. *Parasite Immunol*, 16(5):243–9, May 1994.

[98] Louis H Miller, Hans C Ackerman, Xin-Zhuan Su, and Thomas E Wellems. Malaria biology and disease pathogenesis: insights for new treatments. *Nat Med*, 19(2):156–67, Feb 2013.

[99] Ruth Aguilar, Tiziana Marrocco, Oleksii A Skorokhod, Arnoldo Barbosa, Augusto Nhabomba, Maria N Manaca, Caterina Guinovart, Llorenç Quintó, Paolo Arese, Pedro L Alonso, Carlota Dobaño, and Evelin Schwarzer. Blood oxidative stress markers and plasmodium falciparum malaria in non-immune african children. *Br J Haematol*, 164(3):438–50, Feb 2014.

[100] K Tsuda, K Kimura, I Nishio, and Y Masuyama. Nitric oxide improves membrane fluidity of erythrocytes in essential hypertension: An electron paramagnetic resonance investigation. *Biochem Biophys Res Commun*, 275(3):946–54, Sep 2000.

[101] D Starzyk, R Korbut, and R J Gryglewski. Effects of nitric oxide and prostacyclin on deformability and aggregability of red blood cells of rats ex vivo and in vitro. *J Physiol Pharmacol*, 50(4):629–37, Dec 1999.

[102] D Starzyk, R Korbut, and R J Gryglewski. The role of nitric oxide in regulation of deformability of red blood cells in acute phase of endotoxaemia in rats. *J Physiol Pharmacol*, 48(4):731–5, Dec 1997.

[103] Juliana Rey, Pierre A Buffet, Liliane Ciceron, Geneviève Milon, Odile Mercereau-Puijalon, and Innocent Safeukui. Reduced erythrocyte deformability associated with hypoargininemia during plasmodium falciparum malaria. *Sci. Rep.*, 4:3767, Jan 2014.

[104] Hansen Bow, Igor V Pivkin, Monica Diez-Silva, Stephen J Goldfless, Ming Dao, Jacquin C Niles, Subra Suresh, and Jongyoon Han. A microfabricated deformability-based flow cytometer with application to malaria. *Lab Chip*, 11(6):1065–73, Mar 2011.

[105] Joanne M Kwan, Quan Guo, Dana L Kyluik-Price, Hongshen Ma, and Mark D Scott. Microfluidic analysis of cellular deformability of normal and oxidatively damaged red blood cells. *Am J Hematol*, 88(8):682–9, Aug 2013.

[106] Ruqayyah Almizraq, Jayme D R Tchir, Jelena L Holovati, and Jason P Acker. Storage of red blood cells affects membrane composition, microvesiculation, and in vitro quality. *Transfusion*, 53(10):2258–67, Oct 2013.

[107] Basanta Bhaduri, Mikhail Kandel, Carlo Brugnara, Krishna Tangella, and Gabriel Popescu. Optical assay of erythrocyte function in banked blood. *Sci. Rep.*, 4:6211, Jan 2014.

[108] L M Crespo, E M Bifano, and J C Freedman. Membrane lipid fluidity and filterability of red blood cells from adults and newborns. *Pediatr Res*, 24(4):433–7, Oct 1988.

[109] Willy A Flegel, Charles Natanson, and Harvey G Klein. Does prolonged storage of red blood cells cause harm? *Br J Haematol*, 165(1):3–16, Apr 2014.

[110] Juliet Ho, William J Sibbald, and Ian H Chin-Yee. Effects of storage on efficacy of red cell transfusion: when is it not safe? *Crit Care Med*, 31(12 Suppl):S687–97, Dec 2003.

[111] Keyvan Karkouti. From the journal archives: The red blood cell storage lesion: past, present, and future. *Can J Anaesth*, 61(6):583–6, Jun 2014.

[112] Alan Tinmouth, Dean Fergusson, Ian Chin Yee, Paul C Hébert, ABLE Investigators, and Canadian Critical Care Trials Group. Clinical consequences of red cell storage in the critically ill. *Transfusion*, 46(11):2014–27, Nov 2006.

[113] Thomas J van 't Erve, Claire M Doskey, Brett A Wagner, John R Hess, Benjamin W Darbro, Kelli K Ryckman, Jeffrey C Murray, Thomas J Raife, and Garry R Buettner. Heritability of glutathione and related metabolites in stored red blood cells. *Free Radic Biol Med*, 76C:107–113, Aug 2014.

[114] Steven M Frank, Bagrat Abazyan, Masahiro Ono, Charles W Hogue, David B Cohen, Dan E Berkowitz, Paul M Ness, and Viachaslau M Barodka. Decreased erythrocyte deformability after transfusion and the effects of erythrocyte storage duration. *Anesth Analg*, 116(5):975–81, May 2013.

[115] W Trager and J B Jensen. Human malaria parasites in continuous culture. *Science*, 193(4254):673–5, Aug 1976.

[116] C Lambros and J P Vanderberg. Synchronization of plasmodium falciparum erythrocytic stages in culture. *J Parasitol*, 65(3):418–20, Jun 1979.

[117] Dai Thi Xuan Trang, Nguyen Tien Huy, Tohru Kariu, Kunihiko Tajima, and Kaeko Kamei. One-step concentration of malarial parasite-infected red blood cells and removal of contaminating white blood cells. *Malar J*, 3:7, Mar 2004.

[118] malERA Consultative Group on Drugs. A research agenda for malaria eradication: drugs. *PLoS Med*, 8(1):e1000402, Jan 2011.

[119] Wesley A J Webster and Geoffrey I McFadden. From the genome to the phenome: Tools to understand the basic biology of plasmodium falciparum. *J Eukaryot Microbiol*, Sep 2014.

[120] Y Wu, C D Sifri, H H Lei, X Z Su, and T E Wellems. Transfection of plasmodium falciparum within human red blood cells. *Proc Natl Acad Sci USA*, 92(4):973–7, Feb 1995.

[121] Stephen J Goldfless, Brian J Belmont, Alexandra M de Paz, Jessica F Liu, and Jacquin C Niles. Direct and specific chemical control of eukaryotic translation with a synthetic rna-protein interaction. *Nucleic Acids Research*, 40(9):e64, May 2012.

[122] Stephen J Goldfless. Engineering control of eukaryotic translation with application to the malaria parasite plasmodium falciparum. pages 1–130, Jul 2014.

[123] Jeffrey C Wagner, Stephen J Goldfless, Suresh M Ganesan, Marcus C S Lee, David A Fidock, and Jacquin C Niles. An integrated strategy for efficient vector construction and multi-gene expression in plasmodium falciparum. *Malar J*, 12:373, Jan 2013.

[124] Patrick Guye, Yinqing Li, Liliana Wroblewska, Xavier Duportet, and Ron Weiss. Rapid, modular and reliable construction of complex mammalian gene circuits. *Nucleic Acids Research*, 41(16):e156, Sep 2013.

[125] K Deitsch, C Driskill, and T Wellems. Transformation of malaria parasites by the spontaneous uptake and expression of dna from human erythrocytes. *Nucleic Acids Research*, 29(3):850–3, Feb 2001.

[126] Claudia Pfander, Burcu Anar, Frank Schwach, Thomas D Otto, Mathieu Brochet, Katrin Volkmann, Michael A Quail, Arnab Pain, Barry Rosen, William Skarnes, Julian C Rayner, and Oliver Billker. A scalable pipeline for highly effective genetic modification of a malaria parasite. *Nature Methods*, 8(12):1078–82, Dec 2011.

[127] Jeffrey C Wagner, Randall J Platt, Stephen J Goldfless, Feng Zhang, and Jacquin C Niles. Efficient crispr-cas9-mediated genome editing in plasmodium falciparum. *Nature Methods*, 11(9):915–8, Sep 2014.

[128] L G Pologe and J V Ravetch. A chromosomal rearrangement in a p. falciparum histidine-rich protein gene is associated with the knobless phenotype. *Nature*, 322(6078):474–7, Jan 1986.

[129] Jeffrey Wagner, Stephen Goldfless, Suresh Ganesan, Marcus Lee, David Fidock, and Jacquin Niles. An integrated strategy for efficient vector construction and multi-gene expression in plasmodium falciparum. *Malar J*, 12(1):373–373, Oct 2013.

[130] Judith Straimer, Marcus C S Lee, Andrew H Lee, Bryan Zeitler, April E Williams, Jocelynn R Pearl, Lei Zhang, Edward J Rebar, Philip D Gregory, Manuel Llinás, Fyodor D Urnov, and David A Fidock. Site-specific genome editing in plasmodium falciparum using engineered zinc-finger nucleases. *Nat Meth*, 9(10):993–8, Oct 2012.

[131] Zita Krnajski, Tim-Wolf Gilberger, Rolf D Walter, Alan F Cowman, and Sylke Müller. Thioredoxin reductase is essential for the survival of plasmodium falciparum erythrocytic stages. *J Biol Chem*, 277(29):25970–5, Jul 2002.

[132] Nobutaka Kato, Tomoyo Sakata, Ghislain Breton, Karine G Le Roch, Advait Nagle, Carsten Andersen, Badry Bursulaya, Kerstin Henson, Jeffrey Johnson, Kota Arun Kumar, Felix Marr, Daniel Mason, Case McNamara, David Plouffe, Vandana Ramachandran, Muriel Spooner, Tove Tuntland, Yingyao Zhou, Eric C Peters, Arnab Chatterjee, Peter G Schultz, Gary E Ward, Nathanael Gray, Jeffrey Harper, and Elizabeth A Winzeler. Gene expression signatures and small-molecule compounds link a protein kinase to plasmodium falciparum motility. *Nat Chem Biol*, 4(6):347–56, Jun 2008.

[133] Eliane Droucheau, Aline Primot, Virginie Thomas, Denise Mattei, Marie Knockaert, Chris Richardson, Pina Sallicandro, Pietro Alano, Ali Jafarshad, Blandine Baratte, Conrad Kunick, Daniel Parzy, Laurence Pearl, Christian Doerig, and Laurent Meijer. Plasmodium falciparum glycogen synthase kinase-3: molecular model, expression, intracellular localisation and selective inhibitors. *Biochim Biophys Acta*, 1697(1-2):181–96, Mar 2004.

[134] Ana Rita Gomes, Ellen Bushell, Frank Schwach, Gareth Girling, Burcu Anar, Michael A Quail, Colin Herd, Claudia Pfander, Katarzyna Modrzynska, Julian C Rayner, and Oliver Billker. A genome-scale vector resource enables high-throughput reverse genetic screening in a malaria parasite. *Cell Host Microbe*, Feb 2015.

[135] J I Penny, S T Hall, C J Woodrow, G M Cowan, A M Gero, and S Krishna. Expression of substrate-specific transporters encoded by plasmodium falciparum in xenopus laevis oocytes. *Mol Biochem Parasitol*, 93(1):81–9, May 1998.

[136] Ksenija Slavic, Michael J Delves, Miguel Prudêncio, Arthur M Talman, Ursula Straschil, Elvira T Derbyshire, Zhengyao Xu, Robert E Sinden, Maria M Mota, Christophe Morin, Rita Tewari, Sanjeev Krishna, and Henry M Staines. Use of a selective inhibitor to define the chemotherapeutic potential of the plasmodial hexose transporter in different stages of the parasite's life cycle. *Antimicrobial Agents and Chemotherapy*, 55(6):2824–30, Jun 2011.

[137] Ksenija Slavic, Ursula Straschil, Luc Reininger, Christian Doerig, Christophe Morin, Rita Tewari, and Sanjeev Krishna. Life cycle studies of the hexose transporter of plasmodium species and genetic validation of their essentiality. *Molecular Microbiology*, 75(6):1402–13, Mar 2010.

[138] Jennifer A Doudna and Emmanuelle Charpentier. Genome editing. the new frontier of genome engineering with crispr-cas9. *Science*, 346(6213):1258096, Nov 2014.

[139] Kirsten Moll, Inger Ljungström, Hedvig Perlmann, Artur Scherf, and Mats Wahlgren. Methods in malaria research, updated 2008. pages 1–351, Mar 2008.

[140] Andrea Ecker, Adele Lehane, and David A Fidock. Molecular markers of plasmodium resistance to antimalarials. *Treatment and Prevention of Malaria: Milestones in Drug Therapy*, pages 249–280, 2012.

[141] Frédéric Ariey, Benoit Witkowski, Chanaki Amaratunga, Johann Beghain, Anne-Claire Langlois, Nimol Khim, Saorin Kim, Valentine Duru, Christiane Bouchier, Laurence Ma, Pharath Lim, Rithea Leang, Socheat Duong, Sokunthea Sreng, Seila Suon, Char Meng Chuor, Denis Mey Bout, Sandie Ménard, William O Rogers, Blaise Genton, Thierry Fandeur, Olivo Miotto, Pascal Ringwald, Jacques Le Bras, Antoine Berry, Jean-Christophe Barale, Rick M Fairhurst, Françoise Benoit-Vical, Odile Mercereau-Puijalon, and Didier Ménard. A molecular marker of artemisinin-resistant plasmodium falciparum malaria. *Nature*, 505(7481):50–5, Jan 2014.

[142] T E Wellems, L J Panton, I Y Gluzman, V E do Rosario, R W Gwadz, A Walker-Jonah, and D J Krogstad. Chloroquine resistance not linked to mdr-like genes in a plasmodium falciparum cross. *Nature*, 345(6272):253–5, May 1990.

[143] Wassim Daher, Christophe Biot, Thierry Fandeur, Helene Jouin, Lydie Pelinski, Eric Viscogliosi, Laurent Fraisse, Bruno Pradines, Jacques Brocard, Jamal Khalife, and Daniel Dive. Assessment of plasmodium falciparum resistance to ferroquine (ssr97193) in field isolates and in w2 strain under pressure. *Malar J*, 5:11, Jan 2006.

[144] A S Lim and A F Cowman. Plasmodium falciparum: chloroquine selection of a cloned line and dna rearrangements. *Exp Parasitol*, 83(3):283–94, Aug 1996.

[145] S A Peel, S C Merritt, J Handy, and R S Baric. Derivation of highly mefloquine-resistant lines from plasmodium falciparum in vitro. *Am J Trop Med Hyg*, 48(3):385–97, Mar 1993.

[146] A F Cowman, D Galatis, and J K Thompson. Selection for mefloquine resistance in plasmodium falciparum is linked to amplification of the pfmdr1 gene and cross-resistance to halofantrine and quinine. *Proc Natl Acad Sci USA*, 91(3):1143–7, Feb 1994.

[147] Peter B Bloland. Drug resistance in malaria: a background document for the who global strategy for containment of antimicrobial resistance. *World Health Organization*, 2001.

[148] Ringwald Pascal and Amy Barrette. Global report on antimalarial drug efficacy and drug resistance: 2000-2010. *World Health Organization*, 2010.

[149] J R Zucker, E M Lackritz, T K Ruebush, A W Hightower, J E Adungosi, J B Were, B Metchock, E Patrick, and C C Campbell. Childhood mortality during and after hospitalization in western kenya: effect of malaria treatment regimens. *Am J Trop Med Hyg*, 55(6):655–60, Dec 1996.

[150] J F Trape, G Pison, M P Preziosi, C Enel, A Desgrées du Loû, V Delaunay, B Samb, E Lagarde, J F Molez, and F Simondon. Impact of chloroquine resistance on malaria mortality. *C R Acad Sci III, Sci Vie*, 321(8):689–97, Aug 1998.

[151] Eline L Korenromp, Brian G Williams, Eleanor Gouws, Christopher Dye, and Robert W Snow. Measurement of trends in childhood malaria mortality in africa: an assessment of progress toward targets based on verbal autopsy. *Lancet Infect Dis*, 3(6):349–58, Jun 2003.

[152] Anders Björkman. Malaria associated anaemia, drug resistance and antimalarial combination therapy. *Int J Parasitol*, 32(13):1637–43, Dec 2002.

[153] Emiliana Tjitra, Nicholas M Anstey, Paulus Sugiarto, Noah Warikar, Enny Kenangalem, Muhammad Karyana, Daniel A Lampah, and Ric N Price. Multidrug-resistant plasmodium vivax associated with severe and fatal malaria: a prospective study in papua, indonesia. *PLoS Med*, 5(6):e128, Jun 2008.

[154] M Warsame, W H Wernsdorfer, O Ericsson, and A Björkman. Isolated malaria outbreak in somalia: role of chloroquine-resistant plasmodium falciparum demonstrated in balcad epidemic. *J Trop Med Hyg*, 93(4):284–9, Aug 1990.

[155] R N Price and F Nosten. Drug resistant falciparum malaria: clinical consequences and strategies for prevention. *Drug Resist Updat*, 4(3):187–96, Jun 2001.

[156] M Phillips and P A Phillips-Howard. Economic implications of resistance to antimalarial drugs. *Pharmacoeconomics*, 10(3):225–38, Sep 1996.

[157] Ambrose O Talisuna, Peter Bloland, and Umberto D'Alessandro. History, dynamics, and public health importance of malaria parasite resistance. *Clin Microbiol Rev*, 17(1):235–54, Jan 2004.

[158] A P Dash, Neena Valecha, A R Anvikar, and A Kumar. Malaria in india: challenges and opportunities. *J Biosci*, 33(4):583–92, Nov 2008.

[159] P Nguyen-Dinh and W Trager. Chloroquine resistance produced in vitro in an african strain of human malaria. *Science*, 200(4348):1397–8, Jun 1978.

[160] D A Barnes, S J Foote, D Galatis, D J Kemp, and A F Cowman. Selection for high-level chloroquine resistance results in deamplification of the pfmdr1 gene and increased sensitivity to mefloquine in plasmodium falciparum. *The EMBO Journal*, 11(8):3067–75, Aug 1992.

[161] Roland A Cooper, Michael T Ferdig, Xin-Zhuan Su, Lyann M B Ursos, Jianbing Mu, Takashi Nomura, Hisashi Fujioka, David A Fidock, Paul D Roepe, and Thomas E Wellems. Alternative mutations at position 76 of the vacuolar transmembrane protein pfcrt are associated with chloroquine resistance and unique stereospecific quinine and quinidine responses in plasmodium falciparum. *Mol Pharmacol*, 61(1):35–42, Jan 2002.

[162] C R Brockelman, S Monkolkeha, and P Tanariya. Decrease in susceptibility of plasmodium falciparum to mefloquine in continuous culture. *Bull World Health Organ*, 59(2):249–52, Jan 1981.

[163] C Lambros and J D Notsch. Plasmodium falciparum: mefloquine resistance produced in vitro. *Bull World Health Organ*, 62(3):433–8, Jan 1984.

[164] A M Oduola, W K Milhous, N F Weatherly, J H Bowdre, and R E Desjardins. Plasmodium falciparum: induction of resistance to mefloquine in cloned strains by continuous drug exposure in vitro. *Exp Parasitol*, 67(2):354–60, Dec 1988.

[165] Louis J Nkrumah, Paul M Riegelhaupt, Pedro Moura, David J Johnson, Jigar Patel, Karen Hayton, Michael T Ferdig, Thomas E Wellems, Myles H Akabas, and David A Fidock. Probing the multifactorial basis of plasmodium falciparum quinine resistance: evidence for a strain-specific contribution of the sodium-proton exchanger pfnhe. *Mol Biochem Parasitol*, 165(2):122–31, Jun 2009.

[166] H S Banyal and J Inselburg. Plasmodium falciparum: induction, selection, and characterization of pyrimethamine-resistant mutants. *Exp Parasitol*, 62(1):61–70, Aug 1986.

[167] P K Rathod, T McErlean, and P C Lee. Variations in frequencies of drug resistance in plasmodium falciparum. *Proc Natl Acad Sci USA*, 94(17):9389–93, Aug 1997.

[168] M Korsinczky, N Chen, B Kotecka, A Saul, K Rieckmann, and Q Cheng. Mutations in plasmodium falciparum cytochrome b that are associated with atovaquone resistance are located at a putative drug-binding site. *Antimicrob Agents Chemother*, 44(8):2100–8, Aug 2000.

[169] Richard T Eastman, John White, Oliver Hucke, Kevin Bauer, Kohei Yokoyama, Laxman Nallan, Debopam Chakrabarti, Christophe L M J Verlinde, Michael H Gelb, Pradipsinh K Rathod, and Wesley C Van Voorhis. Resistance to a protein farnesyltransferase inhibitor in plasmodium falciparum. *J Biol Chem*, 280(14):13554–9, Apr 2005.

[170] Nagwa S M Aly, Akiko Hiramoto, Hitomi Sanai, Osamu Hiraoka, Kazuyuki Hiramoto, Hiroyuki Kataoka, Jin-Ming Wu, Araki Masuyama, Masatomo Nojima, Satoru Kawai, Hye-Sook Kim, and Yusuke Wataya. Proteome analysis of new antimalarial endoperoxide against plasmodium falciparum. *Parasitol Res*, 100(5):1119–24, Apr 2007.

[171] Amar Bir Singh Sidhu, Qingan Sun, Louis J Nkrumah, Michael W Dunne, James C Sacchettini, and David A Fidock. In vitro efficacy, resistance selection, and structural modeling studies implicate the malarial parasite apicoplast as the target of azithromycin. *J Biol Chem*, 282(4):2494–504, Jan 2007.

[172] Leah Mwai, Abdi Diriye, Victor Masseno, Steven Muriithi, Theresa Feltwell, Jennifer Musyoki, Jacob Lemieux, Avi Feller, Gunnar R Mair, Kevin Marsh, Chris Newbold, Alexis Nzila, and Céline K Carret. Genome wide adaptations of plasmodium falciparum in response to lumefantrine selective drug pressure. *PLoS ONE*, 7(2):e31623, Jan 2012.

[173] Leila S Ross, Francisco Javier Gamo, Maria José Lafuente-Monasterio, Onkar M P Singh, Paul Rowland, Roger C Wiegand, and Dyann F Wirth. In vitro resistance selections for plasmodium falciparum dihydroorotate dehydrogenase inhibitors give mutants with multiple point mutations in the drug-binding site and altered growth. *Journal of Biological Chemistry*, 289(26):17980–95, Jun 2014.

[174] Marina Chavchich, Lucia Gerena, Jennifer Peters, Nanhua Chen, Qin Cheng, and Dennis E Kyle. Role of pfmdr1 amplification and expression in induction of resistance to artemisinin derivatives in plasmodium falciparum. *Antimicrobial Agents and Chemotherapy*, 54(6):2455–64, Jun 2010.

[175] Neekesh V Dharia, Amar Bir Singh Sidhu, María Belén Cassera, Scott J Westenberger, Selina Er Bopp, Rich T Eastman, David Plouffe, Serge Batalov, Daniel J Park, Sarah K Volkman, Dyann F Wirth, Yingyao Zhou, David A Fidock, and Elizabeth A Winzeler. Use of high-density tiling microarrays to identify mutations globally and elucidate mechanisms of drug resistance in plasmodium falciparum. *Genome Biology*, 10(2):R21, Jan 2009.

[176] Neekesh V Dharia, David Plouffe, Selina E R Bopp, Gonzalo E González-Páez, Carmen Lucas, Carola Salas, Valeria Soberon, Badry Bursulaya, Tadeusz J Kochel, David J Bacon, and Elizabeth A Winzeler. Genome scanning of amazonian plasmodium falciparum shows subtelomeric instability and clindamycin-resistant parasites. *Genome Res*, 20(11):1534–44, Nov 2010.

[177] Ian Chopra, Alexander J O'Neill, and Keith Miller. The role of mutators in the emergence of antibiotic-resistant bacteria. *Drug Resist Updat*, 6(3):137–45, Jun 2003.

[178] Víctor M Castillo-Acosta, Fernando Aguilar-Pereyra, Antonio E Vidal, Miguel Navarro, Luis M Ruiz-Pérez, and Dolores González-Pacanowska. Trypanosomes lacking uracil-dna glycosylase are hypersensitive to antifolates and present a mutator phenotype. *Int J Biochem Cell Biol*, 44(9):1555–68, Sep 2012.

[179] Thomas Helleday, Eva Petermann, Cecilia Lundin, Ben Hodgson, and Ricky A Sharma. Dna repair pathways as targets for cancer therapy. *Nat Rev Cancer*, 8(3):193–204, Mar 2008.

[180] Hajime Honma, Makoto Hirai, Shota Nakamura, Hassan Hakimi, Shin-Ichiro Kawazu, Nirianne Mq Palacpac, Hajime Hisaeda, Hiroyuki Matsuoka, Satoru Kawai, Hiroyoshi Endo, Teruo Yasunaga, Jun Ohashi, Toshihiro Mita, Toshihiro Horii, Mitsuru Furusawa, and Kazuyuki Tanabe. Generation of

rodent malaria parasites with a high mutation rate by destructing proofreading activity of dna polymerase ÎŽ. *DNA Research*, Mar 2014.

[181] J L Martinez and F Baquero. Mutation frequencies and antibiotic resistance. *Antimicrob Agents Chemother*, 44(7):1771–1777, 2000.

[182] A J O'Neill and I Chopra. Use of mutator strains for characterization of novel antimicrobial agents. *Antimicrob Agents Chemother*, 45(5):1599–600, May 2001.

[183] José L Martínez, Fernando Baquero, and Dan I Andersson. Predicting antibiotic resistance. *Nat Rev Micro*, 5(12):958–65, Dec 2007.

[184] Meryl A Castellini, Jeffrey S Buguliskis, Louis J Casta, Charles E Butz, Alan B Clark, Thomas A Kunkel, and Theodore F Taraschi. Malaria drug resistance is associated with defective dna mismatch repair. *Mol Biochem Parasitol*, 177(2):143–7, Jun 2011.

[185] Lara Bethke, Susan Thomas, Kerone Walker, Ronak Lakhia, Radha Rangarajan, and Dyann Wirth. The role of dna mismatch repair in generating genetic diversity and drug resistance in malaria parasites. *Molecular and Biochemical Parasitology*, 155(1):18–25, Sep 2007.

[186] Richard F Trotta, Matthew L Brown, James C Terrell, and Jeanne A Geyer. Defective dna repair as a potential mechanism for the rapid development of drug resistance in plasmodium falciparum. *Biochemistry*, 43(17):4885–91, May 2004.

[187] B M Haltiwanger, Y Matsumoto, E Nicolas, G L Dianov, V A Bohr, and T F Taraschi. Dna base excision repair in human malaria parasites is predominantly by a long-patch pathway. *Biochemistry*, 39(4):763–72, Feb 2000.

[188] Thidarat Suksangpleng, Ubolsree Leartsakulpanich, Saengduen Moonsom, Saranya Siribal, Usa Boonyuen, George E Wright, and Porntip Chavalitshewinkoon-Petmitr. Molecular characterization of plasmodium falciparum uracil-dna glycosylase and its potential as a new anti-malarial drug target. *Malaria Journal*, 13(1):149, Apr 2014.

[189] B J Glassner, L J Rasmussen, M T Najarian, L M Posnick, and L D Samson. Generation of a strong mutator phenotype in yeast by imbalanced base excision repair. *Proc Natl Acad Sci USA*, 95(17):9997–10002, Aug 1998.

[190] B Kavli, G Slupphaug, C D Mol, A S Arvai, S B Peterson, J A Tainer, and H E Krokan. Excision of cytosine and thymine from dna by mutants of human uracil-dna glycosylase. *EMBO J*, 15(13):3442–7, Jul 1996.

[191] Paul Auerbach, Richard A O Bennett, Elisabeth A Bailey, Hans E Krokan, and Bruce Demple. Mutagenic specificity of endogenously generated abasic sites in saccharomyces cerevisiae chromosomal dna. *Proc Natl Acad Sci USA*, 102(49):17711–6, Dec 2005.

[192] P Funchain, A Yeung, J L Stewart, R Lin, M M Slupska, and J H Miller. The consequences of growth of a mutator strain of escherichia coli as measured by loss of function among multiple gene targets and loss of fitness. *Genetics*, 154(3):959–70, Mar 2000.

[193] Claire Daurel, Anne-Laure Prunier, Françoise Chau, Louis Garry, Roland Leclercq, and Bruno Fantin. Role of hypermutability on bacterial fitness and emergence of resistance in experimental osteomyelitis due to staphylococcus aureus. *FEMS Immunol Med Microbiol*, 51(2):344–9, Nov 2007.

[194] Masamitsu Honma. Generation of loss of heterozygosity and its dependency on p53 status in human lymphoblastoid cells. *Environ Mol Mutagen*, 45(2-3):162–76, Jan 2005.

[195] E L Ivanov, I V Fedorova, and S V Koval'tsova. [isolation and characteristics of new mutants of saccharomyces cerevisiae with increased spontaneous mutability]. *Genetika*, 28(5):47–55, May 1992.

[196] A Nasim and T Brychcy. Cross sensitivity of mutator strains to physical and chemical mutagens. *Can J Genet Cytol*, 21(1):129–37, Mar 1979.

[197] B A Montelone, S Prakash, and L Prakash. Hyper-recombination and mutator effects of the mms9-1, mms13-1, and mms21-1 mutations in saccharomyces cerevisiae. *Curr Genet*, 4(3):223–32, Dec 1981.

[198] A Nzila-Mounda, E K Mberu, C H Sibley, C V Plowe, P A Winstanley, and W M Watkins. Kenyan plasmodium falciparum field isolates: correlation between pyrimethamine and chlorcycloguanil activity in vitro and point mutations in the dihydrofolate reductase domain. *Antimicrobial Agents and Chemotherapy*, 42(1):164–9, Jan 1998.

[199] Benoit Witkowski, Antoine Berry, and Françoise Benoit-Vical. Resistance to antimalarial compounds: methods and applications. *Drug Resist Updat*, 12(1-2):42–50, Jan 2009.

[200] Elizabeth A Winzeler and Micah J Manary. Drug resistance genomics of the antimalarial drug artemisinin. *Genome Biology*, 15(11):544, Jan 2014.

[201] Eva S Istvan, Neekesh V Dharia, Selina E Bopp, Ilya Gluzman, Elizabeth A Winzeler, and Daniel E Goldberg. Validation of isoleucine utilization targets in plasmodium falciparum. *Proc Natl Acad Sci USA*, 108(4):1627–32, Jan 2011.

[202] I K Srivastava, J M Morrisey, E Darrouzet, F Daldal, and A B Vaidya. Resistance mutations reveal the atovaquone-binding domain of cytochrome b in malaria parasites. *Molecular Microbiology*, 33(4):704–11, Aug 1999.

[203] D A Fidock, T Nomura, A K Talley, R A Cooper, S M Dzekunov, M T Ferdig, L M Ursos, A B Sidhu, B Naudé, K W Deitsch, X Z Su, J C Wootton, P D Roepe, and T E Wellems. Mutations in the p. falciparum digestive vacuole transmembrane protein pfcrt and evidence for their role in chloroquine resistance. *Mol Cell*, 6(4):861–71, Oct 2000.

[204] D R Brooks, P Wang, M Read, W M Watkins, P F Sims, and J E Hyde. Sequence variation of the hydroxymethyldihydropterin pyrophosphokinase: dihydropteroate synthase gene in lines of the human malaria parasite, plasmodium falciparum, with differing resistance to sulfadoxine. *Eur J Biochem*, 224(2):397–405, Sep 1994.

[205] Jacques Le Bras and Rémy Durand. The mechanisms of resistance to antimalarial drugs in plasmodium falciparum. *Fundam Clin Pharmacol*, 17(2):147–53, Apr 2003.

[206] M T Duraisingh, C J Drakeley, O Muller, R Bailey, G Snounou, G A Targett, B M Greenwood, and D C Warhurst. Evidence for selection for the tyrosine-86 allele of the pfmdr 1 gene of plasmodium falciparum by chloroquine and amodiaquine. *Parasitology*, 114 (Pt 3):205–11, Mar 1997.

[207] C H Sibley, J E Hyde, P F Sims, C V Plowe, J G Kublin, E K Mberu, A F Cowman, P A Winstanley, W M Watkins, and A M Nzila. Pyrimethamine-sulfadoxine resistance in plasmodium falciparum: what next? *Trends in Parasitology*, 17(12):582–8, Dec 2001.

[208] Thomas Spangenberg, Jeremy N Burrows, Paul Kowalczyk, Simon McDonald, Timothy N C Wells, and Paul Willis. The open access malaria box: a drug discovery catalyst for neglected diseases. *PLoS ONE*, 8(6):e62906, Jan 2013.